

# **Physicochemical and Quantitative Cell Viability Assays of Quercetin-Encapsulated Alginate Beads**

**Cahit Özbilenler**

Submitted to the  
Institute of Graduate Studies and Research  
in partial fulfillment of the requirements for the degree of

Master of Science  
in  
Chemistry

Eastern Mediterranean University  
July 2019  
Gazimağusa, North Cyprus

Approval of the Institute of Graduate Studies and Research

---

Prof. Dr. Ali Hakan Ulusoy  
Acting Director

I certify that this thesis satisfies all the requirements as a thesis for the degree of Master of Science in Chemistry.

---

Prof. Dr. İzzet Sakallı  
Chair, Department of Chemistry

We certify that we have read this thesis and that in our opinion it is fully adequate in scope and quality as a thesis for the degree of Master of Science in Chemistry.

---

Asst. Prof. Dr. Ergül Mutlu Altundağ  
Co-Supervisor

---

Prof. Dr. Mustafa Gazi  
Supervisor

---

Examining Committee

1. Prof. Dr. Mustafa Gazi
2. Prof. Dr. Elvan Yılmaz
3. Assoc. Prof. Dr. Terin Adalı
4. Assoc. Prof. Dr. Kerem Teralı
5. Asst. Prof. Dr. Ergül Mutlu Altundağ

---

---

---

---

---

## ABSTRACT

In this thesis, quercetin-encapsulated alginate beads were prepared in two different version; normal ionic cross-linked gel beads and cryogel beads. FT-IR was used to characterize the beads and to check the basic chemical moieties from beads. It was found that quercetin molecules could be trapped into and outside the “egg box” between polymer chains and they would make weak interactions such as polar-polar interactions with the functional groups of alginate. Swelling and drying profiles were studied. Based on release studies, it was found that Mueller Hinton Broth (MHB) was not a suitable release medium for the beads due to the reaction between the ester moiety of casein hydrolysate in MHB and carboxylate groups of alginate would limit the release of quercetin. Therefore, 0.9% saline should be preferred for antimicrobial assays. In addition, sodium ions in RPMI-1640 caused the swelling of beads, which lead to the maximum release of drug.

Release kinetic models showed that release of quercetin from cryogel beads fit to the first order release model in DMSO and this meant that release of quercetin is based on the concentration of quercetin. Release of quercetin from gel beads fit to the Higuchi release model in DMSO and this meant that quercetin concentration was lower in polymer than its solubility and release occurs through the pores in the matrix. Release of quercetin from gel beads and cryogel beads fit to the first order release model in 0.9% saline with 40% DMSO of total solution. Thus, release of quercetin is based on the concentration of quercetin. Cryogel beads and gel beads fit to zero order release model in RPMI-1640 between 12 and 48 hours.

Cell viability, MTT (3-(4,5-dimethylthiazol-2-yl)-2,5-diphenyltetrazolium bromide) assay showed that as the concentration of quercetin released from the beads increases, the percent viability of (B-CPAP) papillary thyroid cancer cells decreases. In addition, DPPH (2,2-diphenyl-1-picrylhydrazyl) assay showed that as the concentration of quercetin release from beads increases the inhibition of free radical increases. However, in time-kill assay to have significant effect on bacteria, the concentration of quercetin in the beads should be increased.

**Keywords:** Quercetin, papillary thyroid cancer cells (B-CPAP) , 3-(4,5-dimethylthiazol-2-yl)-2,5-diphenyltetrazolium bromide (MTT), 2,2-diphenyl-1-picrylhydrazyl (DPPH)

## ÖZ

Bu tez çalışmasında, kuvarsetin yüklü aljinat kürecikleri iki farklı versiyonda hazırlanmıştır; normal iyonik çapraz bağlı jel küreler ve kriyojel küreler. Kürelerin çapları ve kütle ölçümleri yapılmış ve küreleri karakterize etmek ve tanelerin temel kimyasal kısımlarını kontrol etmek için FT-IR spektroskopisi kullanılmıştır. Kuvarsetin moleküllerinin “egg box” içerisine yer aldığı ve aljinatın fonksiyonel gruplarıyla polar-polar etkileşimi gibi zayıf etkileşimler yaptıkları tespit edilmiştir. Şişme ve kurutma profilleri incelenmiştir. Mueller Hinton Broth (MHB), MHB içerisindeki kazein hidrolizatın ester kısmı ile aljinatların karboksilat grupları arasındaki reaksiyonun, kuvarsetin salımını sınırlayacağından küreler için uygun bir salım ortamı olmadığı saptanmıştır. Bu nedenle, antimikrobiyal çalışmalar için % 0.9 salin tercih edilmelidir. Ek olarak, RPMI-1640' daki sodyum iyonları boncukların şişmesine ve böylece ilacın maksimum salınımına yol açtığı belirlenmiştir.

Serbest bırakma kinetik modelleri, DMSO ortamında kriyojel boncuklardan kuvarsetin salınmasının, birinci dereceden serbest bırakma modeline uyduğunu ve bunun kuvarsetin konsantrasyonuna dayandığı anlamına geldi. DMSO ortamında kuvarsetin 'in jel boncuklarından salınması, Higuchi salma modeline uymaktadır ve bunun anlamı, quercetin konsantrasyonunun polimerde çözünürlüğünden daha düşük olması ve salımın matris içindeki gözeneklere yardımıyla gerçekleştiği anlamına gelmektedir. Kriyojel ve jel kürelerden kuvarsetin salımı, hem DMSO hem de %40 DMSO içeren % 0.9 salin solusyonunda birinci dereceden salma modeline uyuyor. Bu da, kuvarsetin salınımının kuvarsetin derişimine bağlı olduğunu gösterir. RPMI-

1640 ortamında kriyojel ve jel kürelerde kuvarsetin salınımı 12 ila 48 saat arasında sıfırncı salma modeline uyar.

Hücre sağkalımı, MTT (3- (4,5-dimetiltiyazol-2-il) -2,5-difeniltetrazolyum bromür) deneyi, kürelerden salınan kuvarsetin derişimi arttıkça, (B-CPAP) papiller tiroid kanser hücrelerinin yüzde canlılığının azaldığını gösterdi. Ayrıca, DPPH (2,2-difenil-1-pikrilhidrazil) deneyi, kürelerden kuvarsetin salınımının derişimi arttıkça serbest radikal inhibasyon yüzdesinin (%) arttırdığını gösterdi. Bununla birlikte, zamana karşı ölüm deneyinde, bakteriler üzerindeki etkiyi görebilmek için, küreler içerisindeki kuvarsetin miktarının artırılması gerektiği gözlemlendi.

**Anahtar Kelimeler:** Kuvarsetin, papiller tiroid kanseri hücreleri (B-CPAP), 3- (4,5-dimetiltiyazol-2-il) -2,5-difeniltetrazolyum bromür (MTT), 2,2-difenil-1-pikrilhidrazil (DPPH)

## DEDICATION

*I dedicate this thesis to my  
family*

## ACKNOWLEDGMENT

I would like to thank to my supervisor Prof. Dr. Mustafa Gazi and my co-supervisor Asst.Prof.Dr.Ergül Mutlu Altundağ for their continuous support and great guidance. I would like to thank to Prof. Dr. Elvan Yılmaz for her great guidance and strong support.

I would also like to thank to vice dean of Medicine Faculty Asst. Prof. Dr. Mümtaz Güran, instructor Gizem Şanlıtürk and research assistant Namık Refik Kerküklü for their advices and help during time kill assay.

I would also like to record my feelings to my close friends;Selma Ustürk, Faisal Mustafa, Erdem Baytunç, and Arwa Abou Rajab, who motivate and support me during the progression of this thesis.



# TABLE OF CONTENTS

ABSTRACT .....	iii
ÖZ .....	v
DEDICATION .....	vii
ACKNOWLEDGMENT .....	viii
LIST OF TABLES .....	xii
LIST OF FIGURES .....	xiii
LIST OF ABBREVIATIONS .....	xvi
1 INTRODUCTION .....	1
1.1 Alginate .....	1
1.2 Quercetin .....	5
1.3 Cryogelation .....	8
1.4 Human Papillary Thyroid Cancer (B-CPAP) Cells.....	9
1.5 Cell Culture.....	10
1.6 Importance of Cargo or Beads in Chemical Storage and Usage.....	11
1.7 Aim of the Thesis.....	11
2 LITERATURE REVIEW.....	12
2.1 Calcium Alginate Gel Beads as Drug Release Media .....	12
2.2 Anticancer, Antioxidant and Antibacterial Activities of Quercetin .....	16
2.2.1 Anticancer Activities .....	16
2.2.2 Antioxidant Activities.....	17
2.2.3 Antibacterial Activities .....	18
3 EXPERIMENTAL .....	19
3.1 Materials .....	19

3.2 Formation of Quercetin-Encapsulated Beads.....	19
3.3 Cryogel Beads Formation.....	21
3.4 Light Microscope Image and the Diameter of the Beads.....	21
3.5 FTIR (Fourier-Transform Infrared Spectroscopy) Measurements.....	22
3.6 Drying Profile of Quercetin-Loaded Beads.....	22
3.7 Swelling Test.....	22
3.8 Calibration Curves.....	23
3.9 Release Studies.....	23
3.9.1 Determination of Percent Quercetin Released.....	24
3.9.2 Determination of Release Kinetics of Quercetin from Alginate Beads...	24
3.9.2.1 Zero Order Release Model.....	24
3.9.2.2 First Order Release Model.....	25
3.9.2.3 Higuchi Release Model.....	25
3.9.2.4 Korsmeyer-Peppas Release Model.....	25
3.10 MTT Assay (Succinate Dehydrogenase Activity Assay).....	26
3.11 Antioxidant Assay – DPPH (2,2-diphenyl-1-picrylhydrazyl)Test.....	28
3.12 Time Kill Assay.....	29
4 RESULTS AND DISCUSSION.....	31
4.1 Quercetin Loaded Beads and Cryogel Beads.....	31
4.2 Cryogel beads.....	32
4.3 Weight , Diameter and Light Microscope Image of the Beads.....	34
4.3.1 Weight Measurements of the Beads.....	34
4.3.2 Diameter Measurements of the Beads.....	36
4.3.3 Light Microscope Image of the Beads.....	40
4.4 FTIR (Fourier-Transform Infrared spectroscopy) Results.....	42

4.5 Results of Drying Profile of Quercetin Loaded Beads.....	48
4.6 Swelling Tests Results.....	51
4.7 Calibration Curves.....	54
4.8 Release Studies.....	60
4.8.1 Observations From Release Studies .....	67
4.8.2 Absorbance Versus Concentration and Concentration Versus Time Graphs.....	72
4.8.3 Release Kinetics Models.....	86
4.8.3.1 Percent Quercetin Released Results .....	86
4.8.3.2 Results of Release Kinetics of Quercetin from Alginate Beads.....	90
4.9 MTT Assay (Succinate Dehydrogenase Activity Assay) and IC50 Determination.....	105
4.9.1 IC50 Determination .....	110
4.10 Antioxidant Assay – DPPH (2,2-diphenyl-1-picrylhydrazyl) Test .....	111
4.11 Time Kill Assay.....	114
5 CONCLUSION.....	116
REFERENCES.....	118

## LIST OF TABLES

Table 1: Masses of beads. ....	34
Table 2: Diameters of dried gel beads.....	36
Table 3: Diameters of cryogel beads.....	37
Table 4: Diameters of gel beads.....	38
Table 5: Diameters of dried gel cryobeads. ....	39
Table 6 : Drying data of the beads. ....	48
Table 7 : Drying data of the cryogel beads. ....	50
Table 8: Observations from release kinetics studies. ....	72
Table 9: Parameters table for four different models. ....	90
Table 10: Types of release mechanism can be determined based on release exponent (n). ....	90
Table 11: Selected concentrations and their effect on B-CPAP Cancer cells after hours in terms of % cell viability. ....	105
Table 12: Colony Forming Units per mL (CFU/mL) for S. aureus at specific time intervals were calculated from number of colonies obtained on blood agar plates	114

## LIST OF FIGURES

Figure 1: Structural features of alginate in three different forms.....	3
Figure 2: “Egg box” structure . .....	4
Figure 3:Structure of quercetin .....	7
Figure 4: Schematic representation of cryogelation.....	9
Figure 5: Experimental setup for preparing quercetin-encapsulated gel beads .....	20
Figure 6: Quercetin-encapsulated alginate gel beads on petri dish .....	21
Figure 7: Formazan crystals formation. ....	26
Figure 8: Quercetin loaded gel beads.....	31
Figure 9: Cryogelation. ....	33
Figure 10: Average weight measurements.....	35
Figure 11: Average diameters of the dried gel beads.....	37
Figure 12: Average diameters of the cryogel beads.....	38
Figure 13: Average diameters of the gel beads.....	39
Figure 14: Average diameters of the dried cryogel beads. ....	40
Figure 15: Light microscope images of gel bead .....	41
Figure 16: Morphologies of four different types of beads. ....	42
Figure 17:FT-IR spectra and the structure of quercetin-encapsulated beads.....	47
Figure 18: Drying rate of the beads.....	49
Figure 19: Drying rate of the cryogel beads.....	51
Figure 20: Average percent swelling profiles. ....	54
Figure 21: Calibration graphs for DMSO. ....	56
Figure 22: Calibration graphs for MHB.....	57
Figure 23: Calibration graphs for RPMI-1640.....	58

Figure 24: Calibration graphs for saline.....	59
Figure 25: Release graphs of quercetin from the beads in different solvents. ....	67
Figure 26: Colour change of quercetin.....	68
Figure 27: Quercetin loaded beads in MHB. ....	69
Figure 28: Percent swelling profiles of alginate beads. ....	71
Figure 29: Absorbance versus concentration and concentration versus time graphs of quercetin in DMSO.....	75
Figure 30: Absorbance versus concentration graph of dried gel beads in 0.9% saline solution with 10% DMSO of total solution. ....	76
Figure 31: Absorbance versus concentration and concentration versus time graphs of quercetin in 0.9% Saline solution with 20% DMSO of total solution.....	77
Figure 32: Absorbance versus concentration and concentration versus time graphs of quercetin in 0.9% Saline solution with 40% DMSO of total solution.....	80
Figure 33: Absorbance versus concentration and concentration versus time graphs of quercetin in MHB solution with 20% DMSO of total solution . ....	81
Figure 34: Absorbance versus concentration and concentration versus time graphs of quercetin in MHB solution with 40% DMSO of total solution. ....	84
Figure 35: Absorbance versus concentration and concentration versus time graphs of quercetin in RPMI1640.....	86
Figure 36: Quercetin released (%) graphs.....	89
Figure 37: Zero order release models for different types of beads in 3 different types of release media .....	95
Figure 38: First order release models for different types of beads in 3 different types of release media.....	98

Figure 39: Higuchi Release Models for different types of beads in 3 different types of release media.....	101
Figure 40: Korsmeyer-peppas models for different types of beads in 3 different types of release media .....	104
Figure 41: Percent viability versus concentration graph.....	106
Figure 42: Invert microscope images of B-CPAP cancer cells after treatment with different concentrations of quercetin. ....	108
Figure 43: Invert microscope images of B-CPAP cancer cells after MTT treatment.....	109
Figure 44: Average % Viability Determination.....	110
Figure 45: DPPH reduction by quercetin .....	112
Figure 46: Reduction of DPPH absorbance values at 515 nm. ....	113
Figure 47: CFU/mL versus time graph. ....	115

## LIST OF ABBREVIATIONS

A	Adenine
ATP	Adenosine Triphosphate
ATR	Attenuated Total Reflectance
B-CPAP	Papillary Thyroid Cancer Cell
CFU	Colony Forming Unit
CoA	Acetyl Coenzyme A
COX	Cyclooxygenase
CVD	Cardiovascular Diseases
DMSO	Dimethyl Sulfoxide
DNA	Deoxyribonucleic Acid
DPPH	2,2-Diphenyl-1-picrylhydrazyl
E	Glutamate
ERK	ExtraCellular Signal-Regulated Kinases
FAD	Adenine Dinucleotide
FBS	Fetal Bovine Serum
FT-IR	Fourier Transform Infrared Spectroscopy
G	Guluronic Acid
LDL	Low Density Lipoproteins
M	Mannuronic Acid
MAPK	Mitogen-Activated Protein Kinases
MHB	Mueller Hinton Broth
MIC	Minimum Inhibitory Concentration
MSSA	<i>Methicillin sensitive staphylococcus aureus</i>



MTT	(3-[4,5-dimethylthiazole-2-yl]-2,5-diphenyl-tetrazolium bromide)
NAD	Nicotinamide Adenine Dinucleotide
NADP	Nicotinamide Adenine Dinucleotide Phosphate
PBS	Phosphate Buffered Saline
Q	Quercetin
RNA	Ribonucleic Acid
RNS	Reactive Nitrogen Species
ROS	Reactive Oxygen Species
T	Thymin
V	Valine

# Chapter 1

## INTRODUCTION

This thesis focuses on the synthesis of alginate gel beads by loading them with quercetin molecules. The method of bead formation conducted according to the method in literature by Bajpai et al., (2004). Following to the beads formation, physicochemical studies were conducted such as characterization with FT-IR spectroscopy, drying profiles and swelling graphs. After that release studies were conducted and release kinetic models were studied according to the methods used by Dash et al., (2010). Following to the release studies, three different applications of the quercetin-encapsulated gel beads were studied; anticancer, antioxidant and antimicrobial activities according to the methods in literature by Mutlu Altundağ et al.,(2016); Adebisi et al., (2017) and Perim et al., (2018).

### 1.1 Alginates

Natural polymers are the polymeric compounds, which are extracted or produced from nature. They are more advantageous compare to other types of polymers, especially in biological/ biomaterial/drug delivery research topics (Asghari et al., 2017). These advantages can be listed as high abundance, economic, environmental friendly and safe. Natural polymers are produced from nature, and extracting polymeric compounds from plants or animals means that there are many source of origin around and plenty of compounds can be obtained (Panzella & Napolitano,2017). Compare to other polymers, which require different techniques and many reagents to synthesize, production of natural polymers is far more

economical and environmental friendly. More importantly, natural polymers are biodegradable and also biocompatible, these two key features make them to perfectly fit to drug delivery in biological organisms research topics (Islam et al., 2017). In biological based application of polymers, non-toxic materials such as natural polymers are desired thereby the side effects of the polymers on biological organisms can be reduced during the biological applications. Natural Polymers can be derived from plant or animal origin (Kulkarni et al., 2012).

Alginates are the most abundant natural polysaccharides in brown algae more than one over third of the dried mass of algae. They are usually coordinated with metal ions in intracellular matrix, these metal ions can be magnesium, sodium and calcium (Jia et al., 2014). It is also the main polymeric structure in algae that's give the algal structural shape and strength (Wang et al., 2014). Alginates are favorable polymers for polymeric materials applications due to its gelation ability, viscosity and stability. Alginates can be synthesized in laboratory or can be extracted from the natural sources (Draget et al., 2006).

Alginates are copolymeric structures, which are composed of guluronic acid (G) and mannuronic acid (M). Thus, under physiological conditions with pH 7.4 they are anionic polymers as shown in Figure 1 (Graulus et al., 2015).

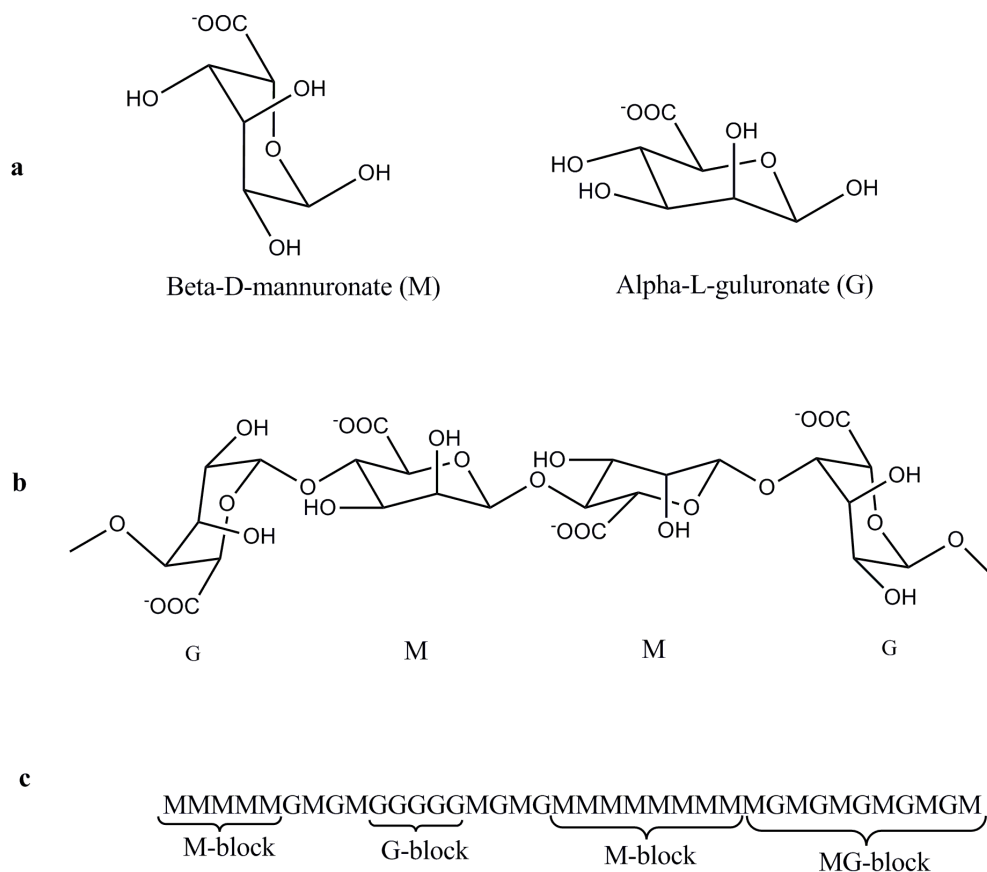


Figure 1: Structural features of alginate in three different forms.

Note: (a) Monomeric residues of alginate.(b) Conformational features of G and M monomers of alginate.(c) The G and M blocks in block polymer form of alginate (ChemDraw image derived from Draget & Taylor, 2011).

Alginates are polyanionic polymers and they have suitable ion binding features, which make them perfect polymers for gel formation applications. Depending on their mannuronate (M) and guluronate (G) composition of alginates, they have an affinity to bind multivalent cations such as calcium ion,  $\text{Ca}^{2+}$  and barium ion,  $\text{Ba}^{2+}$  (Kaygusuz et al., 2016). Although the mannuronate residues are not selective, the selectivity due to presence of polyguluronate blocks was good enough to have characteristic affinity for metal ions. The strength of the affinity of polyanionic alginates to cations can vary (An et al., 2015). For instance, the attraction between the barium ion and the anions of alginates was stronger compare to the attraction between the calcium ions and the anions of alginates. As a result of the binding

properties of alginates to multivalent cations, the “egg-box” shape was resembled as shown in Figure 2 (Li et al., 2015).

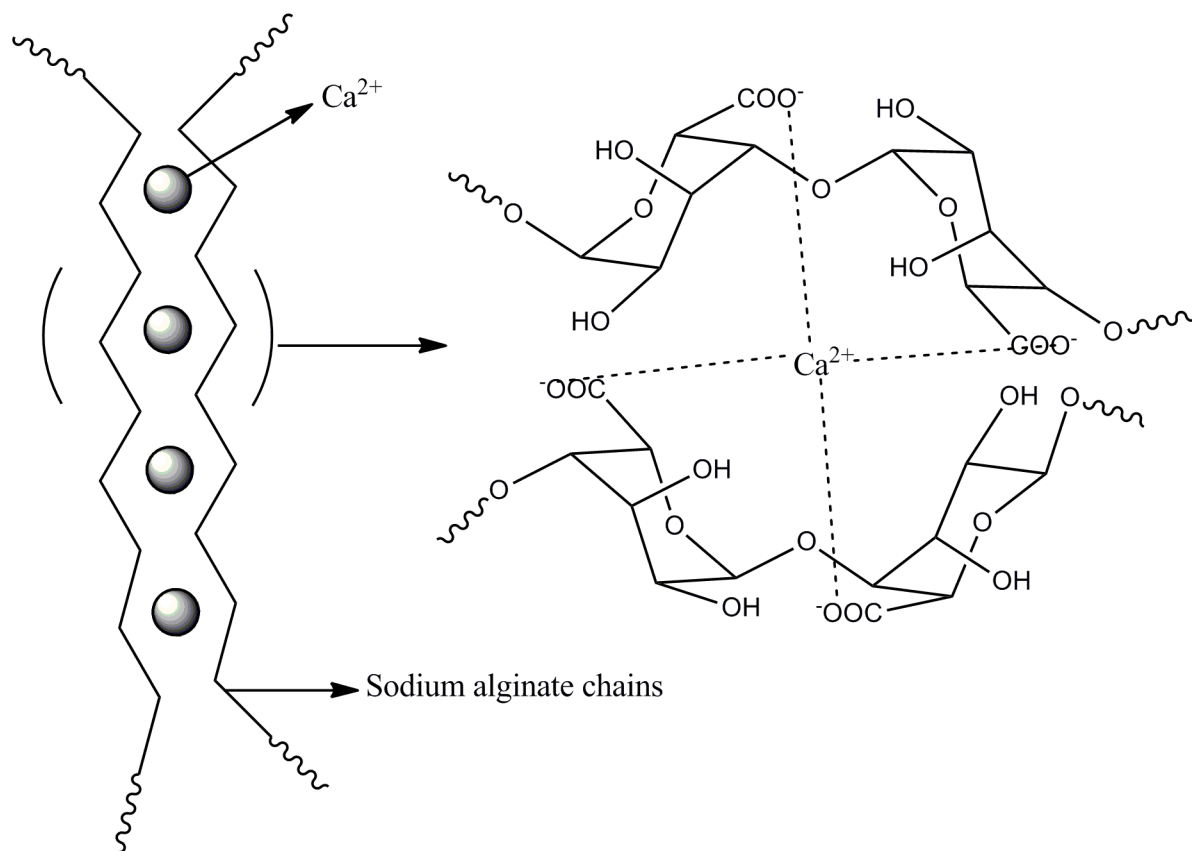


Figure 2: “Egg box” structure.

Note: ChemDraw image derived from Destruel et al., 2016.

Ion binding properties of alginates do not only make them suitable for gel formation, this property makes them perfect polymers for beads formation. Encapsulation of drugs or desired chemicals into alginate polymers preferential among all the other types of polymers. This is due to several advantageous features of alginates. They have high chemical stability and high mechanical stability. Alginate has strong backbone and it has stable structure under physiological conditions at 37 °C and pH 7.4 (Shaari & Kamarudin, 2015). Their swelling features can be regulated. Alginates have carboxylic acid group. At lower pH values carboxylic acid group will be protonated due to higher concentration of proton and at

higher pH values carboxylic acid group will be deprotonated to form negatively charged carboxylate. Negatively charged carboxylate groups can interact with positively charged ions. As a summary, depending on the pH of medium the swelling properties of alginate can be adjusted and this can affect the release of chemicals from alginate beads. Since swelling characteristic can vary depending on the pH of medium, the gastrointestinal track (GIT) of digestive system can be mimicked and this will give more reliable results for biomedical applications (Alegre-Requena et al., 2016). For instance, swelling features of alginates at around pH 1 can be observed by using 0.1 - 0.2 M HCl to mimic the swelling properties of alginates in stomach and pH 7.4 can be created by using buffer solutions (such as phosphate buffer) to mimic the swelling features of alginates in intestines. In addition, they have low toxicity. Alginates are natural polymers. Like many other natural polymers, they can be digested in biological organisms and it can easily decompose in nature (Bang et al., 2016). They also have low pore size distribution. Alginate can form beads with defined and homogenous pore sizes. Similar size of pore is key in polymer science, otherwise, it will be difficult to characterize the physical properties of the beads formed (Orive et al., 2004; Agüero et al., 2017). Beads or any polymeric materials with undefined physical features will have limited applications, specifically it will not fit for drug delivery applications, since it will be difficult to estimate the amount of drug or chemical released from the beads.

## **1.2 Quercetin**

Polyphenols are phytochemicals and they are abundantly found in plant based resources (Williamson, 2017). After the discovery of polyphenolic reduction effect of the rate of cardiovascular diseases (CVD) and neurodegenerative diseases was found, the popularity of polyphenol based researches increased (Rasines-Perea & Teissedre,

2017). Usually polyphenols take part in the reduction of reactive oxygen species (ROS) by helping ROS reducing enzymes, thus, they are considered as strong antioxidants (Feng et al., 2017). Studies show that there are various different polyphenols and they have different features. These features can be listed as antioxidant activity, antibacterial activity, anticancer activity, stability, biocompatibility and bioavailability (Tsao, 2010). Polyphenols can be subdivided into four groups; flavonoids, phenolic acids, stilbenes and lignans. Flavonoids are plant based secondary metabolites and they are excessively found in vegetables and fruits. Flavonoids have multiple biochemical effects such as antimutagenic, antioxidant and anticarcinogenic (Teixeira et al., 2019). Apart from these favourable effects, they can also act as inhibitor for several enzymes such as cyclooxygenase (COX) and phosphoinositide-3- kinase (Panche et al., 2016). Flavonols are the subgroup of flavonoids and they are mostly found in fruits and vegetables. Red wine and tea can also have high amounts of flavonols. Due to high antioxidation activity, they can decrease the risk of Cardiovascular Diseases (CVDs). Flavonols can be subdivided into Quercetin, Myricetin, rutin, morin, and kaempferol (Scarano et al., 2018). Although they can show variation in structure due to methylations, hydroxylations and glycosylations. Generally, flavonols have the ketone group at position 4 of ring C and double bond between position 2 and 3 of ring C. Ring B is attached to ring C at position 2 and hydroxyl group attached to ring C at position 3 (Iwashina,2013).

Quercetin also known as 3, 3', 4', 5, 7-pentahydroxyflavone as shown in Figure 3, and it cannot be synthesized in the body. It has yellow colour and once it dissolves its colour will turn to darker yellow (Bentz, 2017). Quercetin is soluble in alcohols, however insoluble in water. Among all these solvents, the DMSO

(dimethylsulfoxide) can be considered as the best solvent for quercetin. Quercetin is rich in onions, cherries, broccoli, tea and red wines (Anand, 2016; Lakhanpal, 2007). Quercetin has many features such as antioxidant activity, anti-inflammatory activity, anticancer activity and cardiovascular diseases reducing effects.

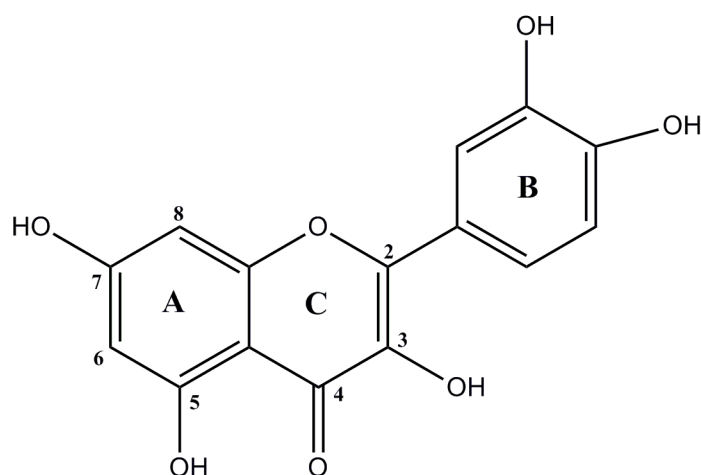


Figure 3: Structure of quercetin.

Note: It has 5 hydroxyl groups, a ketone group, two aromatic rings and one heterocyclic group. (ChemDraw image derived from Bentz, 2017).

Quercetin has three rings and three key functional groups to be considered for inhibition of enzymes such as kinases in signal transduction pathway. Quercetin with its AC-ring system, 5-hydroxyl and 4-carbonyl groups support that quercetin may mimics the adenine moiety of ATP. That's why quercetin can inhibit the kinases to prevent signal transduction pathway (Zhang et al., 2018). Kinases require ATP to phosphorylate the effector proteins on hydroxyl groups of serine or threonine. Phosphorylation may led to activation of proteins (Lu & Hunter, 2018). However, if an inhibitor such as quercetin binds to kinases instead of ATP, it can inhibit the kinases and causes a blockage of signaling pathway. In addition to ATP, quercetin can possibly mimics other adenylate-containing ligands such as CoA, NAD, NADP, and FAD (Athukoralage et al., 2019). Although the B-ring moiety may not be



directly involved in binding to the ATP-binding domain of enzymes, it seems to be determinant of the protein specificity of the inhibitor.

### **1.3 Cryogelation**

Generally gels can be defined as three dimensional form of polymeric structure and they are way too viscous compare to normal solution forms of the polymers. Gels can be prepared from polymeric solution and gel formation requires physical agents to make interactions between the polymer chains or among themselves. These agents are not only required for interactions, but also required for pore formation. Therefore, they are also known as pore forming elements or progeny. Salts, sugars and living bacteria can be used as progeny in gelation mixture (Huang et al., 2007; Wei & Ma, 2009; Xu et al., 2011). Progeny are essential for gel formation, however, they should be removed post-gelation. Removal of progeny are often require wash solvents and it's may let to trace amounts of wash solvents to stuck inside the scaffolds of gels. In addition, not all the porogens can be removed even after extensive washes with suitable solvents (Fellinger, 2017). Due to the removal problems of porogens and wash solvents, an alternative way of gelation was preferred. This alternative way is cryogelation. Cryogelation is the formation of porous gels without using any porogens as shown in Figure 4. During cryogelation, the polymeric solution will be kept at lower temperature (lower than the freezing temperature of the solvent), thus, the solvent will form crystals. On the other hands, polymeric solution itself will be in liquid form while solvent forms crystals. These crystals act as porogens at low temperatures and interconnect the polymeric structures to form porous gels. Removal of crystals is not required , just the gelation medium should be placed at room temperature , so that solvent crystals will melts and porous cryogels will be formed without any requirement for removal of gel forming elements. The freezing and

thawing of gelation medium can be repeated for several times depending on the requirement of the size of the pores (Henderson et al., 2013).

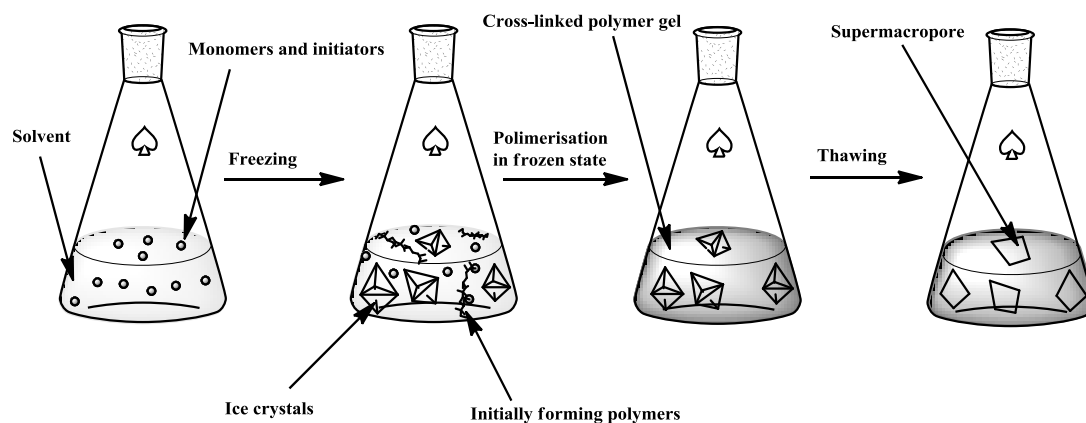


Figure 4: Schematic representation of cryogelation.  
Note: ChemDraw image derived from Plieva et al., 2004.

#### 1.4 Human Papillary Thyroid Cancer (B-CPAP) Cells

Cancer cells are formed due to division and multiplication of cells in an uncontrollable manner that leads to disfunctioning of the cells. The most common type of cancer in endocrine cancers is the thyroid cancer (Kondo et al., 2006). There are six mutational thyroid cancer lines (WRO, FTC133, BCPAP, TPC1, K1 and 8505C) (Saiselet et al., 2012). B-CPAP is a cell line of a papillary thyroid carcinoma. These cancer cells have BRAF V600E mutation in their genome. It is a point mutation of T (thymine) to A (adenine) on exon 15, this mutation leads to substitution of valine (V) with glutamate (E) at the amino acid position 600. Presence of glutamate causes the pathogenic activities in cells by activating extracellular signaling pathway via the activation of extracellular signal-regulated kinases (ERK) (Mutlu A. E., 2016; Falini B., 2016). ERK pathway is also known as MAPK (mitogen-activated protein kinases). Alternative name of the pathway is Ras-Raf-MEK-ERK pathway. It is a signaling pathway, which enables the communication via

phosphorylation starting from receptors on cell membrane to the DNA in the nucleus (Chen et al., 2018). In BRAF V600E mutation, the negative charge of Glu600 causes it to be phosphomimetic. This mimics the phosphorylation of the nearby T599 and S602 residues in the activation segment of BRAF, which are used to activate the WT form of the protein (Murugan et al., 2016).

## **1.5 Cell Culture**

Cell culture is a biological method of growing and developing the cells outside the organism. First cell culture was started by Ross Harrison in 1907 by keeping the frog neurons alive in saline solution for few days. In cell culture, the aim is to provide a medium with enough nutrients for the cells and also with some antibiotics to prevent the development of undesired organisms in the culture medium (Birch & Arathoon, 2018). Although there are trypsinized and suspended cell cultures, they both have the same cell culture procedures, only difference is to check the cell viability trypsinized cells should get detached via trypsin (Lynn, 2009).

Cell viability is the capability of the cells to keep themselves alive by maintaining their metabolic reactions in certain medium (Kabay, 2019). For healthy cells, the cell medium or chemicals used in that medium should enhance the proliferation of the cells or at least it should provide enough materials to keep the cells alive. However, for cancer cells the reverse scenario is desired. Cancer cells should not maintain their metabolic reactions in the medium or due to the chemical used and their numbers should decrease (Catalani, 2017). Overall, this reduction in the number of cancer cells in cell medium was called as reduction of cancer cell viability.

## **1.6 Importance of Cargo or Beads in Chemical Storage and Usage**

The main advantage of chemical loaded beads compare to direct application of chemicals is control release mechanism. Metabolic pathways in organisms have tendency to metabolize and discard any chemicals applied to body, therefore, cargo mechanisms such as beads enable the release of the chemicals slowly. Slow release of chemicals is the key to keep the level of chemicals in the body at the effective concentrations. In addition, beads can prevent the quick degradation of the chemicals. Since the half-lives of chemicals are extended, their effect on organism will be longer compare to chemicals with short half-lives.

## **1.7 Aim of the Thesis**

The aim of this thesis is to prepare calcium alginate gel beads and to encapsulate quercetin into the beads prepared. The quercetin release behavior from the alginate gel beads were studied in different cell culture and bacterial media to find out the quercetin release in these specific media. As applications; anticancer, antioxidant and antimicrobial activities of quercetin released based on the release studies were conducted.

## Chapter 2

### LITERATURE REVIEW

#### 2.1 Calcium Alginate Gel Beads as Drug Release Media

Controlled release mechanism is a desirable feature in drug delivery systems. Researchers were focussed on the slow release of chemical for a longer period of time at a therapeutic dosage (Thombre et al., 2019). To establish slow release active chemical that they are responsible with the therapy usually administered together with some other chemicals, which are known as excipients. Excipients are preferentially should be inactive and have no side effects either on the activity of the active chemical or on to the applied organism (Lawal et al., 2019). Polymers considered as excipients that contribute the control released mechanism of drug. Similar to many other industry and cosmetic companies, in drug delivery systems, biodegradable and natural polymers are preferred over the other types of polymers (Pongjanyakul & Rongthong, 2010). Alginate and chitosan are the common two natural polymers used in many industrial application, specifically pharmaceutical industries (Murawski et al., 2019). Alginate gels were formed via the presence of multivalent cations such as calcium and barium. Electrostatic forces between the negatively charged carboxylate groups of alginate and the metal cations causes the gel formation (Abedini et al., 2018). Thus, presence of chelating agents such as monovalent metal cation (i.e.  $\text{Na}^+$ ), lactate or phosphate will be sufficient for the degradation of the alginate gels. Without chelating agents, calcium alginate gels are very stable and they can hold active chemicals without any leakage (Danks et al.,

2016). Once the chelating agents were introduced into medium, chelating agents can cause the destabilization of calcium alginate gels by displacing the calcium ions around the alginate and this will leads to slow release of active chemical into medium. The release of active chemical from calcium alginate gels is not only dependent on the presence of chelating agents or the concentration of chelating agents. L-guluronate contents and the viscosity of the alginate affect the degradation or the dissolution of the calcium alginate gels (Soukoulis et al., 2016). Guluronate unit of alginate is required for the formation of ‘egg box’ structures. If there are more guluronate subunits on the alginate , this indicate that alginate gels are more ordered and it will be difficult and time consuming for the chelating agents to displace many calcium ions from the “egg box” structures (Hecht & Srebnik, 2016) . In addition, not all alginate polymers have the same molecular weight. Calcium alginate gels formed from molecular weight alginate polymers can leads to slow release of active chemicals into release medium (Kumar et al., 2015). When a faster drug release mechanism required for calcium alginate beads, the L-guluronate units of alginate and also the molecular weight of the alginate should be low. Calcium alginate beads can be easily preserve for a long period of time without any release of active chemical in the presence of calcium ion containing solutions (Yang et al., 2016).

Alginate gels can preserve their stability even in the presence of chelators. This can be established via the combination of polycationic polymers such as polypeptides, chitosan or polyethyleneimine. Presence of polycationic polymers not only stabilize the alginate gels, but also decreases the level of porosity in the gel formed to establish slow release of active chemicals from the gels (Caliari & Burdick, 2016).

Although alginate itself is a autoclavable polymer, usually the calcium alginate gels that they are prepared from autoclaved alginate , have tendency to release the chemical faster than the unautoclaved alginate gels. This indicate that autoclaving the alginate can causes a decrease in the viscosity of the polymer due to the low level of degradation. To prevent fast release of chemicals from such kind of autoclaved alginate gels, ethylene oxide can be used to preserve the stability of alginate (Sachan et al., 2009; Aijaz et al., 2017).

Types of cross-linkers can affect the release of chemicals from alginate gels. Although the chemical cross-linkers are making strong chemical linkages between different polymer chains of alginate to formgels or gel beads, they require chemical cross-linkers (Mane et al., 2015). Chemical cross-linkers are usually toxic and they are not preferred for drug release mechanisms. On the other hand, with ionic cross-linkers such as calcium gels or beads can easily formed at physiological pH and at room temperature (Luo &Wang, 2014). The gels formed will be pH responsive and non-toxic, which are the preferential features for the drug release mechanisms.

Recently, alginate matrices or alginate gels are used as viscosity modifying agent, as a stabilizer or thickening agent for controlled release mechanisms. Release of drug from the alginate gel matrices can be usually occur via a diffusion mechanism, which is dependent on pH of the release medium (Sachan et al., 2009; Schuster et al., 2016).

Ceftriaxone is an antibiotic used for several different kind of bacterial infections. However, intraperitoneal injection of this antibiotic showed side effects such as cocaine relapse-like or alcohol-drinking like behaviors due to activation of glutamate

transporter 1 (GLU-1) (de Souza Armini et al., 2015; Patel et al., 2016). However, oral administration of water soluble ceftriaxone is not possible due to its acid labile property and poor permeability of gastrointestinal epithelial cells. Therefore, to enable the oral administration of ceftriaxone, calcium alginate beads were produced with the combination of some other polymers such as Sodium carboxymethyl cellulose. All parameters were optimized such as drug- polymer ratio, concentration of cross-linkers and ratio between alginate and other polymers to produce the desired alginate gel beads (Patel et al., 2016). It was found that although beads can swell in conditions similar to stomach such as pH 1.2, the drug would release in a sustained manner at pH 6.8 medium, which resemble intestinal environment. Stability of alginate polymer was used as advantage for oral administration of antibiotic.

Guar gum succinate - sodium alginate (GGS-SA) beads were synthesis by using barium ions as an ionic cross-linker for the delivery of ibuprofen. Swelling features of alginate was used to target specific delivery of ibuprofen, due to its pH sensitivity beads would only release the ibuprofen at colon (pH ~7.4) and therefore it is also called colon-specific drug releasing system (Seeli et al., 2016).

Temperature-controlled extrusion–dripping method was used to synthesize ultra high concentration calcium alginate hydrogel beads loaded with methylene blue. It is found that ultra high concentration beads have extended drug release time, which is a desired feature for drug release systems and also beads have high stiffness (Voo et al., 2016). Thus, it can be concluded that calcium alginate beads can be used to increase the stiffness and the extension of drug release time.



## **2.2 Anticancer, Antioxidant and Antibacterial Activities of Quercetin**

### **2.2.1 Anticancer Activities**

Reactive oxygen species may induce oxidative stress, which may damage the DNA and eventually leads to cancer (Lushchak, 2014). Thus, antioxidants such as quercetin play a crucial role in anticancer activities. In addition, quercetin can down regulate the p53 proteins. When the p53 proteins were inhibited, cells could not proliferate due to cell cycle arrest at G2-M phase in breast cancer cells. Therefore, cancer cells could not proliferate in an uncontrollable manner (Lou et al., 2015).

The numbers of gastric and leukemia cancer cells were reduced in the presence of quercetin. Quercetin causes inhibition of p53 protein and G1 checkpoint of cell cycles was under the control of p53 protein (Zhang et al., 2018). Thus, cancer cells would be arrested in G1 phase and they could not proliferate.

Intravenous administration of quercetin may block the activity of tyrosine kinases for about one hour. It was found that since quercetin resemble the similar chemical structure with adenine. It could bind to tyrosine kinase instead of ATP molecules and it inhibit the binding of ATP molecules (Baby et al., 2018). Thus, tyrosine kinase could not phosphorylate the proteins in growth hormone signaling pathway. This leads to inhibition of growth hormone signal transduction pathway, therefore, cancer cells could not proliferate in an uncontrollable manner.

It was found that quercetin can inhibit HepG2 cell proliferation and cause inhibition of apoptosis of cancerous cells. In vivo tests on mice after intraperitoneal administration of quercetin were showed that due to the inhibition of cyclin D1

expression, tumour growth was inhibited and average survival time for the mice was improved (Zhou et al., 2017).

Quercetin and green tea applications causes the reduction in HL-60 xenografts human leukemia cancer cells due to decrease in anti-apoptotic proteins such as BCL-2 and rise in pro-apoptotic protein such as BAX. It was found that quercetin and green tea affect the signaling at apoptosis, cell cycles and autophagy (Calgorotto et al., 2018). This was a good indication that quercetin can be used as anticancer, natural agent.

### **2.2.2 Antioxidant Activities**

Organisms have defense systems for many unwanted chemicals and reactions to reduce their damages. There are two main types of antioxidant defense mechanisms; enzyme-dependent and enzyme independent. Both mechanisms preserve the organism from reactive oxygen or reactive nitrogen species by controlling their levels and this prevent any oxidative damage on cellular levels (Baghel et al., 2012). Enzyme dependent antioxidant mechanisms mainly composed of glutathione peroxidase, superoxide dismutase and catalases. These three enzymes directly scavenge the radicalic reactive species and they prevent any cellular damage (Ighodaro & Akinloye, 2018). Non-enzymatic antioxidant mechanism involve chemicals such as vitamin C or flavonoids such as quercetin (Rahal et al., 2014). These chemicals scavenge the radicals and prevent the radicalic compounds to react with other molecules, thus, they prevent the propagation of oxidation chain. Quercetin has direct scavenging activity for radicalic chemicals . This inhibit oxidation of LDL (Low Density Lipoproteins). Modifications of LDL usually cause mechanism of inflammatory and immunology to activate that leads to macrophage

foam cells formation and this events promote the atherosclerosis, since, quercetin is inhibiting modification of LDL, it also prevent cardiovascular diseases such as atherosclerosis (Baghel et al., 2012; Jaiswal & Rizvi, 2014).

Production of nitric oxide activates its own production by activating nitric oxide synthase (Mattila & Thomas, 2014). High concentration of nitric oxide causes the reaction between reactive radical species to produce peroxynitrite, which causes permanent, serious cell membrane damages (Toklu & Tumer, 2015). Quercetin molecules reduce the radical species in the medium and this prevent the formation of oxidized form of LDL, which causes cell damages. In addition, quercetin directly reduces the amount of nitric oxide in the medium (Li et al., 2016).

### **2.2.3 Antibacterial Activities**

Antibacterial activity of quercetin in some specific types of bacterial cells such as *S.aureus* and *staphylococcus epidermidis* was known (Farhadi et al., 2019). It also have inhibitory activity on oral microbes such as porphyromonas gingivalis and its MIC value is 0.0125 µg/mL (Geoghegan et al., 2010). In addition, quercetin was found to have synergistic activity on bacterial strains with the combination of some other chemicals such as curcumin (Güran et al., 2019). It was also found that flavonols such as quercetin can reverse bacterial resistance to antibiotics specifically β-lactams (Ayaz et al., 2019).

## Chapter 3

### EXPERIMENTAL

#### 3.1 Materials

Quercetin (Sigma-Aldrich), DMSO (Merck), Calcium Chloride Dihydrate (Merck), Alginic acid sodium salt (AppliChem Panreac ITW Companies), Sodium Chloride (Merck), MHB (Mueller Hinton Broth) (Sigma-Aldrich), DPPH (2, 2-diphenyl-1-picrylhydrazyl) (Sigma-Aldrich), MTT (3-[4, 5-dimethylthiazole-2-yl]-2, 5-diphenyltetrazolium bromide) (Sigma-Aldrich), RPMI-1640 (Cell Culture Medium) (Sigma-Aldrich), FBS (Fetal Bovine Serum) (Sigma-Aldrich), Penicillin and Streptomycin (p/s) (Sigma-Aldrich), Amphotericin (Sigma-Aldrich), Gentamicin (Sigma-Aldrich), Gallic Acid (Sigma-Aldrich), Methanol (Sigma-Aldrich), Trypan Blue (Sigma-Aldrich) were used as received.

#### 3.2 Formation of Quercetin-Encapsulated Beads

Alginate solution was prepared by dissolving 0.5 g alginic acid sodium salt into 16.7 mL distilled water to have sodium alginate solution with 3% (w/v) concentration. In order to have complete dissolution magnetic stirrer was used at 1400 rpm at room temperature. After that quercetin solution was prepared by dissolving 0.05 g quercetin into 2 mL DMSO to have quercetin solution with 82.7 mM. Following to this, sodium alginate solution is mixed together with quercetin solution to have homogenized final solution. After that calcium chloride solution was prepared by dissolving 1 g calcium chloride in 100 mL distilled water to have calcium chloride solution with concentration of 1% (w/v). For the formation of the beads, transfer the

homogenized solution into clean syringe and then adjust the tip of syringe by using a drip controller, so that controller enables the addition of homogenized solution drop by drop to calcium chloride solution (Figure 5). Magnetic stirrer should be used in calcium chloride solution at 230 rpm at room temperature. Also, the distance between the syringe and calcium chloride solution was about 15 cm. Filter the beads from calcium chloride solution and rinse the beads with distilled water for several times.

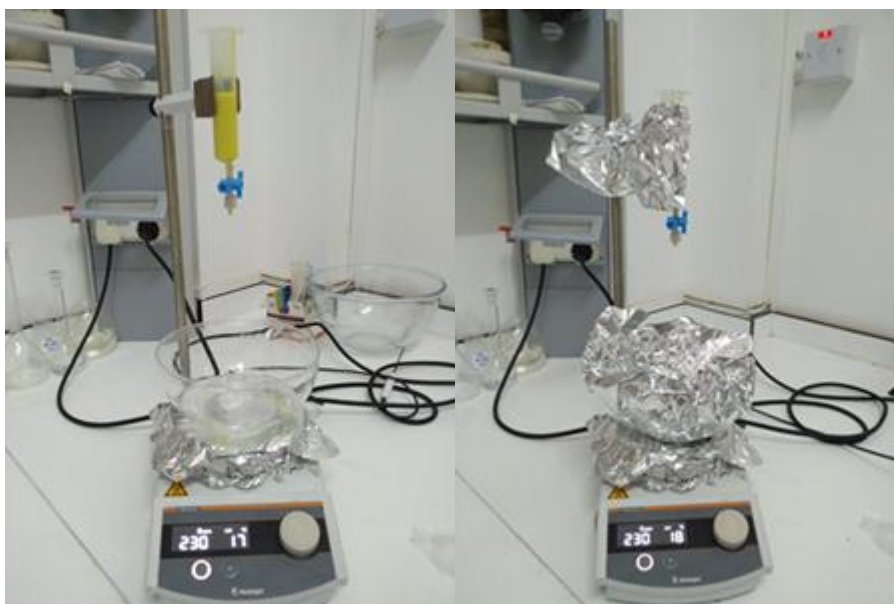


Figure 5: Experimental setup for preparing quercetin-encapsulated gel beads.

Then, the mass of empty petri dish was measured . Beads were placed onto petri dish and the initial mass of the beads were recorded (Figure 6).

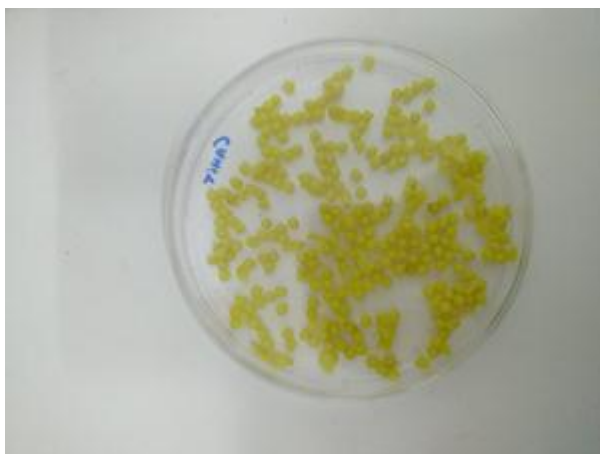


Figure 6: Quercetin-encapsulated alginate gel beads on petri dish.

After the formation of the beads directly release kinetics studies can be conducted. Following to physicochemical studies, biochemical and antimicrobial assays can be sequentially. In addition, once the beads are formed, drying profile of the beads can be examined and the release kinetics studies can be carried out starting from completely dried form of the beads.

### **3.3 Cryogel Beads Formation**

Following to bead formation, beads were placed on petri dish and they were transferred to freezer at  $-20^{\circ}\text{C}$  for 24 hours for cryo gelation. Then, beads were transferred from freezer ( $-20^{\circ}\text{C}$ ) to refrigerator at  $4^{\circ}\text{C}$  for 24 hours. One freeze-thaw cycle has 24 hours at  $-20^{\circ}\text{C}$  and 24 hours at  $4^{\circ}\text{C}$ . These cycles were repeated for three times. Even in the freezer petri dishes were covered with aluminum foil to prevent the entry of light, which might affect the chemical properties of quercetin.

### **3.4 Light Microscope Image and Diameter of the Beads**

For both beads surface morphologies examination and diameter size measurements computer aided LEICA DM750 model of light microscope with LEICA DFC295 attachment was used. For diameter measurement each measurement was triplicated to increase the accuracy of the experiment.

### **3.5 FTIR (Fourier-transform infrared spectroscopy) Measurements**

%Transmittance application of FTIR was used to determine the loaded quercetin to alginate beads. PerkinElmer FT-IR spectrometer was used with ATR used. Each sample to be analysed with ATR was used in powder form.

### **3.6 Drying Profile of Quercetin Loaded Beads**

Drying profile of the beads and the cryobeads were measured at regular intervals to observe the decrease in mass of the beads starting from the known initial mass. Beads are placed under the fume hood and it should be tuned on full vacuum power to increase the speed of drying process of the beads.

### **3.7 Swelling Test**

The initial masses of two types of beads; cryobeads and dried alginate beads were measured by using analytical balance (SHIMADZU-TW423L).

The mass measurements were made in triplicate to repeat the swelling test 3 times. These repetitions of experiment enhance the accuracy of the results by calculating their average percent (%) swelling.

$$\%Swelling = \frac{W_s - W_d}{W_d} * 100 \quad (1)$$

$W_s$  = Weight of Swollen Beads

$W_d$  = Weight of Dried Beads

Following to mass measurements beads are immersed into phosphate buffer at room temperature, the pH of buffer should be adjusted to 7.4 by using 0.1 M Sodium Hydroxide (NaOH) and 0.1 M Hydrochloric Acid (HCl).

### **3.8 Calibration Curves**

Calibration Curves was drawn for four different solvents; DMSO (Dimethyl Sulfoxide), RPMI-1640 (Cell Culture Medium), 0.9 % Saline Solution and MHB (Mueller Hinton Broth). Calibration curve was constructed based on the measurements of absorbance of the sample with a known concentration at  $\lambda_{\max}$  (maximum absorbance). Expected  $\lambda_{\max}$  for quercetin was around 370 nm. For each solvent serial dilution was conducted, thus, based on absorbance values of serial dilutions of quercetin solutions the calibration curve will be constructed. Calibration curves were later be used to determine the amount of quercetin release from quercetin loaded beads in specific solvents. CT-2200 Spectrophotometer was used to measure the absorbance values.

### **3.9 Release Studies**

Release studies were conducted at eight different solvents or cell culture media; DMSO (Dimethyl Sulfoxide), RPMI-1640 (Cell Culture Medium), 0.9 % Saline Solution containing 10%DMSO (i.e.90mL 0.9% saline solution +10 mL DMSO), 0.9 % Saline Solution containing 20%DMSO, 0.9 % Saline Solution containing 40%DMSO ,MHB (Mueller Hinton Broth) containing 10%DMSO, MHB containing 20%DMSO and MHB containing 30%DMSO. In addition, the releases of three different types of beads were investigated; dried beads, cryobeads and newly produced beads in each type of solvents.

For release studies, glass test tubes were used. For each test tube two beads with known masses were placed and 5 mL of solvent was added. Each test tube was placed on orbital shaker (WiseShake SHO-2D) at 130 rpm. In the case of high absorbance value, the measurements were repeated with a higher volume of solvents.



Based on release studies for each solvent and bead type, absorbance versus time graphs were constructed.

### **3.9.1 Determination of Percent Quercetin Released**

The percent quercetin released was determined by using orbital shaker at 130 rpm, which mimics the gastrointestinal tract mobility. Quercetin released (%) was calculated as follow;

$$\text{Quercetin released (\%)} = (m / m_0) \times 100 \quad (2)$$

$m$  is the amount of quercetin released (in terms of mass (g))

$m_0$  is the amount of quercetin encapsulated in beads (in terms of mass (g))

### **3.9.2 Determination of Release Kinetics of Quercetin from Alginate Beads**

To understand the type of mechanism of release kinetic models 4 different types of models was studied; Zero order release model, first order release mode 1, Higuchi release model and Korsmeyer-peppas release model. For each model appropriate graph should be drawn to determine the correlation coefficient ( $R^2$ ). The desired and best model has the correlation coefficient value 1. Thus, the best fit model should give the correlation coefficient value closer to one. The model with closest  $R^2$  to 1 will be defined as best fit model.

#### **3.9.2.1 Zero Order Release Model**

$$C_t = C_0 + k_0 t \quad (3)$$

$C_0$  = percent drug left to release in cargo

$C_t$  = percent drug released at time “t”

$k_0$  = Zero order release constant

t= time in hours

Since, usually  $C_0 = 0$

Hence,

$$C_t = k_0 t$$

### 3.9.2.2 First Order Release Model

$$\ln(100 - C_t) = \ln C_0 - k_1 t \quad (4)$$

Or

$$100 - C_t = C_0 e^{-k_1 t}$$

$C_0$  = percent drug left to release in cargo

$C_t$  = percent drug released at time “t”

$k_1$  = First order release constant

t = time in hours

### 3.9.2.3 Higuchi Release Model

Usually Higuchi model was fit to release of chemical due to diffusion.

$$C_t = k_H t^{1/2} \quad (5)$$

Or

$$m_t/m_0 = k_H t^{1/2}$$

$C_t$  = percent drug released at time “t”

$k_H$  = Higuchi release constant

t = time in hours

$m_t$  = Amount of drug released at time “t”

$m_0$  = Total amount of drug in terms of dosage used

### 3.9.2.4 Korsmeyer-Peppas Release Model

$$\log(C_t/100) = k_p t^n \quad (6)$$

$C_t$  = percent drug released at time “t”

$k_p$  = Peppas release constant

t = time in hours

n= release exponent

### 3.10 MTT Assay (Succinate Dehydrogenase Activity Assay)

MTT Assay is a way of measuring the cell viability of the cell culture. 3-[4, 5-dimethylthiazole-2-yl]-2, 5-diphenyltetrazolium bromide (MTT) was reduced to MTT-formazan crystals via the help of succinate dehydrogenase. Therefore, mitochondrial succinate dehydrogenase activity gives a measure of cell viability by using this assay. MTT results can be measured by using multiplate reader in terms of absorbance at 570nm. Higher the absorbance value indicate the presence of formazan crystals and more formazan crystals means that the most of the cells are still alive (Chacon, 1997) Figure 20.

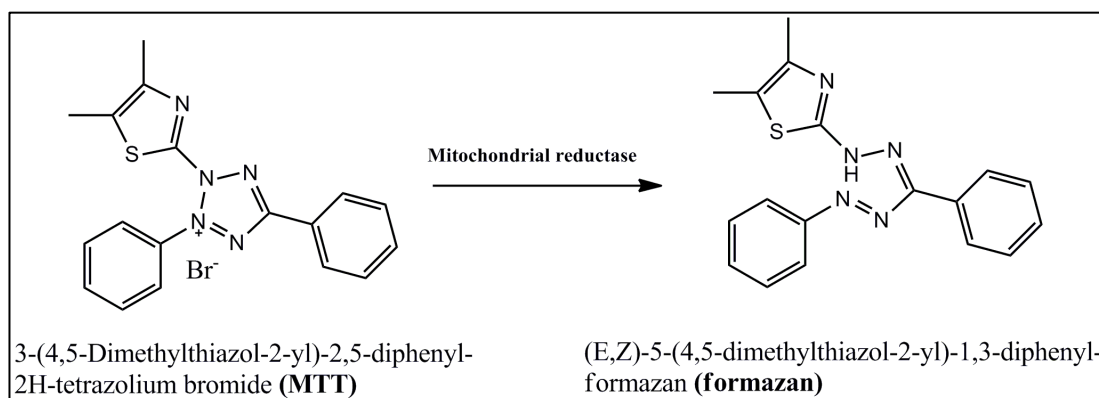


Figure 7: Formazan crystals formation.

(Note: MTT (3-[4, 5-dimethylthiazole-2-yl]-2, 5-diphenyltetrazolium bromide) was reduced to formazan crystals due to cellular metabolic activities (ChemDraw image derived from Kuete, 2017).

Cancer cells or health cell lines were stored in -80°C freezer in cryoflasks. Cells were transferred into 15 mL falcon and 4 mL PBS (Phosphate buffered saline) was added to the cells. Following to the addition of PBS, falcon was placed into centrifuge for 5 minutes at 1500 rpm. Centrifuge enables the cells to be collected as pellet at the bottom of the falcon tube and discard the supernatant. Following to this, 10 mL medium (RPMI-1640) was added to the pellet and by using pipette, cells were

suspended in RPMI-1640. RPMI-1640 contains 10% FBS (fetal bovine serum), 1% penicillin/streptomycin (p/s), 0.1% amphotericin, 0.1% gentamicin. Kanamycin was not required. Although all ingredients such as FBS, P/S, amphotericin-B, 0.01% gentamicin should be stored in freezer at -20°C as aliquots, once they added to RPMI-1640, they can be stored at 4°C. Following to the suspension of cells in the RPMI-1640, 10 µL from this solution was taken and mixed with 10 µL of trypan blue on parafilm. Then, the number of cells were counted by using hemocytometer. Thus, once the dye and cells were mixed, they could be placed on hemocytometer. Preferentially invert microscope should be used. However, LEICA DM500 light microscope was used to count the cells. i.e. count the number of cells in five square of hemocytometer and sum them up, then divide by 5. In the case of low number of cells, the number of cells on all squares can be counted. Then, to find the total number of cells:

=Number of Cells on microscope X Constant X Factor of Trypan Blue X Dilution Factor

Constant =  $10^4$  Factor of Trypan Blue = 2 Dilution Factor = 10 mL

= Number of Cells on microscope X  $10^4$  X 2 X 10 (7)

For MTT Assay cells should be transferred into 96 well plates. After that Quercetin solutions based on release kinetic data and RPMI-1640 should be added to each wells. For this purpose, quercetin solutions should be prepared. Firstly, one main stock solution with 500 000 µM (or 500 mM) concentration should be prepared. Therefore, 0.7556 gram of quercetin was dissolved in 5 mL DMSO to have main quercetin stock with 500 000 µM concentration. Then, from this main stock solution, another more dilute stock could be prepared. 1000 µM new stock was prepared from 500 000 µM stock solution. Thus, 2 µL from 500 000 µM stock solution was taken

and mixed with 998  $\mu\text{L}$  of RPMI-1640 to have new quercetin stock solution with 1000  $\mu\text{M}$  concentration. The aim of the new stock solution is to not to exclude 0.1 % DMSO in solution. Above 0.1 % DMSO in the medium causes toxic effects on the cells. Following to this, the quercetin solutions based on release studies were prepared. After the preparation of quercetin concentrations how much from cell solution would be added to each well should be calculated. For each wells usually between 5000 and 7000 cells should be added. Each released quercetin concentrations were measured as triplicate. Then, the 96 wells plate was placed into incubator (EC160 Nüve CO<sub>2</sub> incubator), 5% CO<sub>2</sub> at 37 °C for 24 hours. After 24 hours incubation, 10  $\mu\text{L}$  of 5 mg/mL MTT solution was added for each well. Then, the 96 well plate was placed into incubator at 37 °C with 5% CO<sub>2</sub> for 3 hours. After 3 hours incubation, 100  $\mu\text{L}$  of DMSO was added. Then, after 15 minutes, 96 well microplate was read by using multiplate reader at 570 nm.

### **3.11 Antioxidant Assay – DPPH (2, 2-diphenyl-1-picrylhydrazyl)**

#### **Test**

DPPH test was carried out based on the protocol used by Adebisi et al (Adebisi et al., 2017). 0.025 mg/mL DPPH solution was prepared by dissolving 0.00125 gram DPPH powder in 50 mL methanol. Gallic acid concentrations were prepared as a reference. One main stock solution of gallic acid was prepared at concentration of 5000  $\mu\text{M}$  (or 0.005 M) by dissolving 0.004253 gram gallic acid in 5 mL methanol.

Different concentrations of gallic acid solutions were required; 5  $\mu\text{M}$ , 50  $\mu\text{M}$ , 100  $\mu\text{M}$ , 200  $\mu\text{M}$ , 400  $\mu\text{M}$  and 500  $\mu\text{M}$  to compare with quercetin concentrations. These concentrations of gallic acid solution were prepared from 5000  $\mu\text{M}$  stock solution in eppendorf tubes. After the preparation of gallic acid concentrations, the quercetin solutions based on release kinetics studies were prepared. 5  $\mu\text{L}$  from each sample

was transferred into 96 well plates and then, 195  $\mu$ L freshly made DPPH solution was transferred to each well. Each sample was repeated for 4 times. DPPH solution alone was used as blank. After incubation in dark place for 20 minutes, multiplate reader at 515 nm was used to read the results.

### **3.12 Time Kill Assay**

Day before the time kill assay blood agar plates were prepared. MHB, 0.9% saline solution and all the glasswares were autoclaved before the assay. Again day before the assay, *MSSA (Methicillin-Sensitive Staphylococcus aureus ATCC)* was plated on agar plates for to make the bacteria ready for assay. On the day of time kill assay; before the experiment, depending on time intervals of release, the number of petri dishes were determined and labeled. (Time intervals used; 0, 5 min., 10 min., 15 min., 30 min., 1 hr, 2 hr, 3 hr, 6 hr, 8 hr, 10 hr, 12 hr and 24 hr.). Then, before the experiment after labeling petri dishes, 96 well plates (ELIZA PLATES) were labeled in order to make dilution. After labeling, bacteria from day before in incubator were taken out and few colonies were taken by using inoculation loop and they were placed into 10 mL 0.9% saline solution. For *S.aureus* in order to have  $10^9$  bacteria/mL, by using DEN-1 McFarland Densitometer; MF-Unit was adjusted to 0.5 MFU. After that the release medium was prepared, which is 0.9% saline containing 40 % DMSO. (Total volume of solution should be 50 mL, therefore, 20 ml DMSO and 30 mL 0.9 % saline solutions were mixed together). Three 100 mL conical flasks were filled with 50 mL 0.9% saline solution containing 40 % DMSO. Then, 50  $\mu$ L from the bacterial solution was added to each conical flask. Following to this, for first erlenmeyer flask 10 beads were added, for second flask 10 cryobeads were added and no beads were added to control. Immediately, after addition of beads, 10  $\mu$ L from each flask was taken and should be diluted by 10X, 100X and 1000X in 96

well plates by using MHB. To do this dilutions; firstly, 90  $\mu$ L MHB was added to all wells. Then, 10  $\mu$ L from the conical flask was transferred into well 1. This gave 10X dilution. Then, it was pipetted up and down to have homogenization and 10  $\mu$ L was transferred to into well 2. Thus, in well 2, there would be 100X dilution. After that 10  $\mu$ L was transferred from well 2 to well 3 to obtain 1000X dilution. Then, 20  $\mu$ L was taken from each well and dropped onto labeled place on blood agar plates.

Petri dishes were half opened for drying. After when they were completely dried. They were placed into incubator at 37 °C until the colonies were formed about 18 hours. After incubation the countable dilutions were counted and CFU/mL (Colony-forming unit per mL) values were calculated.

$$\text{CFU/mL} = \frac{\text{No.of colonies counted X Dilution factor (e.g.100X)}}{\text{Volume of culture plated (mL)}} \quad (8)$$

## Chapter 4

### RESULTS AND DISCUSSION

#### 4.1 Quercetin Loaded Beads and Cryogel beads

Rotation of each droplets of viscous quercetin-alginate solution in the air enabled us to have regular bead sizes. In addition to this, magnetic stirrer at 230 rpm prevents adhering together. Stirring is the key during the beads formation, otherwise, newly formed beads can clamp together and this will let to deformation in the shapes of the beads. In the case of irregular beads formation, irregular shaped beads should be omitted and they should not be used for further studies. At the end of the beads formation, only the beads with the similar sizes should be saved for further study to prevent any further error due to irregular shaped beads (Figure 8).



Figure 8: Quercetin loaded gel beads.

Note: Quercetin loaded beads with similar sizes were chosen for further analysis.



## **4.2 Cryogel Beads**

The aim of the cryogelation is to increase the size of pores in the beads by generating ice crystals upon freezing. When these ice crystals melt, they leave pores in the beads (Figure 9). Increasing the size of pores or increasing the surface area of the beads may be required when a quick release of quercetin to the medium is necessary. Increased pore size means that more of the solutions from medium will enter into beads and quercetin will be released faster than the normal sized porous beads due to the maximum contact surface between solution and quercetin in the beads. In each cryogelation cycle, there are two steps; 24 hours at 20 °C and 24 hours at 4 °C and for preparation of cryogel beads these cycles were repeated for three times as given in Figure 9.


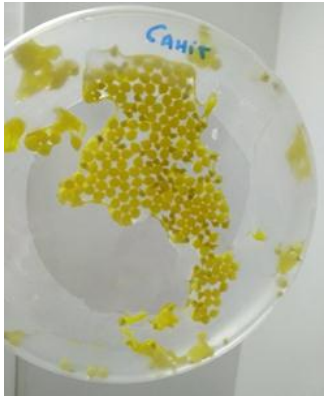
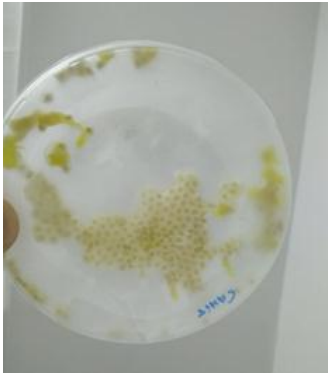

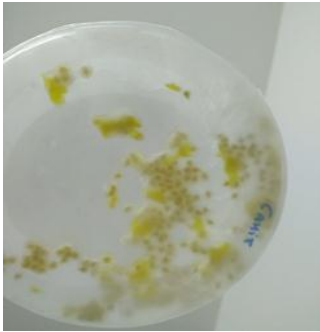
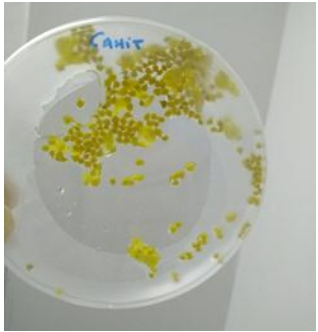
	After 24 hours at -20°C	After 24 hours at 4°C
<b>CYCLE 1</b>	<b>A</b>	<b>B</b>
		
<b>CYCLE 2</b>	<b>C</b>	<b>D</b>
		
<b>CYCLE 3</b>	<b>E</b>	<b>F</b>
		

Figure 9: Cryogelation.

Note: After the formation of quercetin loaded beads, cryogelation was conducted.

## 4.3 Weight, Diameter and Light Microscope Image of the Beads

### 4.3.1 Weight Measurements of the Beads

Weight measurements of the beads for four types of the beads , which can be listed as dried gel beads, gel beads, cryogel beads and dried cryogel beads were conducted as shown in Table 1 and Figure 10.

Table 1: Masses of beads.

<b>Beads Weight Measurements</b>				
	<b>Dried gel beads</b>	<b>Cryogel beads</b>	<b>Gel beads</b>	<b>Dried cryogel beads</b>
<b>Measurements:</b>	<b>Total Mass of 10 Dried beads (g)</b>	<b>Total Mass of 5 Cryobeads (g)</b>	<b>Mass of Not Dried Bead (Freshly made beads) (g)</b>	<b>Total Mass of 10 Dried beads (g)</b>
<b>First set of beads</b>	<b>0,024</b>	<b>0,05</b>	<b>0,032</b>	<b>0,018</b>
<b>Second set of beads</b>	<b>0,024</b>	<b>0,034</b>	<b>0,032</b>	<b>0,019</b>
<b>Third set of beads</b>	<b>0,024</b>	<b>0,04</b>	<b>0,033</b>	<b>0,019</b>
<b>Fourth set of beads</b>	<b>0,025</b>	<b>0,032</b>	<b>0,032</b>	<b>0,019</b>
<b>Fifth set of beads</b>	<b>0,024</b>	<b>0,043</b>	<b>0,032</b>	<b>0,019</b>
<b>Average</b>	<b>0,0242</b>	<b>0,0398</b>	<b>0,0322</b>	<b>0,0188</b>
<b>Standard deviation</b>	<b>± 0,0004</b>	<b>± 0,006462198</b>	<b>± 0,0004</b>	<b>± 0,0004</b>

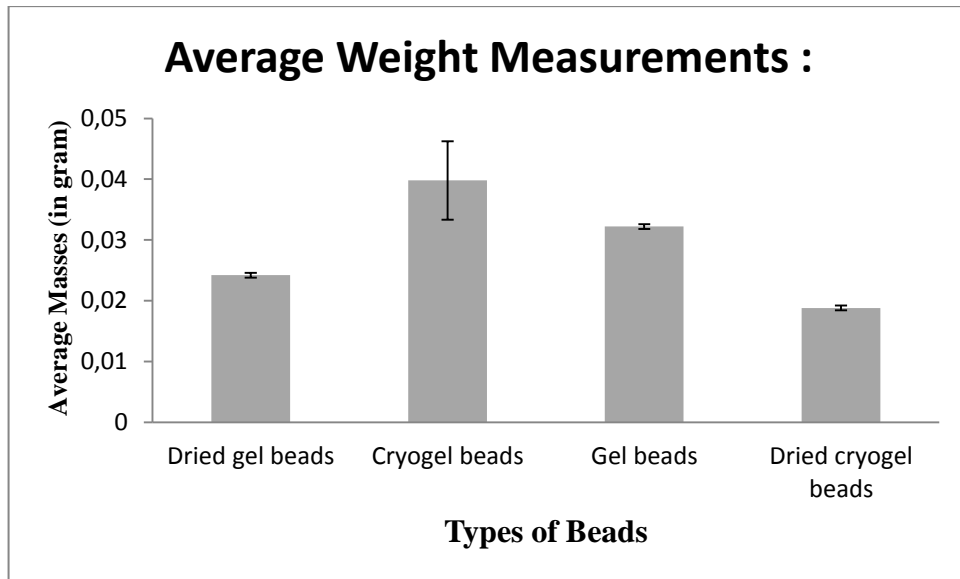


Figure 10: Average weight measurements.

Note: Average weight for each type of beads is illustrated in the bar chart with a standard deviation.

Based on average weight measurement graphic (Figure 10), cryogel beads showed the greatest standard deviation, this can be because of the uneven formation of porous structure in the beads during the cryogelation. Therefore, some of the cryogel beads can hold much more solvent than the others and this makes them heavier than the other cryogel beads. Standard deviation for the other three types of beads (dried gel beads, gel beads and dried cryogel beads) showed the same standard deviation by 0.0004 g , since this standard deviation value is so small , it can be concluded that apart from cryogel beads , all other types of beads showed homogenized weights measurements. Homogenized bead masses were desired property, which enable us to determine physicochemical properties easily compare to unhomogenized bead masses

### 4.3.2 Diameter Measurements of the Beads

Diameters of the each form of beads measured by taking triple measurements of three different beads (see Table 2,3,4,5 and Figure 11, 12, 13, 14). There were not huge differences between the diameter values , which indicate that beads were homogenized in terms of size. Only cryogel beads showed the greatest standard deviation between its own diameter measurements, this can be because of tail structure of the beads. Although the beads for studies are carefully selected to be the same and homogenized in size, some of the beads can have a little bit of tail. This tails can affect the diameter measurements of the beads.

Table 2: Diameters of dried beads.

<b>Dried Gel Beads:</b>					
<b>Sample Name</b>	<b>Measurement 1</b>	<b>Measurement 2</b>	<b>Measurement 3</b>	<b>Average of the Measurements</b>	<b>Standard deviation</b>
<b>Sample 1</b>	<b>1200</b>	<b>1300</b>	<b>1400</b>	<b>1300</b>	<b>± 81,6</b>
<b>Sample 2</b>	<b>1300</b>	<b>1400</b>	<b>1400</b>	<b>1367</b>	<b>± 47,1</b>
<b>Sample 3</b>	<b>1500</b>	<b>1200</b>	<b>1300</b>	<b>1333</b>	<b>± 124,7</b>

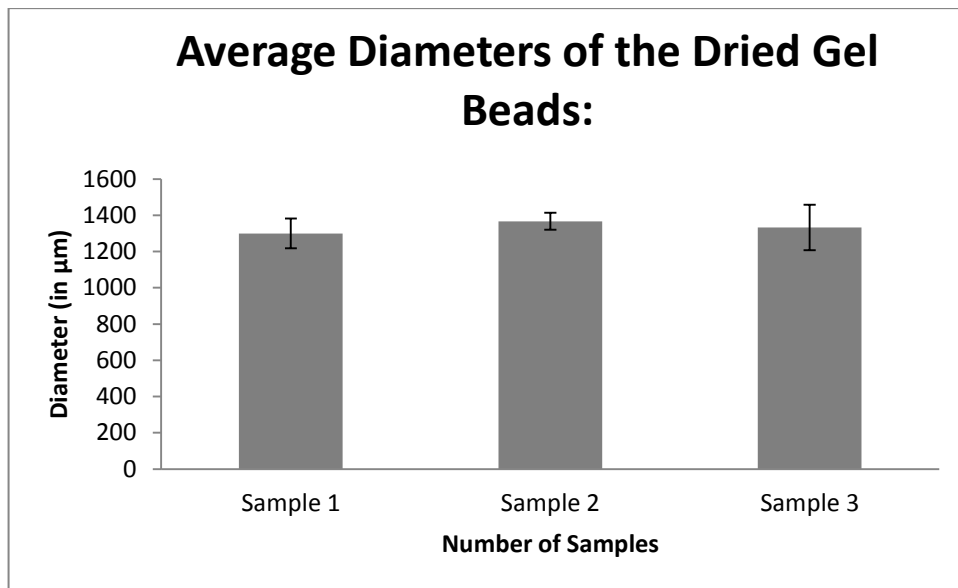


Figure 11: Average diameters of the dried gel beads.

Table 3: Diameters of cryogel beads.

Cryogel beads:					
Sample Name	Measurement 1	Measurement 2	Measurement 3	Average of the Measurements	Standard deviation
Sample 1	3000	2100	2500	2533	$\pm 368,2$
Sample 2	2200	2300	2400	2300	$\pm 81,6$
Sample 3	2300	2200	2000	2167	$\pm 124,7$

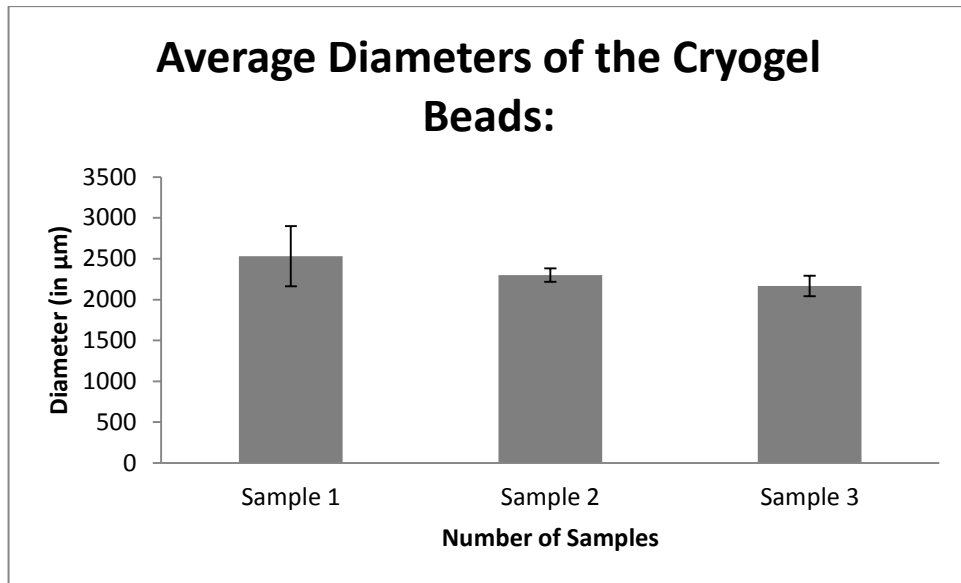


Figure 12: Average diameters of the cryogel beads.

Table 4: Diameters of gel beads.

<b>Gel Beads:</b>					
<b>Sample Name</b>	<b>Measurement 1</b>	<b>Measurement 2</b>	<b>Measurement 3</b>	<b>Average of the Measurements</b>	<b>Standard deviation</b>
<b>Sample 1</b>	<b>3300</b>	<b>3700</b>	<b>3800</b>	<b>3600</b>	<b>± 216,0</b>
<b>Sample 2</b>	<b>3800</b>	<b>3600</b>	<b>4000</b>	<b>3800</b>	<b>± 163,3</b>
<b>Sample 3</b>	<b>3700</b>	<b>3500</b>	<b>4100</b>	<b>3800</b>	<b>± 249,4</b>

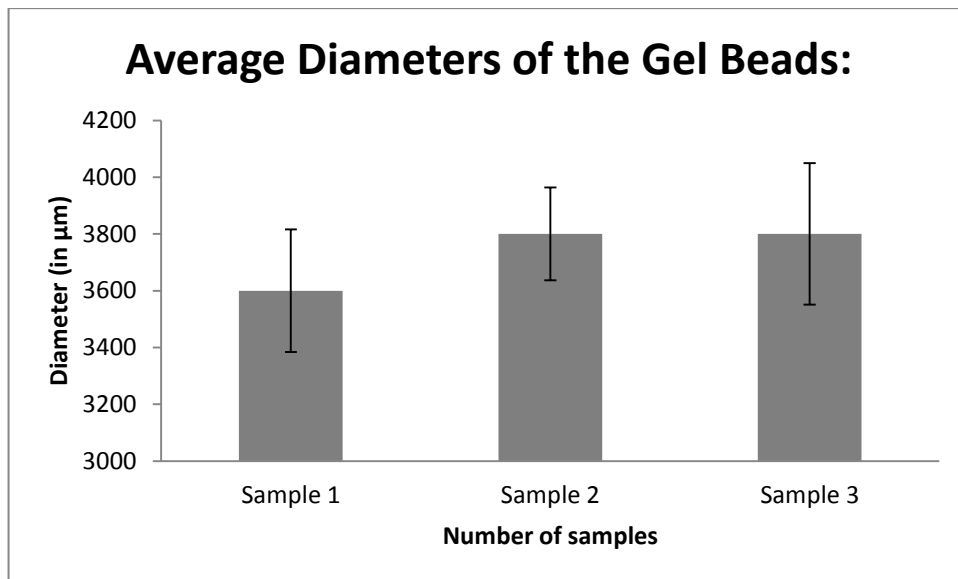


Figure 13: Average diameters of the gel beads.

Table 5: Diameters of dried cryogel beads.

<b>Dried Cryogel beads:</b>					
<b>Sample Name</b>	<b>Measurement 1</b>	<b>Measurement 2</b>	<b>Measurement 3</b>	<b>Average of the Measurements</b>	<b>Standard deviation</b>
<b>Sample 1</b>	<b>1100</b>	<b>1200</b>	<b>1200</b>	<b>1167</b>	<b><math>\pm 47,1</math></b>
<b>Sample 2</b>	<b>1100</b>	<b>1300</b>	<b>1100</b>	<b>1167</b>	<b><math>\pm 94,3</math></b>
<b>Sample 3</b>	<b>1200</b>	<b>1100</b>	<b>1000</b>	<b>1100</b>	<b><math>\pm 81,6</math></b>



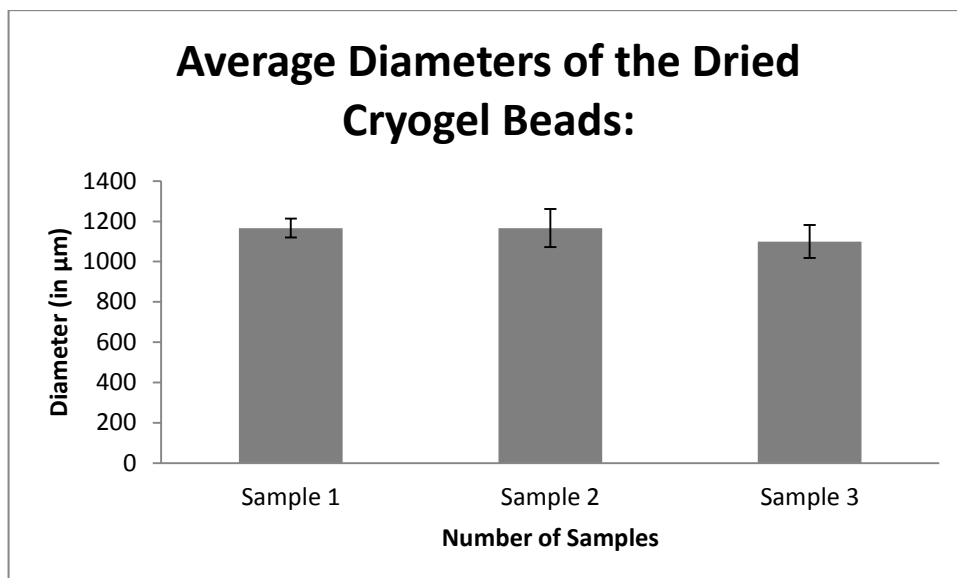


Figure 14: Average diameters of the dried cryogel beads.

#### 4.3.3 Light Microscope Image of the Beads:

For both beads image and diameter size measurements computer aided LEICA DM750 model of light microscopy with LEICA DFC295 attachment was used.

Light microscope images of the beads do not have high enough resolution to assess the degree of porosity of the beads, however, it enabled to observe some pore like structures on the surface of the beads as shown in Figure 15 and Figure 16. For further analysis of the beads morphologies and porosities SEM (scanning electron microscope) images are required. Figure 16 shows that the surface of gel bead is smooth among the others. Since, it is not dried, it is expected to have faster releasing feature compare to others. Cryobead has the most irregular surface structure, it is expected that wrinkled surface structure to increase the surface area to volume ratio for rapid quercetin release in short period of time by increasing the contact time between the solvent and the bead. In dried bead pictures, it was hard to detect the pores, which indicate that the rate of release more likely to be slower compared to other beads.

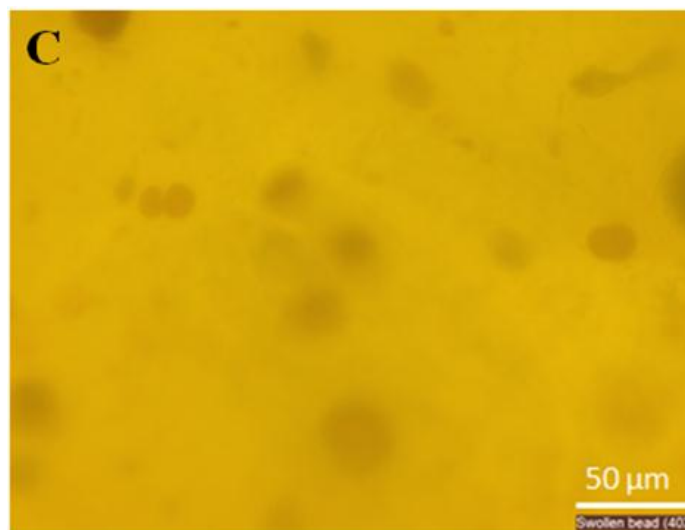
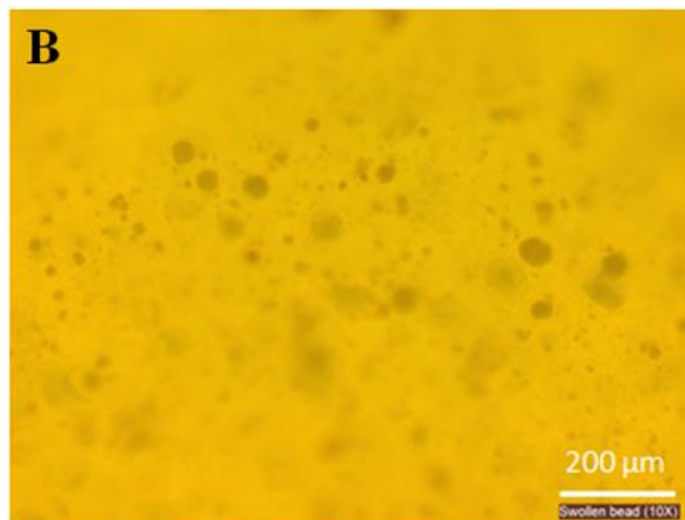
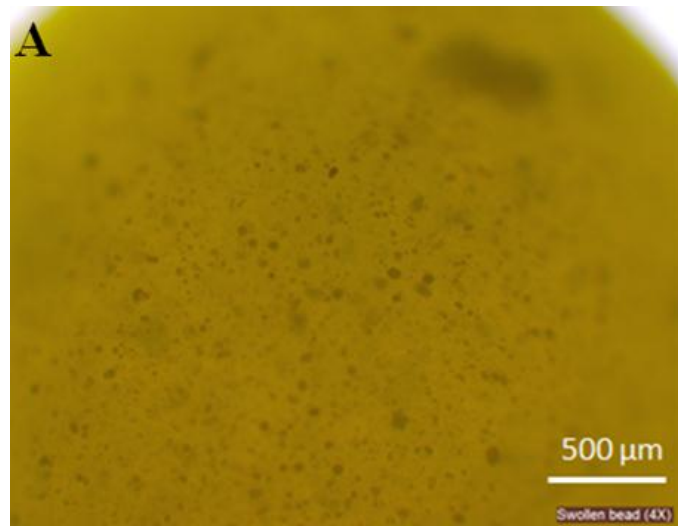


Figure 15: Light microscope images of gel bead.  
Note: Surface morphology of a gel bead was captured by using LEICA DM750 microscopy at 3 different objectives; (A) 4X, (B) 10X, (C) 40X.

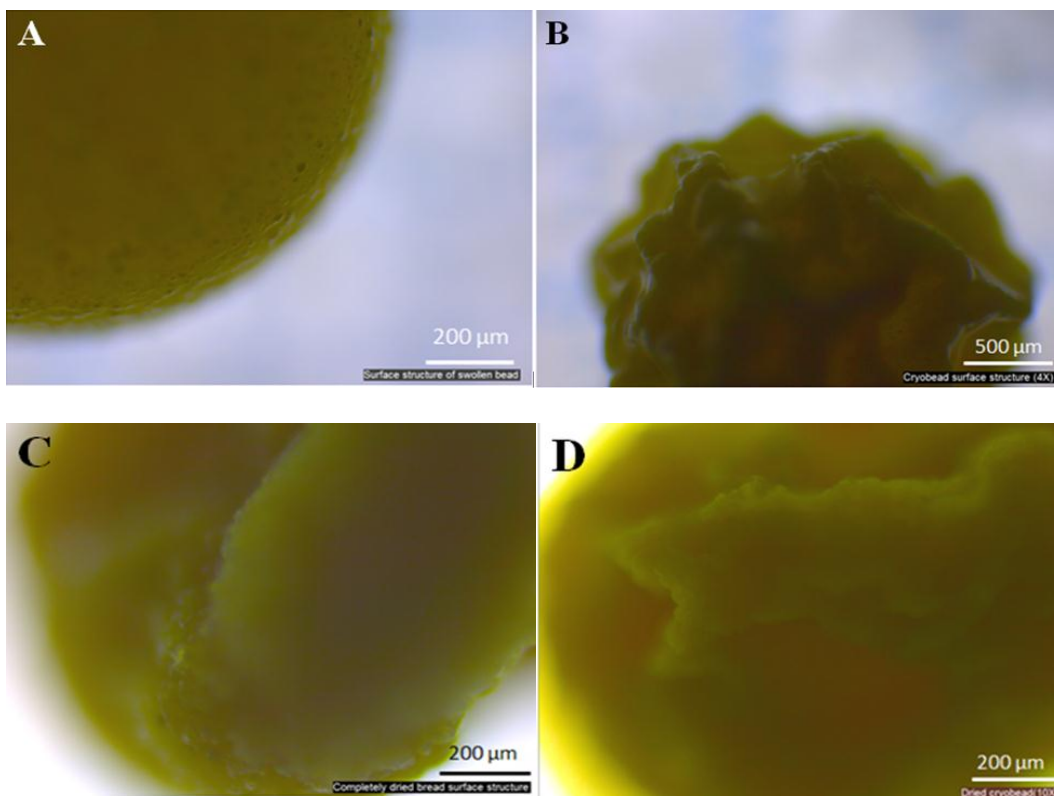


Figure 16: Morphologies of four different types of beads.

Note: (A) 10X objective picture of gel bead with a smooth surface. (B) 4X objective picture of cryogel bead with an irregular surface. (C) 10X objective picture of dried gel bead. (D) 10X objective picture of dried cryogel bead.

#### 4.4 FTIR (Fourier-Transform Infrared Spectroscopy) Results

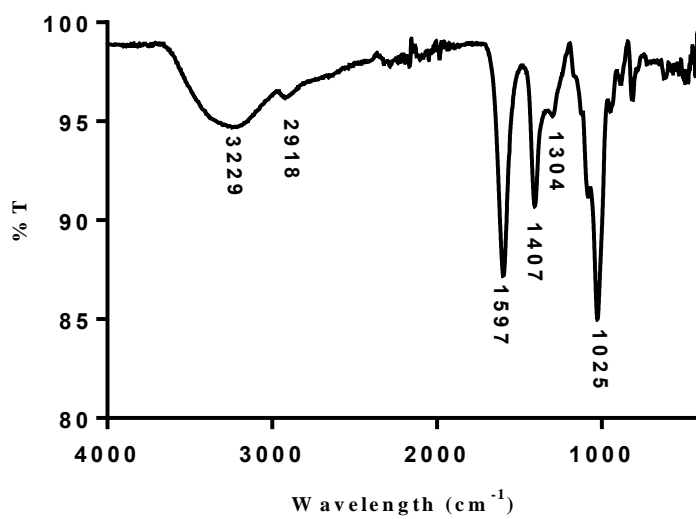
FT-IR results for sodium alginate, quercetin and quercetin-loaded beads are given in Figures 17a, 17b, 17c, 17d and 17e. As it is observed from FT-IR spectrum of sodium alginate; it has asymmetric stretch of C-O-C (ether) structures which it is usually causes the formation of peak between  $1000\text{ cm}^{-1}$  and  $1300\text{ cm}^{-1}$ . In the case, the peak at  $1304\text{ cm}^{-1}$  was a good indication of C-O stretch. Due to the vibrations of O-H bonds, there is broad band between  $3000\text{ cm}^{-1}$  and  $3600\text{ cm}^{-1}$ . This broad band is centered at  $3229\text{ cm}^{-1}$ . Due to strong characteristic broad band of O-H stretch, it should be concluded that there is -COOH groups, not only -OH groups of alcohols. Vibrational stretchings of aliphatic groups (C-H) were showed a peak at  $2918\text{ cm}^{-1}$ . Carboxylate groups of sodium alginate were showed asymmetric stretching at  $1597$

$\text{cm}^{-1}$ , the peak at  $1407 \text{ cm}^{-1}$  usually also represents stretching of carboxylate group symmetrically. Characteristic peaks around  $1025 \text{ cm}^{-1}$  was due to the vibrational stretches of 6-membered carbon rings together with the effects of C-C-H and C-O-H moieties (Daemi and Barikani, 2012).

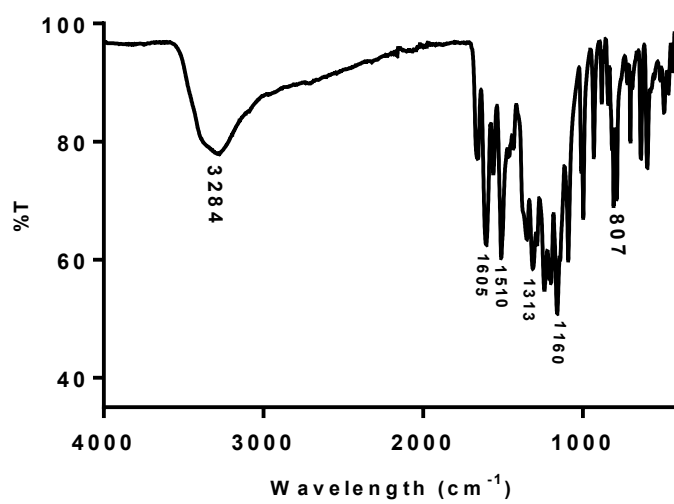
FT-IR spectrum of Quercetin; the band centered at  $3284 \text{ cm}^{-1}$  is due to vibrational stretches of -OH groups of alcohol. Peak at  $1313 \text{ cm}^{-1}$  represent -CRH bridges in the quercetin structure. Asymmetrical vibrational stretches of C-C-OH was observed at  $1240 \text{ cm}^{-1}$ . Quinone structures and ring moieties with six carbons were detected via the peaks at  $1605 \text{ cm}^{-1}$  and  $1510 \text{ cm}^{-1}$ . Sharp peak at  $1160 \text{ cm}^{-1}$  indicates the presence of vibrational of C-O single bond, and -CH<sub>2</sub>OH functional groups (Yadav et al., 2007; Wang et al., 2010; Chiang et al., 2002). Peaks at  $807 \text{ cm}^{-1}$  is due to C-H bends and it is a good indication of presence of aromatic rings.

Spectral result of quercetin encapsulated alginate beads; vibrational stretches of -OH groups of alcohols usually cause a broad band at around  $3500 \text{ cm}^{-1}$  to  $3300 \text{ cm}^{-1}$ . In the quercetin encapsulated alginate beads, this band is centered at  $3298 \text{ cm}^{-1}$ . Presence of peak at  $1598 \text{ cm}^{-1}$ , indicate that there is carboxylate group present in the structure and the detection of small peak at  $1521 \text{ cm}^{-1}$  indicate the presence of -CO-group of carbonyl from quercetin. Asymmetrical stretchings of carboxylate groups shifted from  $1407 \text{ cm}^{-1}$  to  $1419 \text{ cm}^{-1}$  compare to alginate spectrum. This can be due to the ionic interactions between calcium and carboxylate groups. Peak at  $1317 \text{ cm}^{-1}$  was not found in the structure of sodium alginate, however, it is detected in the structure of the quercetin loaded beads. This is because of carbon bridges -CRH- from quercetin cause the formation of peak at  $1317 \text{ cm}^{-1}$ . The peak at  $1025 \text{ cm}^{-1}$  of alginate that is responsible due to ring structures together with C-C-H and C-OH

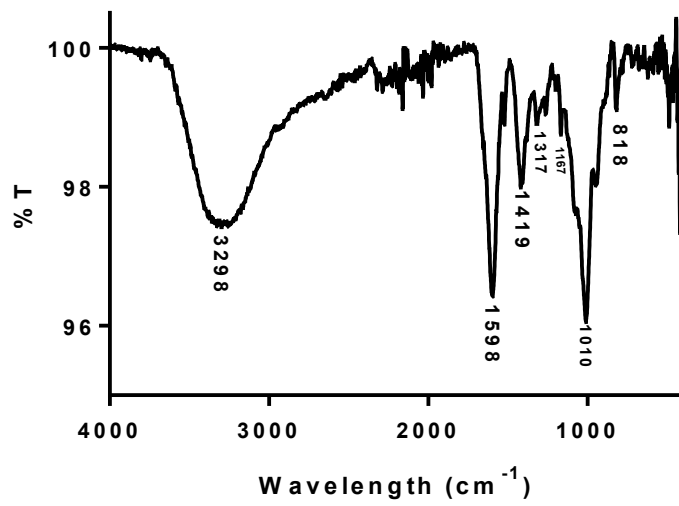
vibrations was shifted to  $1010\text{ cm}^{-1}$  in the spectrum of the beads. In addition, the small peak at  $1167\text{ cm}^{-1}$  indicates the vibrational stretches of  $-\text{CO}$  single bond, and  $-\text{CH}_2\text{OH}$  functional groups. Besides, presence of C-H bends at  $818\text{ cm}^{-1}$  as a single peak is a good indication of aromatic rings in the structure. This is indicating that definitely quercetin, which is an aromatic polyphenol, encapsulated into beads. Overall, the spectrum of quercetin loaded beads is similar to the spectrum of alginate. There are few novel peaks recorded as mentioned above compare to sodium alginate structure, this is new peaks are formed due to the presence of quercetin in the beads. Since, quercetin is not covalently bound to alginate structure, it is just causing slight shifts in the spectrum of sodium alginate. In the case of covalently bound quercetin, FT-IR spectrum of beads will shift considerably, however, in this study covalently bound quercetin to alginate is not desired. Quercetin should be released from the beads, this could be only established by small, weak intermolecular forces between quercetin and the alginate such as polar-polar interactions and ion-polar interactions as shown in Figure 17 (e).



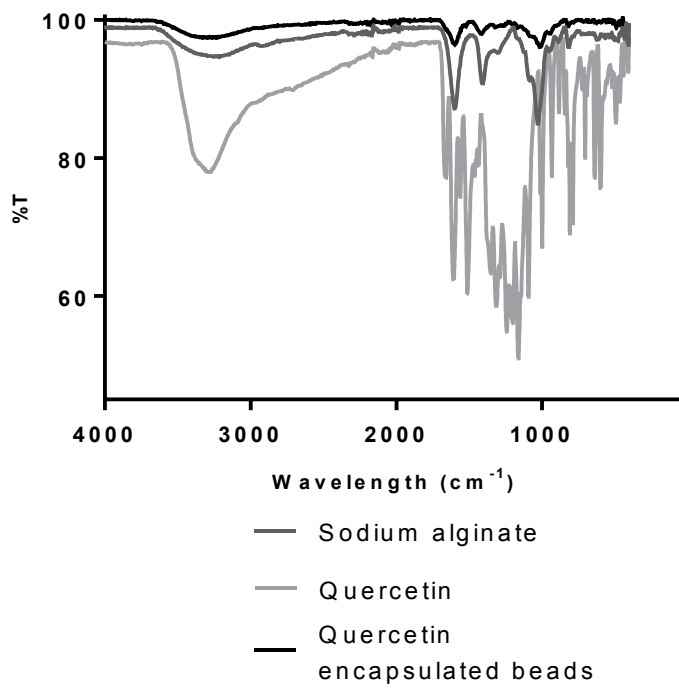
(a)



(b)



**(c)**



**(d)**

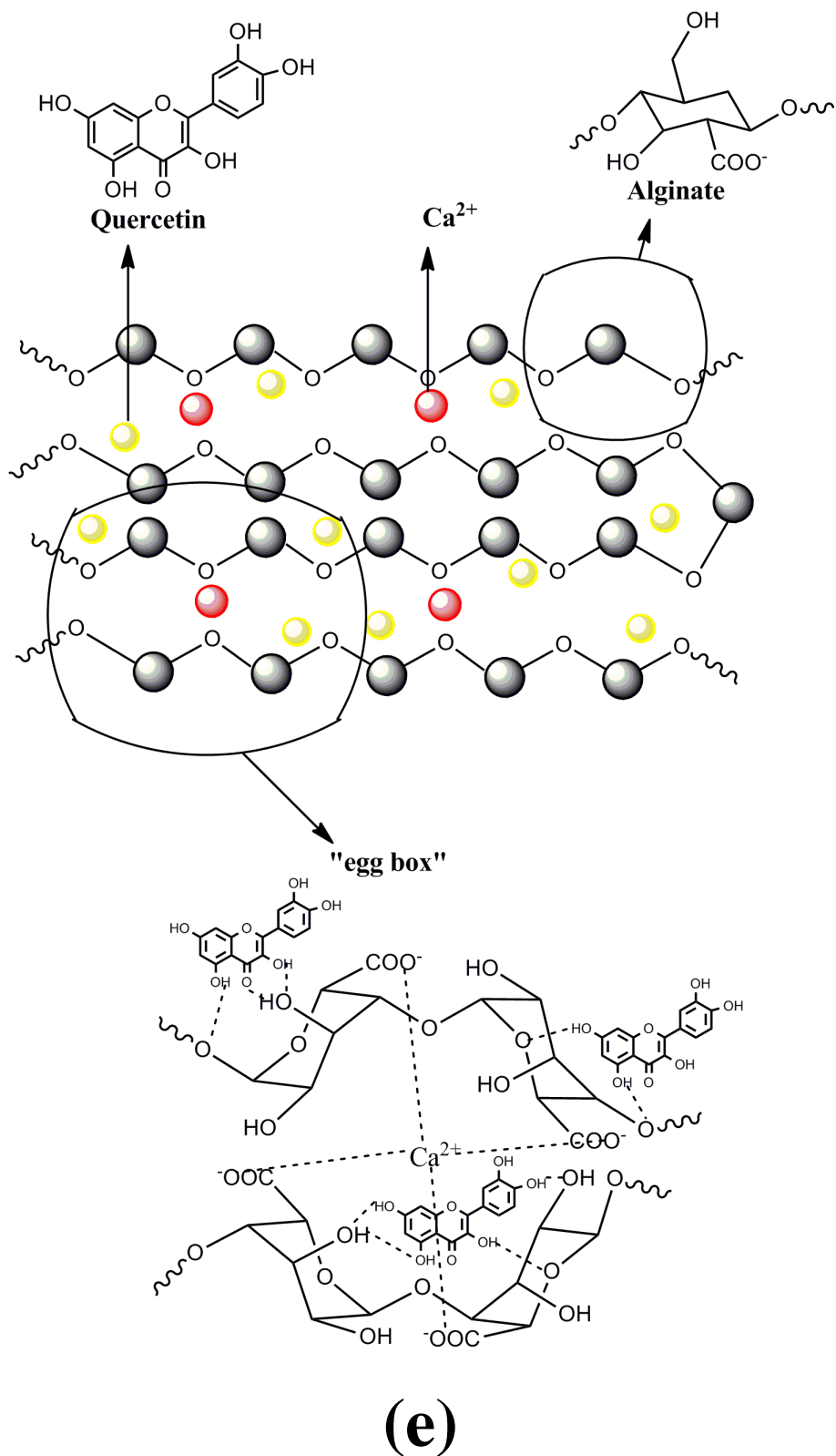


Figure 17: FT-IR spectra and the structure of quercetin-encapsulated beads.  
 Note: (a) FT-IR spectrum of sodium alginate. (b) FT-IR spectrum of quercetin. (c) FT-IR spectrum of quercetin encapsulated beads. (d) FT-IR spectra of sodium alginate, quercetin and quercetin- encapsulated beads. (e) Closer look to the structure of quercetin-encapsulated bead (Drawn in ChemDraw Ultra).



#### 4.5 Results of Drying Profile of Quercetin Loaded Beads

Immediately after the formation of the beads, drying rate should be monitored. Although during the formation of the beads drip controller was used to obtain similar sizes of beads, some of the beads were deformed and they had irregular shapes. Beads with irregular shapes should be eliminated to prevent errors in the drying rate data, because, the beads with different surface area to volume ratio compare to others will have slightly different drying rate. Beads with similar sizes chosen and they transferred into petri dish covered with aluminum foil to prevent light enter and then holes are created by using needle on top of aluminum foil to enable the excess solvent to evaporate . Beads containing petri dish was placed into fume hood at room temperature and the total weights of the beads were measured at constant time intervals until all the beads are completely dried (Table 1, Table 2, Figure 18 and Figure 19).

Table 6: Drying data of the beads.

Drying Rate Profile for Beads	
Weight (in gram)	Time (in hours)
10.284	0
10.058	0.25
9.864	0.5
9.687	0.75
9.486	1
9.152	1.25
8.806	1.5
8.444	1.75
7.994	2
7.302	2.5
6.472	3
5.738	3.5
5.130	4
4.523	4.5
3.926	5
3.318	5.5
2.784	6
2.323	6.5

1.840	7
1.356	7.5
1.047	8
0.852	8.5
0.756	9
0.731	9.5
0.719	10
0.695	15
0.695	17
0.695	19
0.695	21

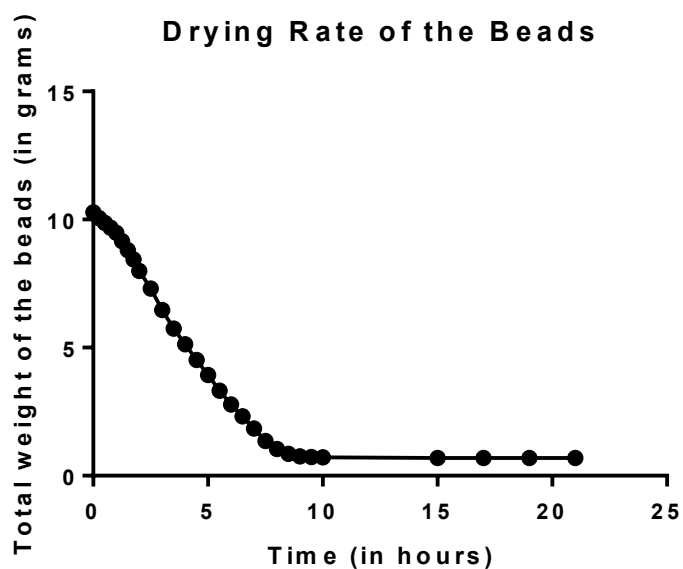


Figure 18: Drying rate of the beads.

Note: Graph indicates that 10 hours of drying under the fume hood at room temperature will be sufficient to have completely dried beads.

Table 7: Drying data of the cryogel beads.

Drying Rate Profile for Cryogel beads	
Weight (in gram)	Time (in hours)
0,2	0
0,172	0.25
0,145	0.5
0,114	0.75
0,097	1
0,08	1.25
0,075	1.5
0,074	1.75
0,073	2
0,072	2.5
0,072	3
0,072	3.5
0,072	4
0,072	4.5
0,072	5

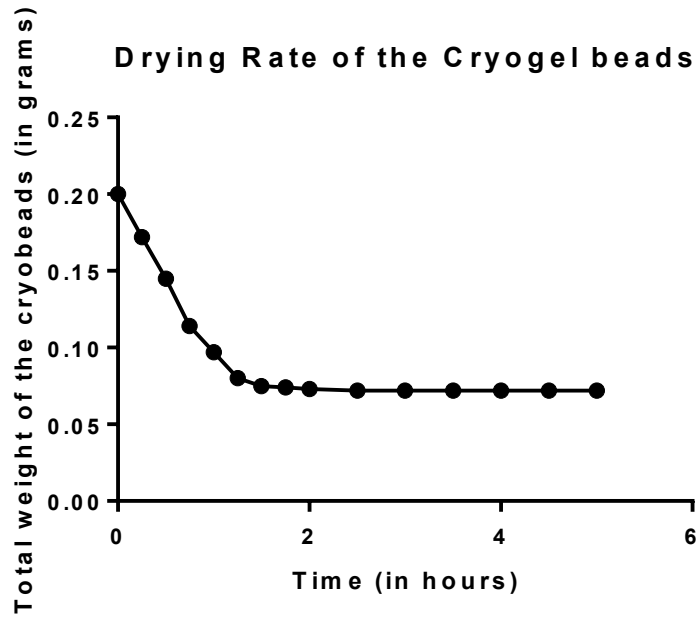


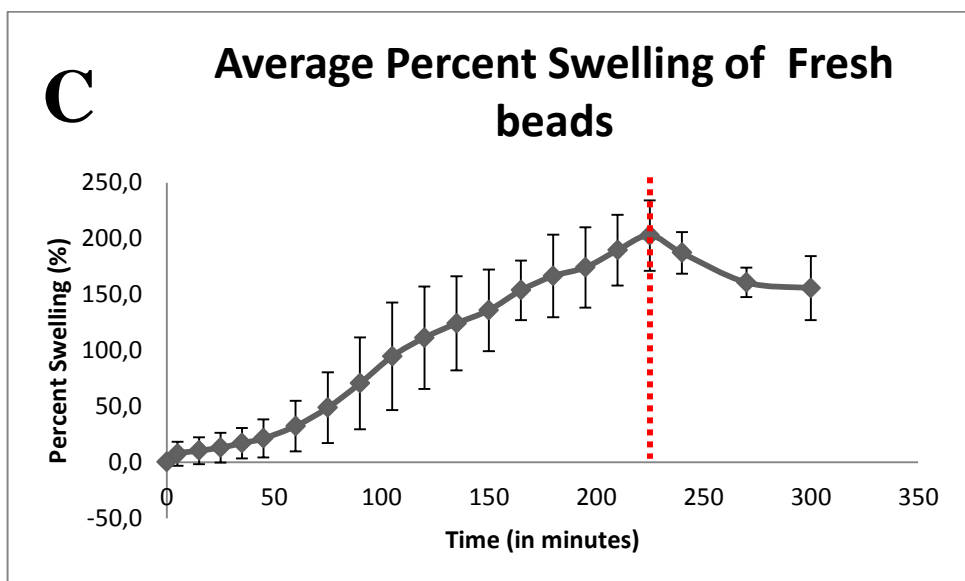
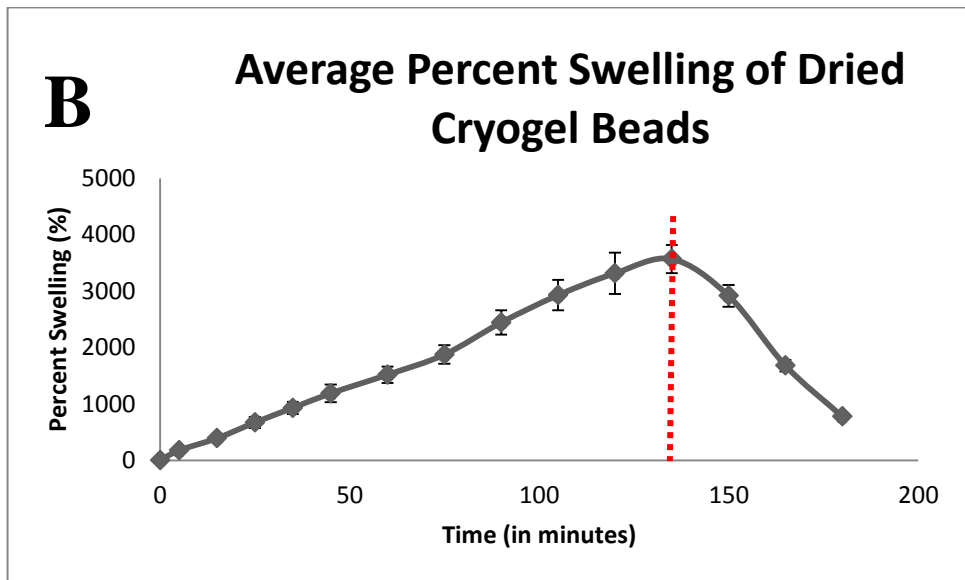
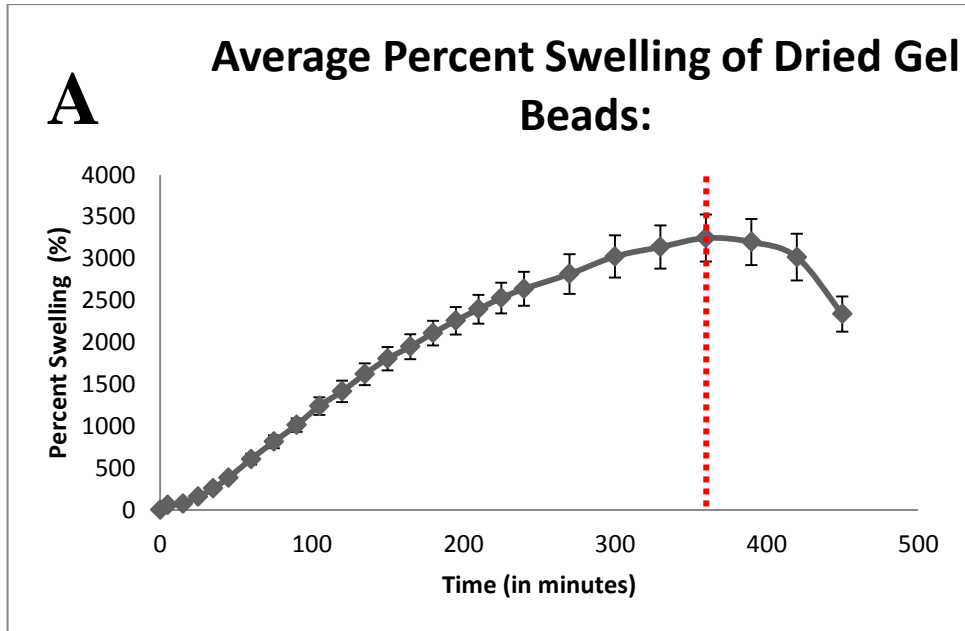
Figure 19: Drying rate of the cryogel beads.

Note: Graph indicates that 5 hours of drying under the fume hood at room temperature will be sufficient to have completely dried cryobeads.

#### 4.6 Swelling Tests Results

Figure 20 indicates the average percent swellings for dried gel beads, dried cryogel beads, gel beads and cryogel beads in phosphate buffer at pH 7.4. Each type of beads showed different maximum average swelling in PBS (Phosphate Buffered Saline). Maximum average swelling percentages of dried gel beads, dried cryogel beads, gel beads and cryogel beads were found as  $3247, 6 \pm 281, 2 \%$ ,  $3568, 2 \pm 250, 2 \%$ ,  $202, 8 \pm 31, 5 \%$  and  $824, 4 \pm 123, 2 \%$ , respectively. In both fresh and dried versions of the beads; cryogel beads showed higher swelling percent than the gel beads due to the presence of the high level of porosity. After the maximum swelling percent, the percent weight change decreased, this is mainly because of dissolution. Beads were started to dissolve in the PBS. Swelling in the alginate beads was established due to the presence of sodium ions in PBS. Sodium ions in PBS can displace some of the calcium ions in beads, since the calcium ion is an ionic cross linker and it makes ion-

ion interactions with negatively charged carboxylate groups ( $-\text{COO}^-$ ) of alginate, when it is displaced with sodium ions, some of the  $-\text{COO}^-$  groups will be free from ion-ion interactions. Thus,  $-\text{COO}^-$  groups will repel each other due to the same charges (electrostatic repulsion). Meanwhile, calcium ions will be trapped by phosphate ions to form calcium phosphate. Since,  $-\text{COO}^-$  groups repel each other, this will cause the swelling of the structure (Bajpai & Shubhra, 2004). As sodium ions replace the calcium ions and calcium phosphates formed, swelling occurs until maximum swelling. After maximum swelling, dissolution will start and swellings continuous until all the beads were completely dissolved.



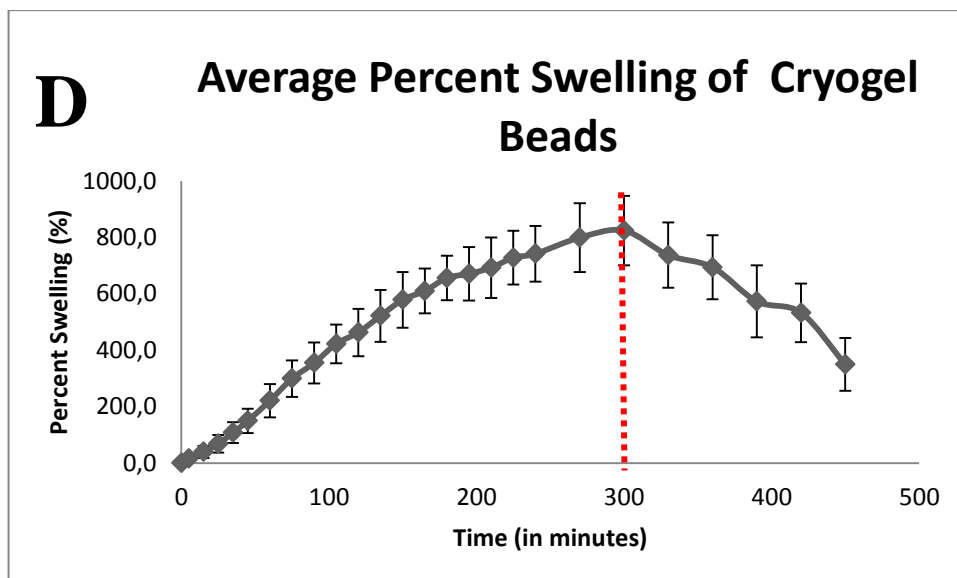


Figure 20: Average Percent Swelling Profiles.

Note: (A) Average percent swelling of dried gel beads until. (B) Average percent swelling of dried cryogel beads (C) Average percent swelling of gel beads. (D) Average percent swelling of cryogel beads.

#### 4.7 Calibration Curves

Calibration curves were prepared for release kinetic studies. Since, four different solvents/cell culture media were predetermined for release kinetic studies; DMSO, MHB, RPMI-1640 (culture medium) and saline (0.9% saline solution), calibrations curves for these solvents were prepared. All the absorbance versus wavelength graphs for these solvents were studied between 350 nm wavelength and 450 nm wavelength to determine the specific lambda max ( $\lambda_{max}$ ) values for each solvents. In order to draw absorbance versus wavelength graphs of quercetin in different solvents, serial dilutions of quercetin in specific solvent was prepared to mimic the release of quercetin in this solvent. After the determination of the lambda max at specific wavelength, only the absorbance values for each dilution at that wavelength ( $\lambda_{max}$ ) was chosen to draw a calibration curve (Absorbance versus concentration curve) for each solvent. All the dilutions were prepared by using quercetin main stock with 82700  $\mu\text{M}$  concentration. From release studies ,

absorbance versus time graphs will be obtained, so that absorbance versus concentration graphs were required to determine specific concentration of quercetin released at the regular time intervals (Figure 21, Figure 22, Figure 23 & Figure 24).



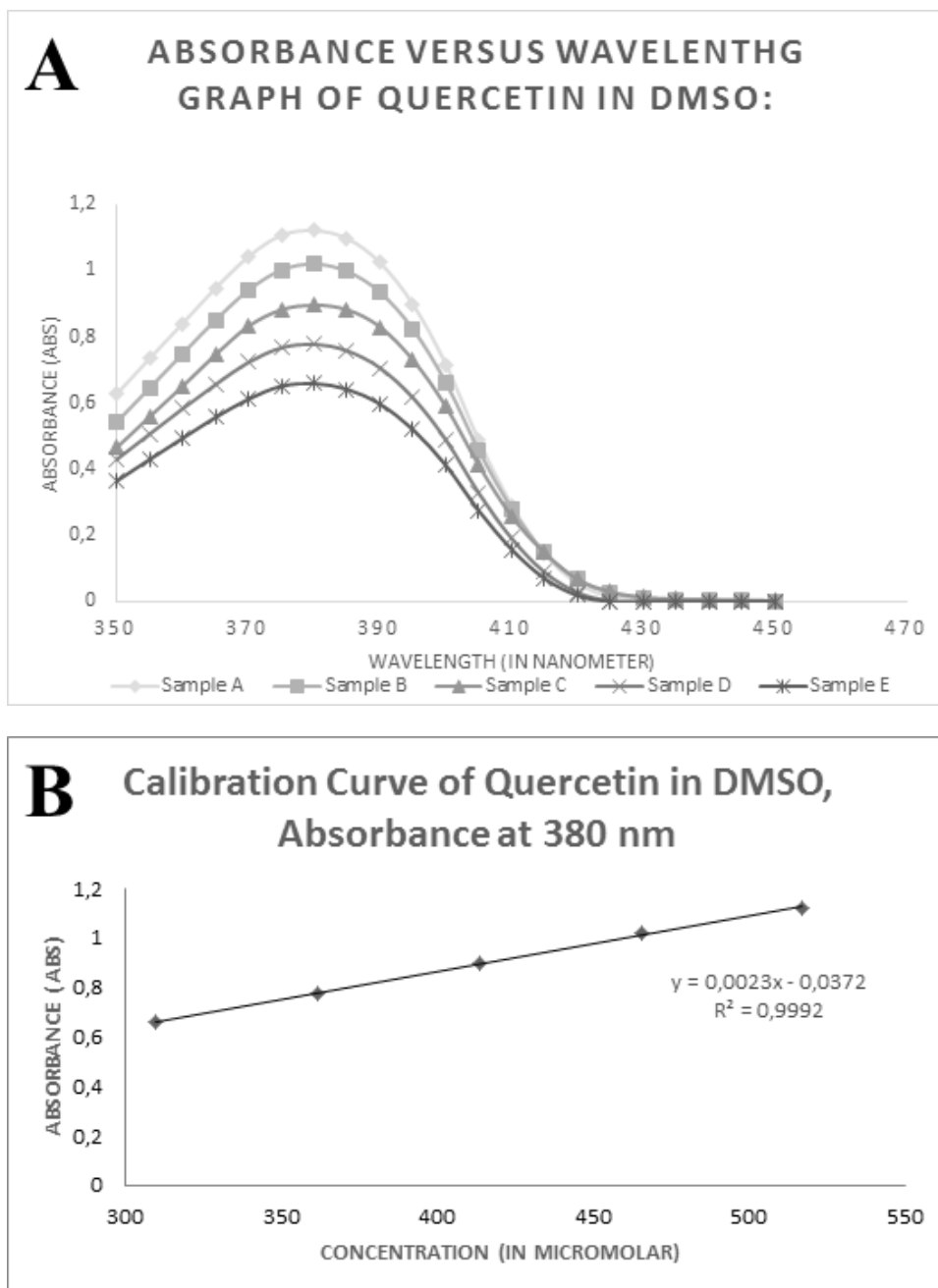


Figure 21: Calibration graphs for DMSO.  
Note: (A) Absorbance versus wavelength graph of quercetin in DMSO. (B) Calibration Curve of Quercetin in DMSO, Absorbance at 380 nm.

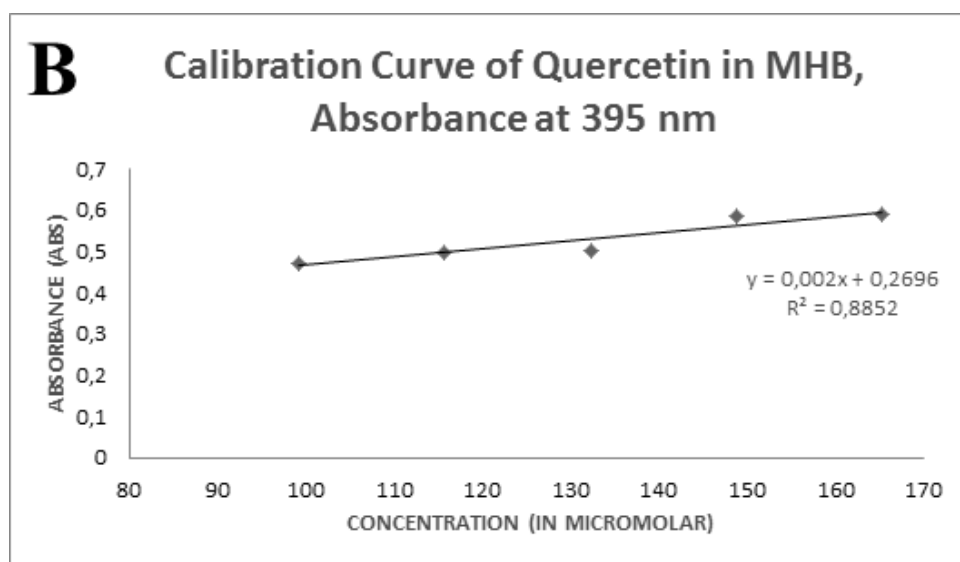
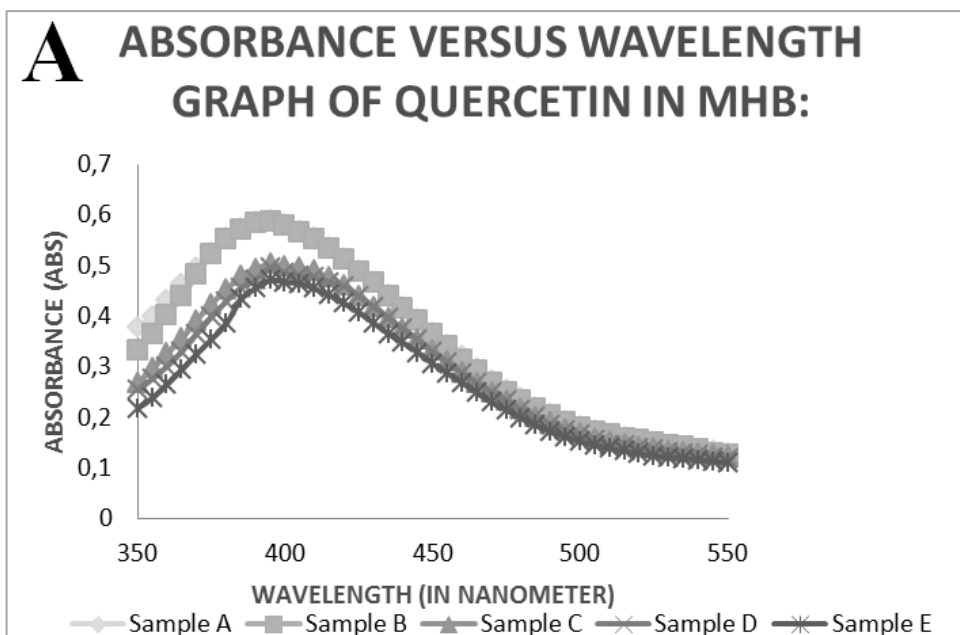


Figure 22: Calibration graphs for MHB.

Note: (A) Absorbance versus wavelength graph of quercetin in MHB. (B) Calibration Curve of Quercetin in MHB, Absorbance at 395 nm.

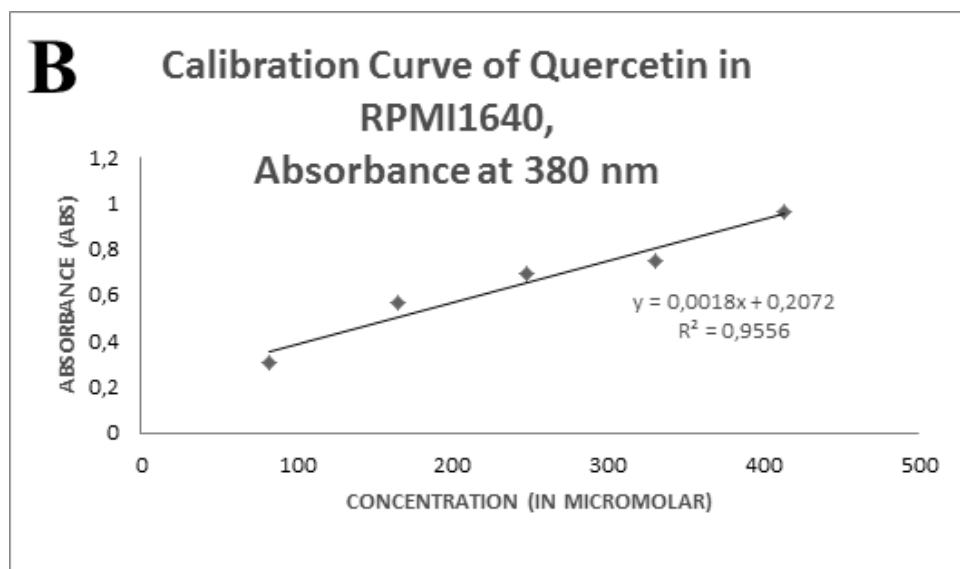
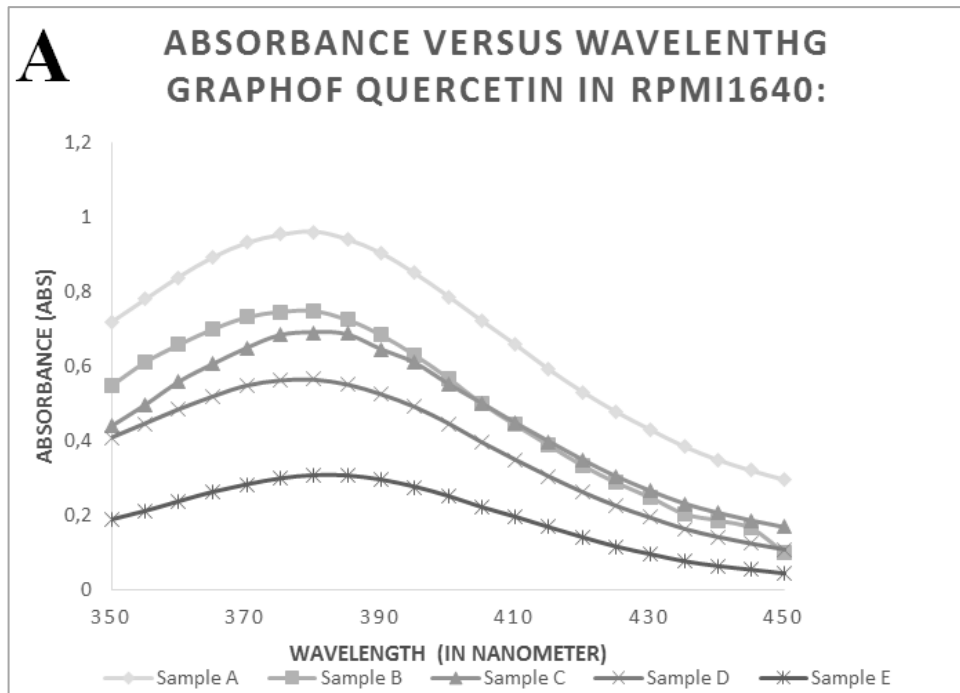


Figure 23: Calibration graphs for RPMI-1640.  
 Note: (A) Absorbance versus wavelength graph of quercetin in RPMI-1640. (B) Calibration Curve of Quercetin in RPMI-1640, Absorbance at 380 nm.

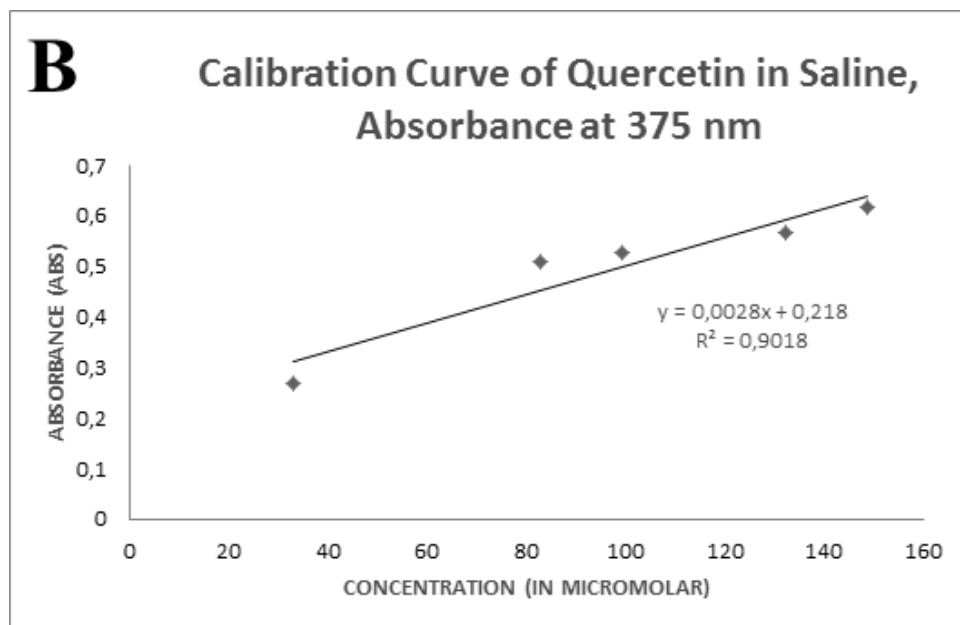
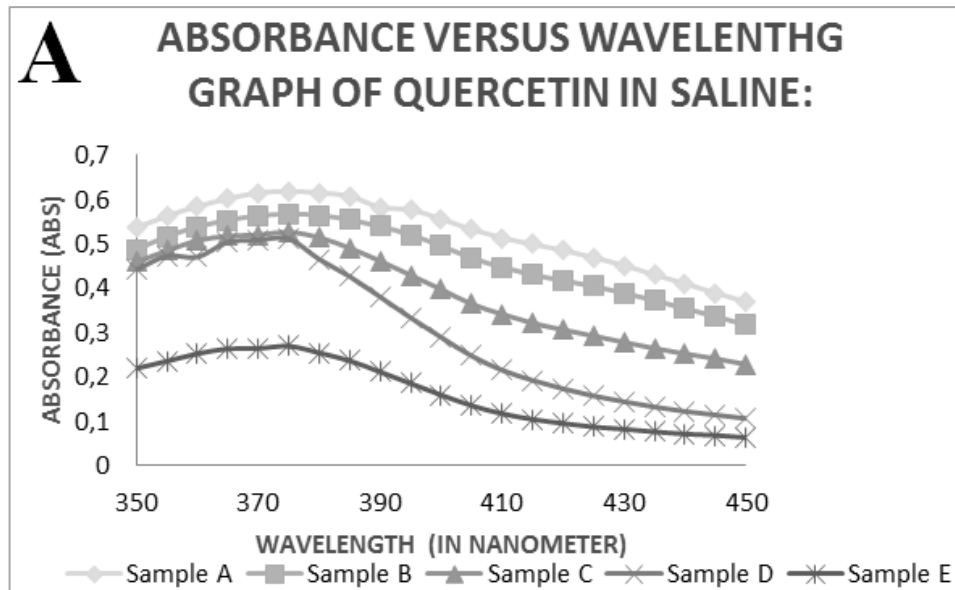


Figure 24: Calibration graphs for saline.  
Note: (A) Absorbance versus wavelength graph of quercetin in saline (0.9% saline).  
(B) Calibration Curve of Quercetin in 0.9% saline, Absorbance at 375 nm.

## 4.8 Release Studies

Release studies were conducted by using four different types of release media, which are DMSO, 0.9% saline with 3 different DMSO percents (10%, 20% and 40%), MHB with 3 different DMSO percents (10%, 20% and 40%) and RPMI-1640. Since the best solvent for quercetin was DMSO, release of quercetin from the beads firstly done by using DMSO as release medium. 0.9% saline solution and MHB solution were chosen for release studies, due to the requirement of these release media during the antibacterial activity studies. Three different percentages of DMSO with 10%, 20% and 40% for both saline and MHB were studied. This is due to the toxicity of DMSO, DMSO was required in the medium for quercetin to be released from the beads. However, the lowest amount of DMSO in the release medium was preferential to prevent any side effects and toxicity on bacteria during antimicrobial test. Thus, three different DMSO percents were used to choose the optimal one. RPMI-1640 was used as release medium for to study release, since it is used as culture medium to grow the cells.

Based on Figure 25 (A), release graph of quercetin from beads in DMSO, gel beads and cryogel beads showed the highest release, therefore, the absorbance values are higher than the dried gel beads. It took 6 hours (360 minutes) for all types of beads to release maximum amount of quercetin.

In Figure 25 (B), release graph of quercetin from beads in 0.9% saline with 10% DMSO of total solution. Gel beads and cryogel beads showed the highest absorbance with about 0.1 Abs. Although, it seems like dried beads release the highest amount of quercetin by absorbance about 0.27 Abs, dried gel beads release the lowest amount

of quercetin compare to cryogel beads and gel beads. The reason of dried gel beads showed higher absorbance is because of during the release studies gel beads and cryogel beads , higher volume of release medium was used compare to dried gel beads to not to exceed absorbance value higher than 2.

In Figure 25 (C), release graph of quercetin from beads in 0.9% saline with 20% DMSO of total solution. The highest amount of quercetin released by gel beads and dried gel beads showed the lowest quercetin released compare to other types.

In Figure 25 (D), release graph of quercetin from beads in 0.9% saline with 40% DMSO of total solution. Gel beads and cryogel beads showed the highest absorbance, therefore, the highest amount of quercetin released. However, the absorbance value was too high and the volume of release medium was increased to have lower, valid absorbance values. Almost the same amount of quercetin was released from the both cryogel beads and gel beads with absorbance about 0.3 Abs.

In Figure 25 (E), release graph of quercetin from beads in MHB with 10% DMSO of total solution. In this case, cryogel beads showed the highest absorbance, which indicates the highest amount of quercetin released and it took about 23 hours (1380 minutes) to reach the highest amount of quercetin released. Gel beads showed the second highest absorbance and the lowest absorbance, or the lowest quercetin release was recorded with dried gel beads.

In Figure 25 (F), release graph of quercetin from beads in MHB with 20% DMSO of total solution. In this case, again 23 hours (1380 minutes) was required to have maximum release of quercetin from each type of beads into release medium. The

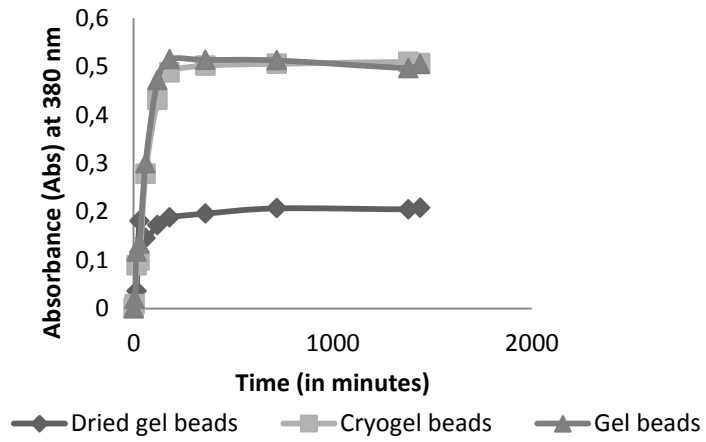
highest and the lowest absorbance values were detected by gel beads (with 0.3 Abs) and dried gel beads (with 0.05 Abs), respectively.

In Figure 25 (G), release graph of quercetin from beads in MHB with 40% DMSO of total solution. In this case, cryogel beads showed much lower absorbance values compare to gel beads about 0.57 Abs. Although increasing DMSO in the medium increases the release of quercetin from the beads in MHB. Increasing level of DMSO in total solution is much more effective for gel beads and it showed the highest absorbance with about 2.3 Abs.

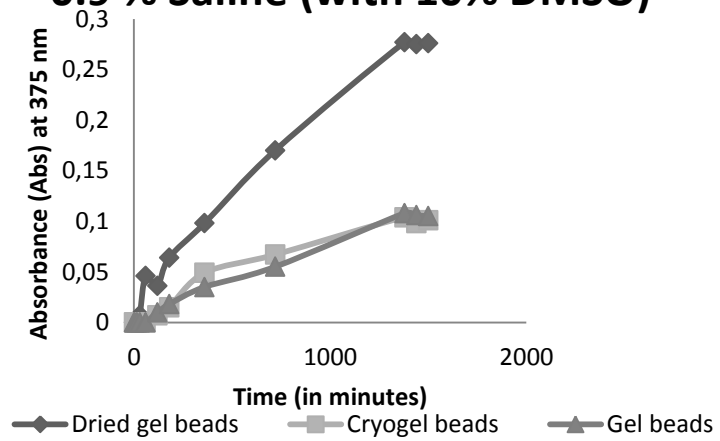
In Figure 25 (H), release graph of quercetin from beads in RPMI-1640, the release of quercetin was started after 720 minutes of shaking at 130 rpm in the release medium. This can be due to the demand for swelling of the beads in the RPMI-1640 medium. After 720 minutes, beads may swell and they start to release the quercetin. The highest absorbance values were recorded with cryogel beads with absorbance of 1 Abs. Again dried gel beads showed the lowest absorbance, thus, the lowest quercetin release among the other types of beads.

Overall, in all graphs either cryogel beads or gel beads were showed the highest absorbance, thus, the highest amount of quercetin released. This is related to the presence and size of porosity. Cryogel beads have bigger pores compare to dried gel beads, therefore, they showed higher absorbance value and also gel beads have pores, which are ready to release the quercetin.

### A Release of Quercetin From Beads in DMSO

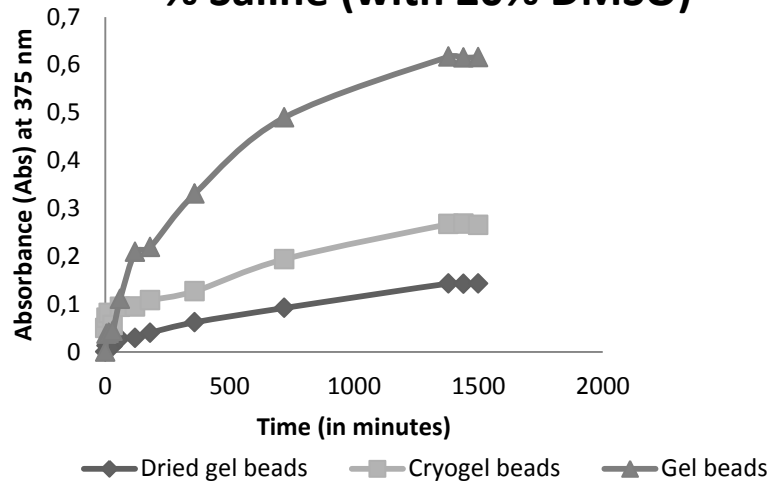


### B Release of Quercetin From Beads in 0.9 % Saline (with 10% DMSO)

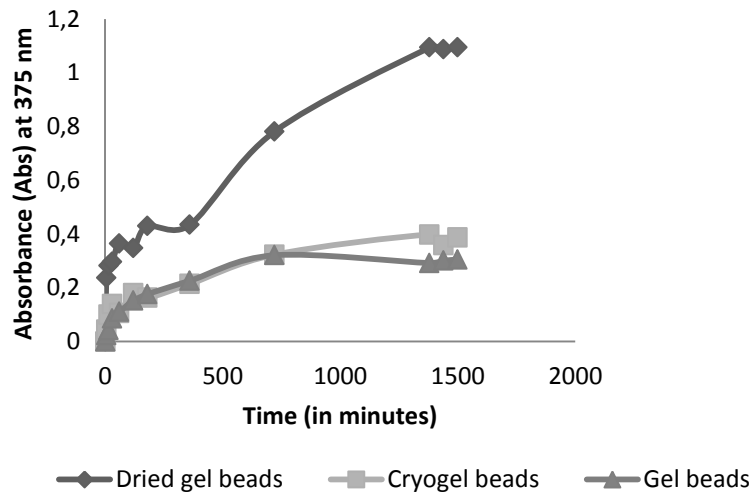




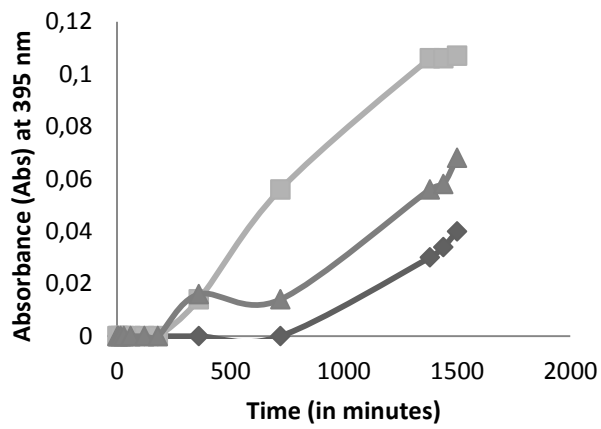
### C Release of Quercetin From Beads in 0.9 % Saline (with 20% DMSO)



### D Release of Quercetin From Beads in 0.9 % Saline (with 40% DMSO)

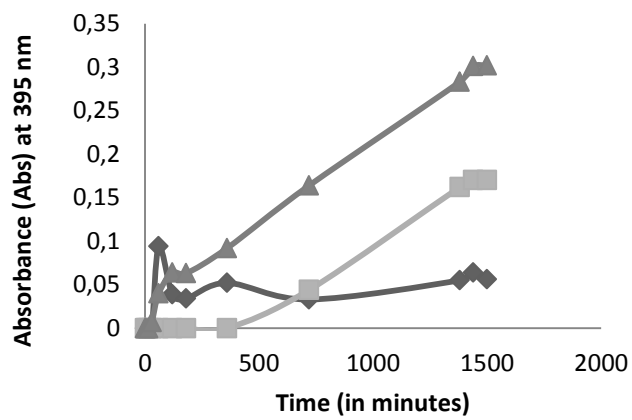


### E Release of Quercetin From Beads in MHB(with 10% DMSO)



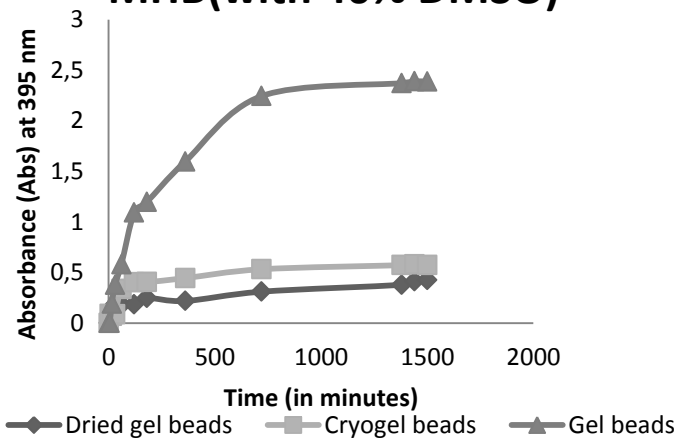
◆ Dried gel beads    ■ Cryogel beads    ▲ Gel beads

### F Release of Quercetin From Beads in MHB(with 20% DMSO)

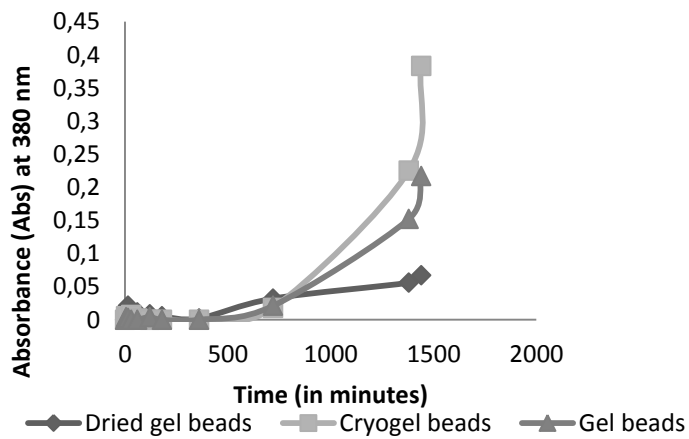


◆ Dried gel beads    ■ Cryogel beads    ▲ Gel beads

### G Release of Quercetin From Beads in MHB(with 40% DMSO)



### H-i Release of Quercetin From Beads in RPMI1640



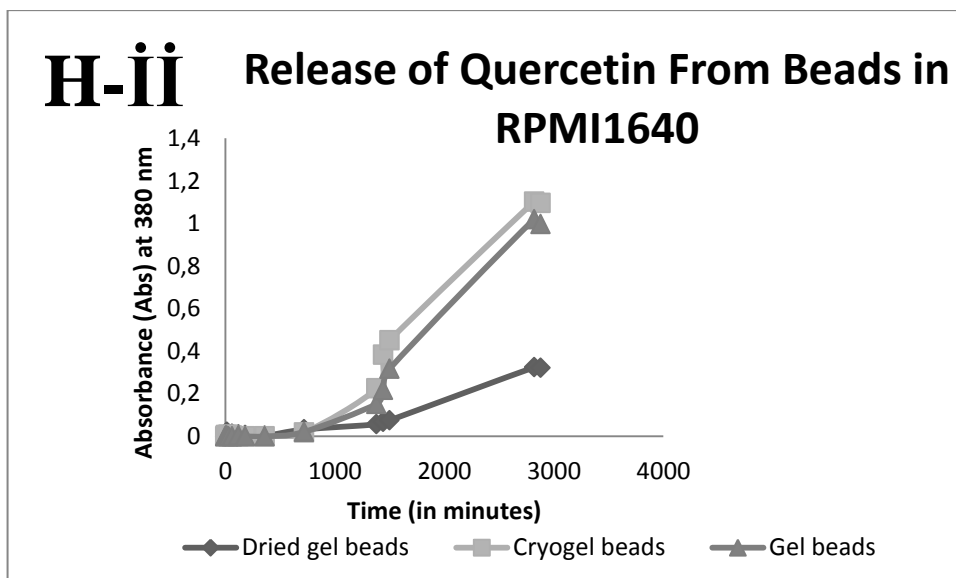


Figure 25: Release graphs of quercetin from the beads in different solvents.  
 Note: (A) Release graph of quercetin from 3 different types of beads in DMSO for 24 hours.(B) Release graph of quercetin from 3 different types of beads in 0.9% Saline (with 10% DMSO) for 25 hours.(C) Release graph of quercetin from 3 different types of beads in 0.9% Saline (with 20% DMSO) for 25 hours.(D) Release graph of quercetin from 3 different types of beads in 0.9% Saline (with 40% DMSO) for 25 hours.(E) Release graph of quercetin from 3 different types of beads in MHB (with 10% DMSO) for 25 hours.(F) Release graph of quercetin from 3 different types of beads in MHB (with 20% DMSO) for 25 hours.(G) Release graph of quercetin from 3 different types of beads in MHB (with 40% DMSO) for 25 hours.(H-I) Release graph of quercetin from 3 different types of beads in RPMI-1640 for 24 hours. (H-II) Release graph of quercetin from 3 different types of beads in RPMI-1640 for 48 hours.

#### 4.8.1 Observations From Release Studies

It is observed that when freshly made quercetin encapsulated gel beads are used, it is more likely to have almost complete release of quercetin from the beads. This deduction is based on the colour change of beads; they were yellow, which is a colour of the quercetin, before release and after release they become colourless (Table 8, Figure 26).

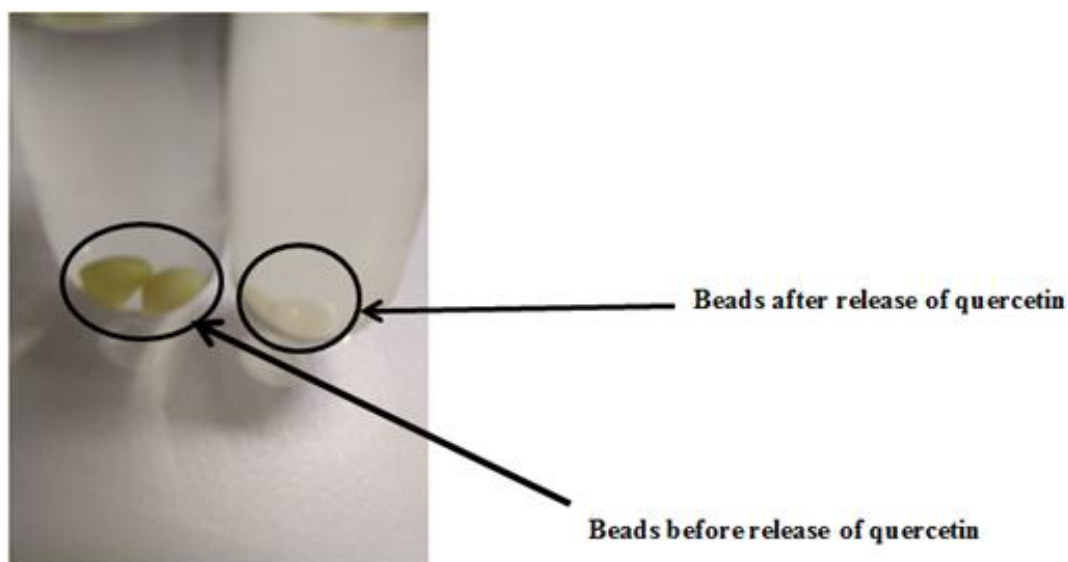
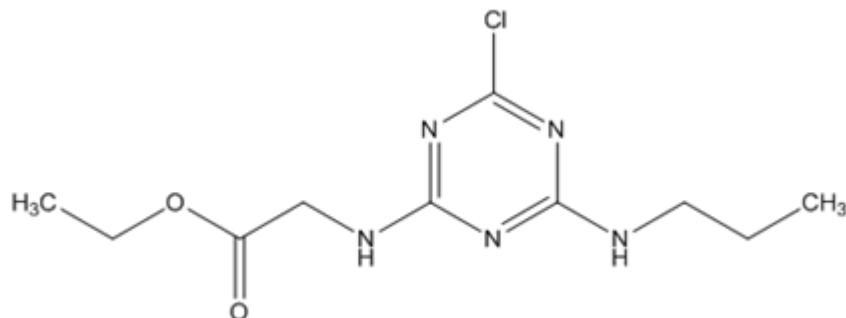


Figure 26: Colour change of quercetin.

Note: Before release the quercetin loaded beads are yellow and after release they become colourless.

In MHB (Mueller Hinton Broth), specifically in 10 % DMSO containing MHB solution beads' surfaces are covered with brown colour. This may indicate that chemicals in MHB may react with carboxylate groups of alginate beads to form brownish outer layer around the beads, this outer layer will affect the release of quercetin from the alginate beads, and therefore, MHB was not suitable for the quercetin release studies (Figure 27). The reason of the formation of brownish layer around beads can be explained by checking the ingredients of MHB. MHB contains beef extracts, starch and casein hydrolysate. Starch has many hydroxyl groups on it, but they can only do ion-polar interactions with the carboxylate groups of alginate. On the other hand, Casein hydrolysate with a chemical structure as follows;



Casein hydrolysate has ester group and it may react with carboxylate group of alginate extending from the beads. This may lead to the formation of brownish layer around the beads and it may prevent the release of quercetin from the beads.

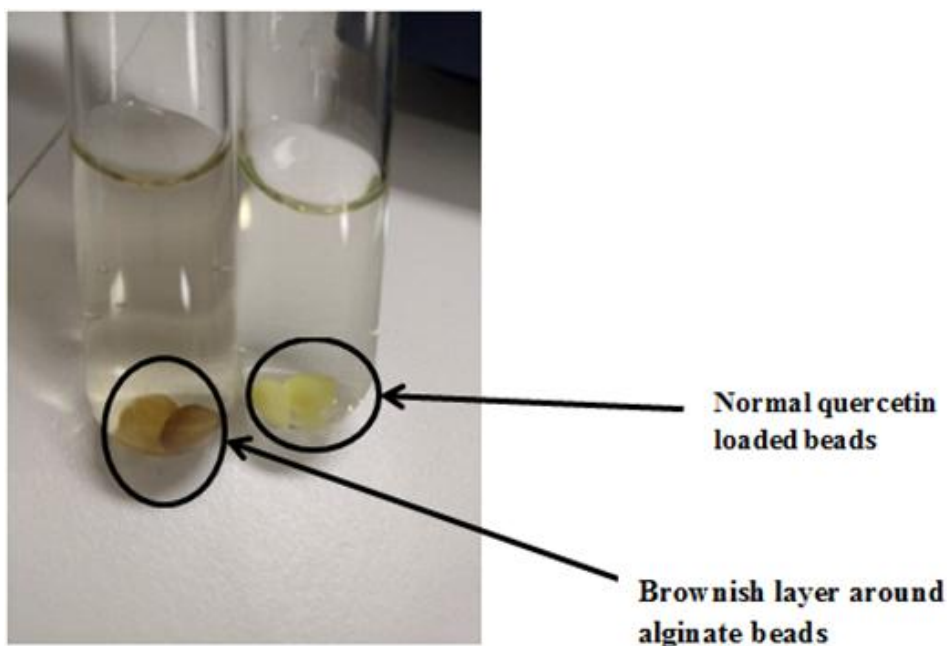


Figure 27: Quercetin loaded beads in MHB.

Note: Since carboxylate groups of alginate beads react with MHB, they will form brownish layer around the beads.

In RPMI-1640, all beads are swollen but no release until first 360 minutes. Then, after 12 hours in RPMI-1640, the absorbance values are increased. This can be the result of two factors, first and most optimistic one is maybe alginate beads sufficiently swollen in RPMI-1640 to make detectable release of quercetin. Another

reason of increased absorbance can be contamination. Not only the increased concentration of quercetin causes increase in absorbance value. In addition to this, any organismal growth in the RPMI-1640 can let to rise in absorbance values. To clarify the reason of increase in absorbance values, swelling test in RPMI-1640 should be conducted (Figure 28). Figure 28 indicates that quercetin loaded beads require about 720 minutes to swell in both only alginate beads and quercetin encapsulated beads. These percent swelling graphs suggest that there is a relation between swelling of beads and release of quercetin from the beads in RPMI-1640 medium. It is concluded that quercetin loaded beads swell in first 720 minutes and as the swelling continuous after 720 minutes, the beads will release the quercetin to the RPMI-1640 medium. RPMI-1640 is a multiple components containing cell culture medium. It is composed of inorganic salts (such as calcium nitrate tetrahydrate, potassium chloride, sodium bicarbonate, sodium chloride, and sodium phosphate dibasic), 21 different amino acids (some of them with modified versions such as L-Tyrosine.2Na.dihydrate), vitamins and other additional chemicals such as phenol red sodium. Thus, the main reason of swelling of beads in the RPMI-1640 is the sodium ions coming from the inorganic salts and from the modified forms of the amino acids. These sodium ions will displace the calcium ions in the beads and since sodium is monovalent cation, it will cause the loosening of the beads and the solvents will enter into the beads. This will lead to the swelling of the beads

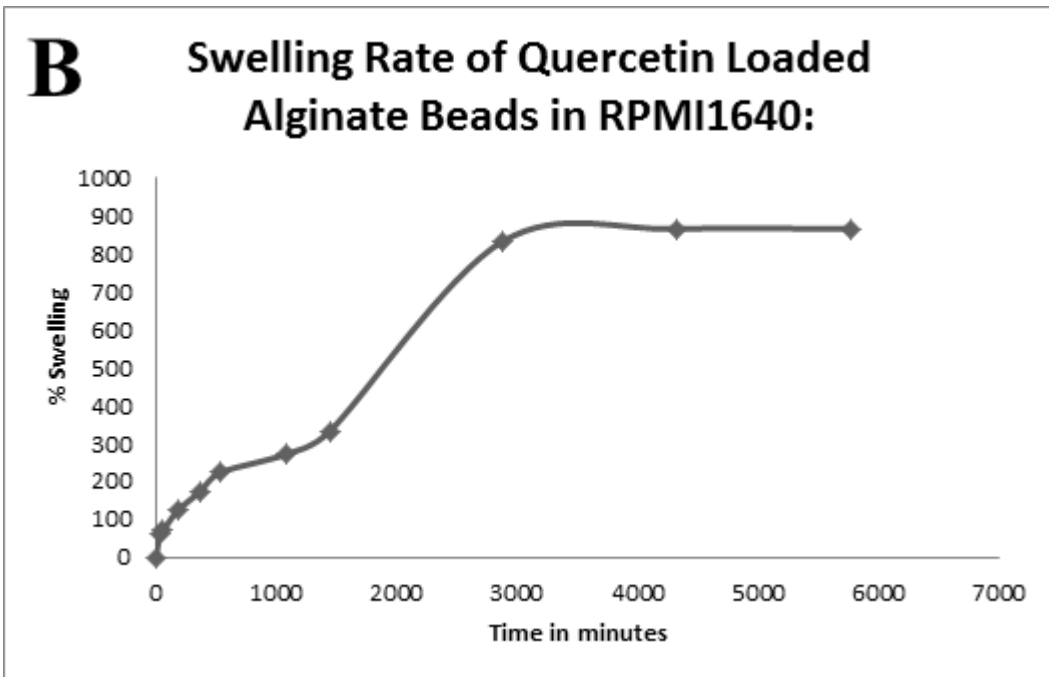
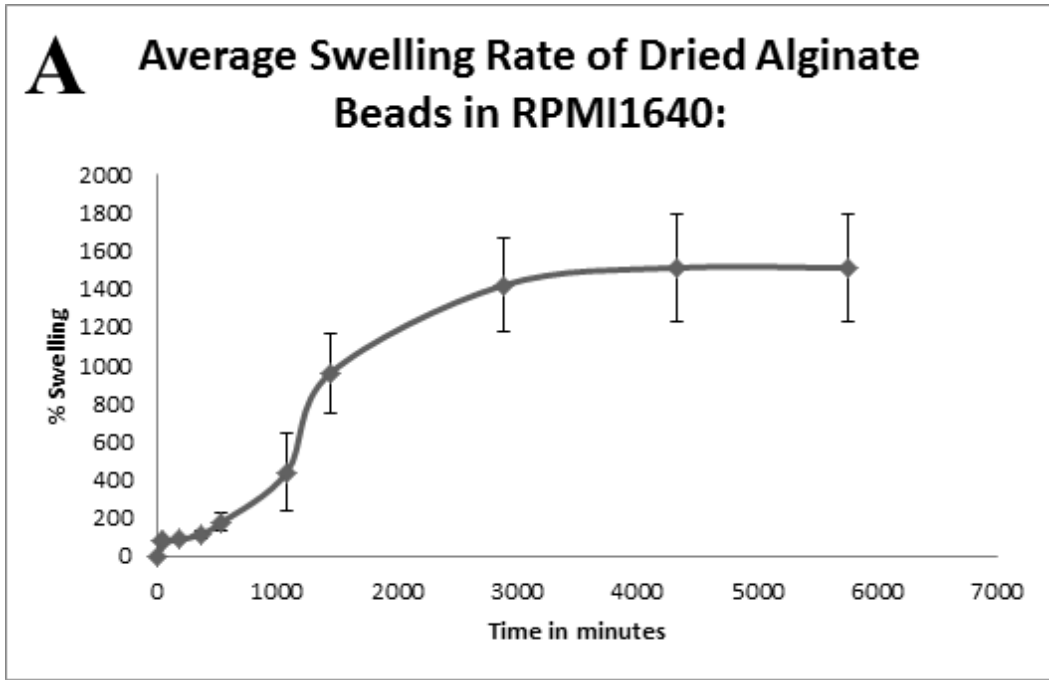


Figure 28: Percent swelling profiles of alginate beads.  
 Note: (A) Average Swelling Rate of Dried Alginate Beads in RPMI-1640. (B) Swelling Rate of Quercetin Loaded Alginate Beads in RPMI-1640.



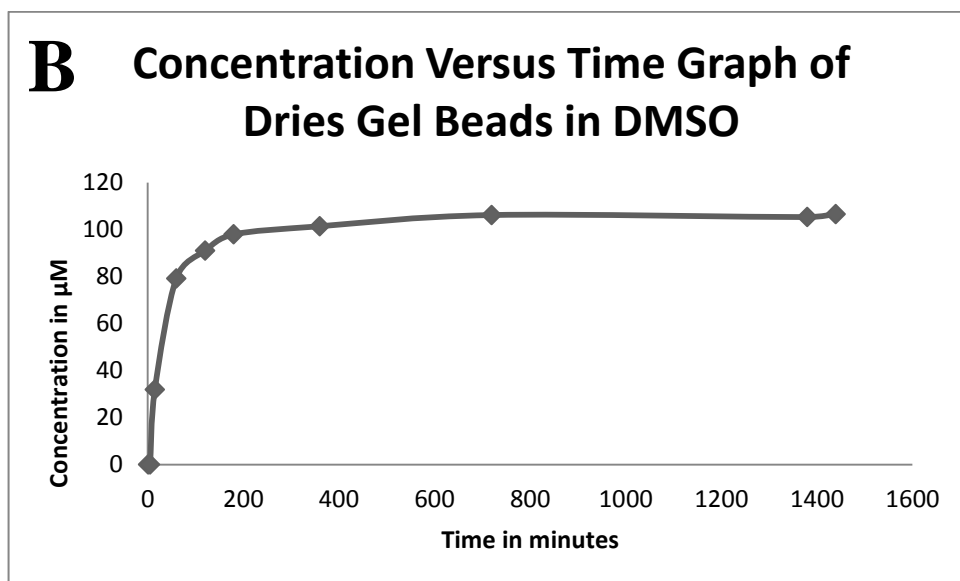
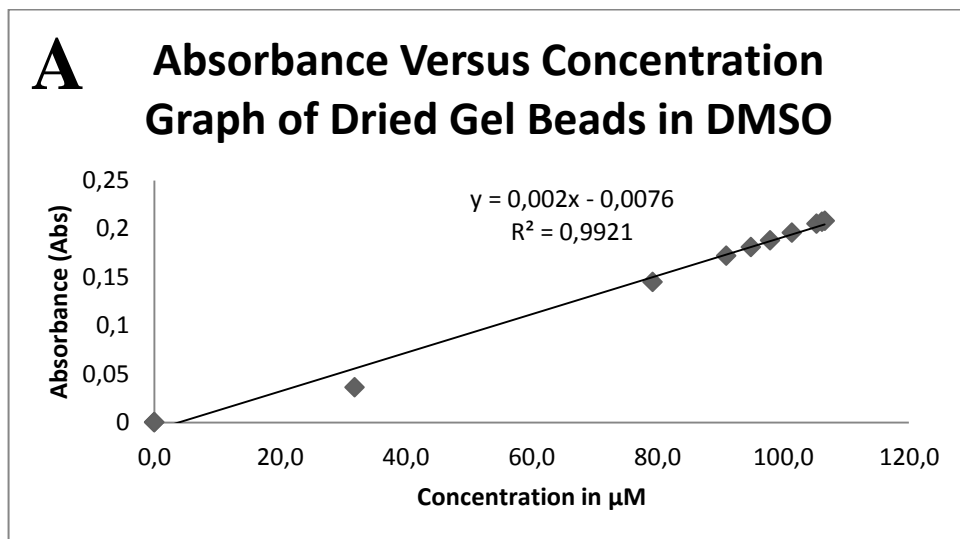
Table 8: Observations from release kinetics studies.

Name of Solution for Release:	Type of Beads:	Observations Criteria:	
		Swelling:	Colour of Beads (after release study)
DMSO	Dried Beads	No observable swelling	still bit yellow
	Cryobeads	No observable swelling	still bit yellow
	Freshly made beads	No observable swelling	colourless
0.9% Saline (10% DMSO)	Dried Beads	No observable swelling	still bit yellow
	Cryobeads	No observable swelling	still bit yellow
	Freshly made beads	No observable swelling	still bit yellow
0.9% Saline (20% DMSO)	Dried Beads	No observable swelling	still bit yellow
	Cryobeads	No observable swelling	still bit yellow
	Freshly made beads	Yes observable swelling	still bit yellow
0.9% Saline (40% DMSO)	Dried Beads	No observable swelling	still bit yellow
	Cryobeads	No observable swelling	still bit yellow
	Freshly made beads	Yes observable swelling	colourless
MHB (10% DMSO)	Dried Beads	Yes observable swelling	still bit yellow and brown coat from outside
	Cryobeads	Yes observable swelling	still bit yellow and brown coat from outside
	Freshly made beads	Yes observable swelling	still bit yellow and brown coat from outside
MHB (20% DMSO)	Dried Beads	No observable swelling	still bit yellow and little brown coat from outside
	Cryobeads	Yes observable swelling	still bit yellow and little brown coat from outside
	Freshly made beads	Yes observable swelling	still bit yellow and little brown coat from outside
MHB (40% DMSO)	Dried Beads	No observable swelling	still bit yellow and no brown coat from outside
	Cryobeads	No observable swelling	still bit yellow and no brown coat from outside
	Freshly made beads	Yes observable swelling	still bit yellow and no brown coat from outside
RPMI1640	Dried Beads	Yes observable swelling	still bit yellow
	Cryobeads	Yes observable swelling	still bit yellow
	Freshly made beads	Yes observable swelling	still bit yellow

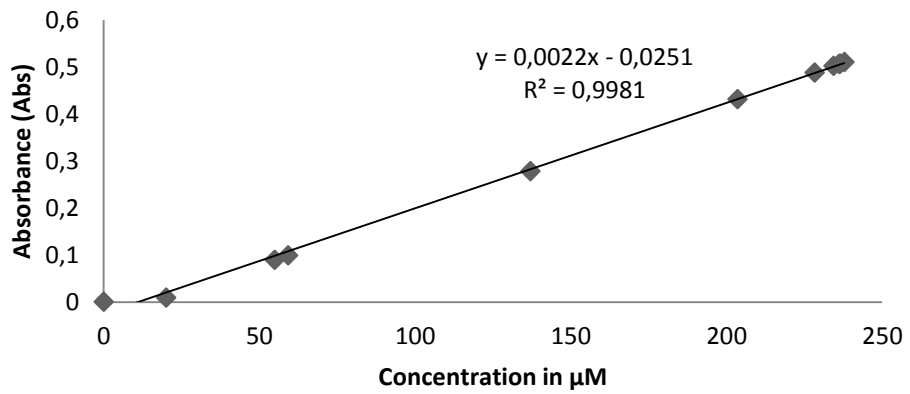
#### 4.8.2 Absorbance Versus Concentration and Concentration Versus Time Graphs

In order to determine the amount of quercetin in terms of concentration (in  $\mu\text{M}$ ), both the calibration curves (absorbance versus concentration graphs of known concentration of quercetin solution in desired solvents) and release graphs for quercetin (Absorbance versus time graphs) were required and they were precalculated. To find the concentration of quercetin corresponds to the absorbance values from release graphs; the absorbance value from the release graphs should be substituted as y value into linear equation of calibration curve. For instance, for DMSO, linear equation of calibration curve is  $y=0,0023x-0,0372$ . x value is the concentration and y value is the absorbance. Therefore, to find the concentration of specific known absorbance, the equation should be rearranged as  $x=(y+0,0372)/0,0023$ , so that x value will give the concentration correspond to the absorbance. In addition to absorbance versus concentration curves, concentration versus time graphs

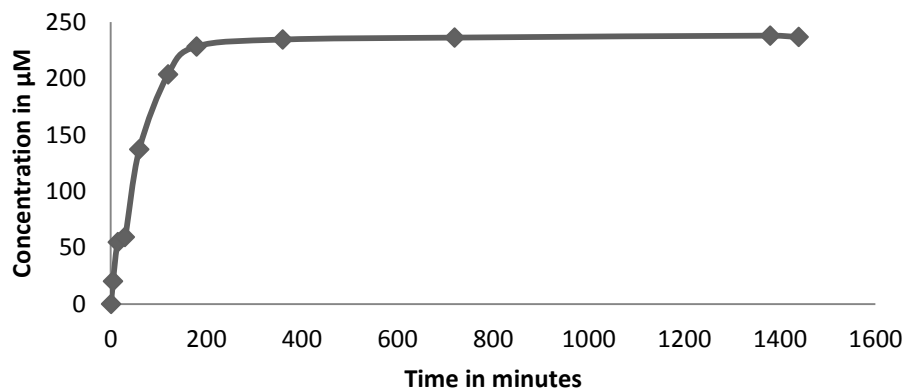
can also be constructed by using release graphs and calibration curves (Figure 29, Figure 30, Figure 31, Figure 32, Figure 33, Figure 34 & Figure 35). Based on results shown in Figures between 29 and 35, cryogel beads and gel beads in 40% saline solution with 10% DMSO of total solution were chosen for antimicrobial activity, specifically for time kill assay. Since, MHB was reacting with carboxylate group of alginate beads, it was not chosen for time kill assay. For cell culture application, the concentrations based on release studies from cryogel and gel beads were chosen.



### C Absorbance Versus Concentration Graph of Cryogel Beads in DMSO



### D Concentration Versus Time Graph of Cryogel Beads in DMSO



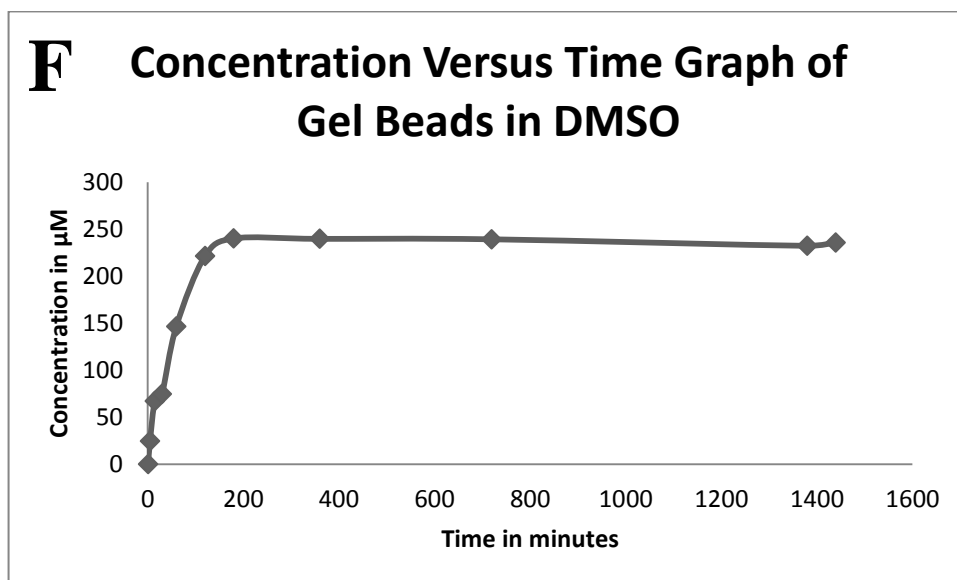
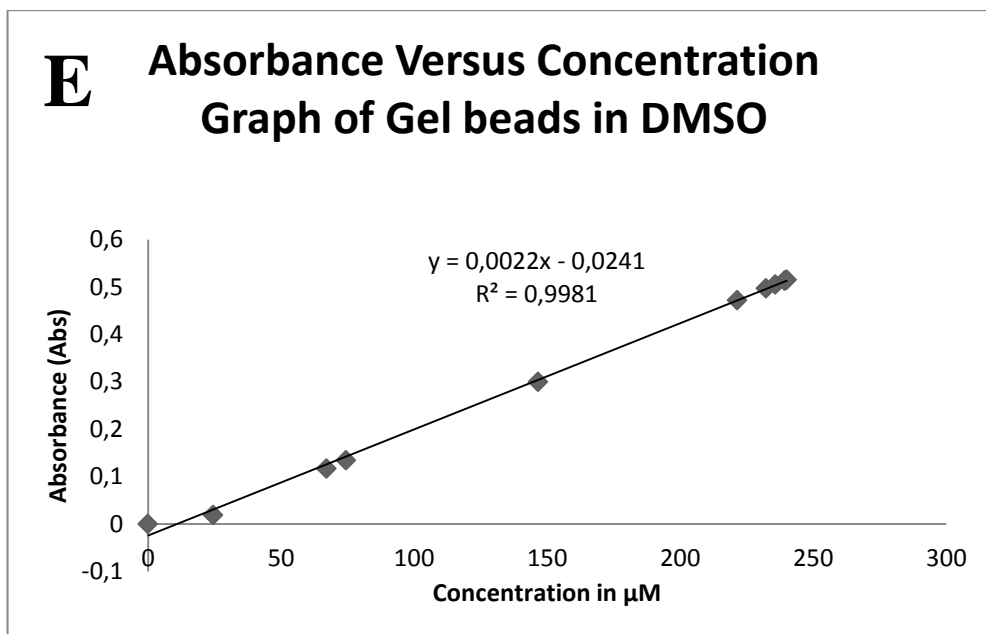


Figure 29: Absorbance versus concentration and concentration versus time graphs of quercetin in DMSO.

Note: (A) Absorbance versus concentration graph of dried gel beads in DMSO.(B) Concentration versus time graph of dried gel beads in DMSO.(C) Absorbance versus concentration graph of cryogel beads in DMSO.(D) Concentration versus time graph of cryogel beads in DMSO.(E) Absorbance versus concentration graph of gel beads in DMSO.(F) Concentration versus time graph of gel beads in DMSO.

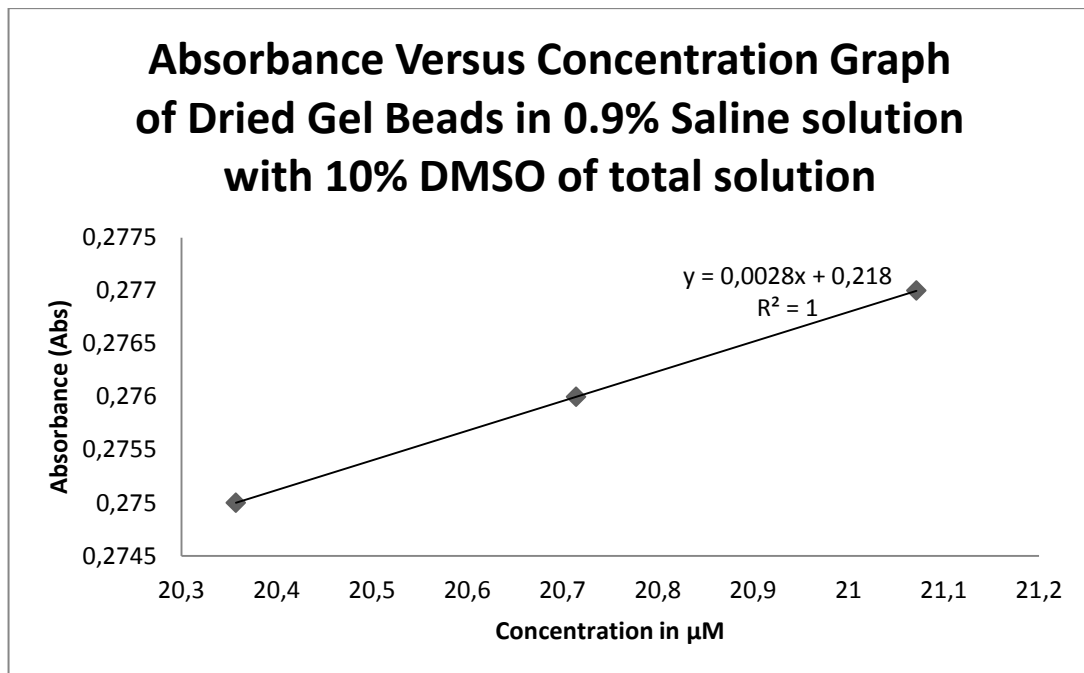
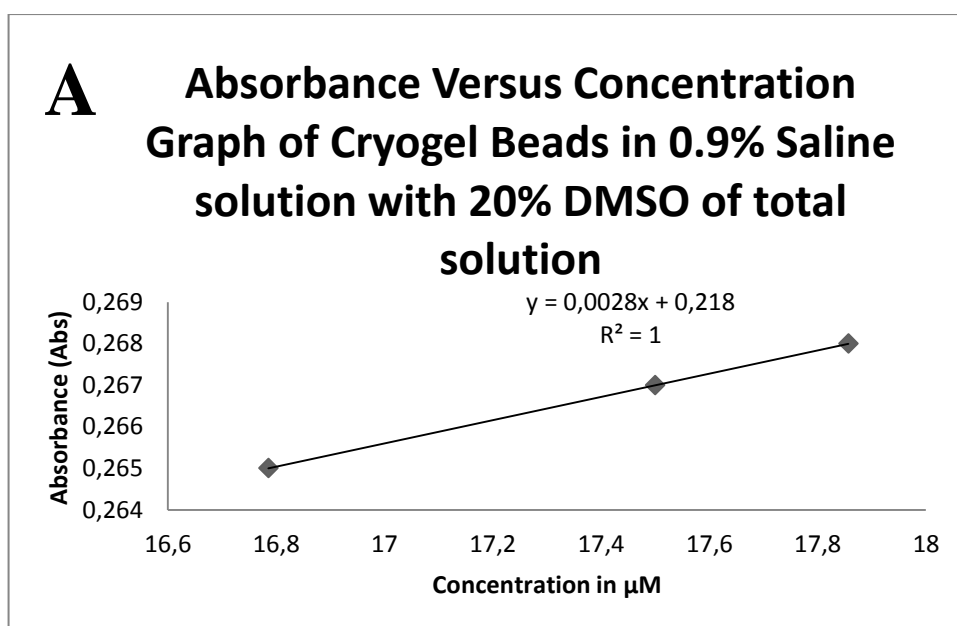
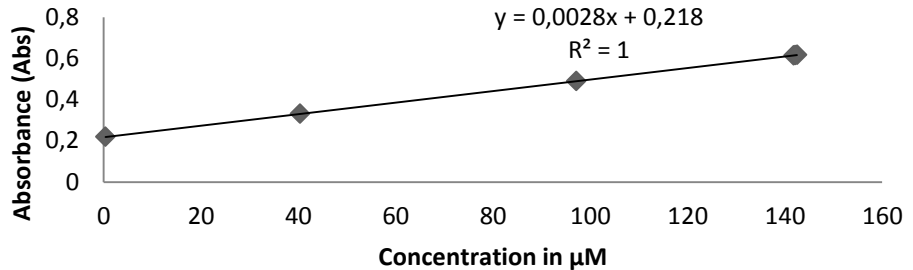


Figure 30: Absorbance versus concentration graph of dried gel beads in 0.9% saline solution with 10% DMSO of total solution.



**B** Absorbance Versus Concentration  
Graph of Gel Beads in 0.9% Saline  
solution with 20% DMSO of total  
solution



**C** Concentration Versus Time Graph of  
Gel beads in 0.9% Saline solution  
with 20% DMSO of total solution

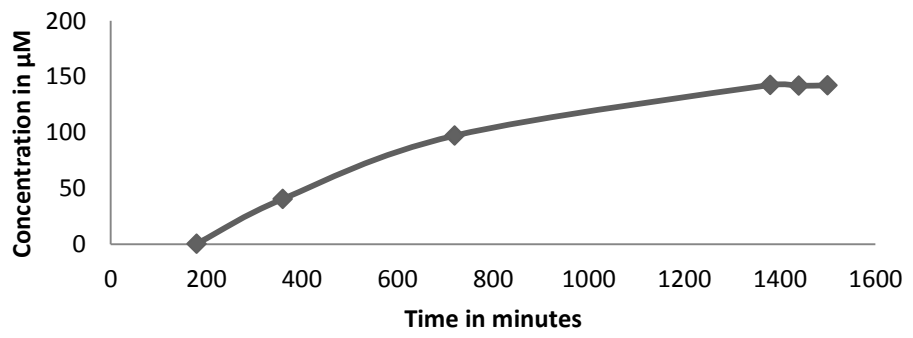
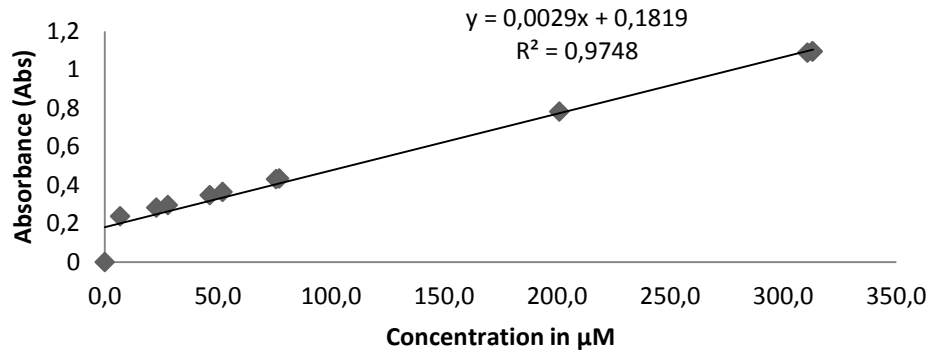


Figure 31: Absorbance versus concentration and concentration versus time graphs of quercetin in 0.9% Saline solution with 20% DMSO of total solution.

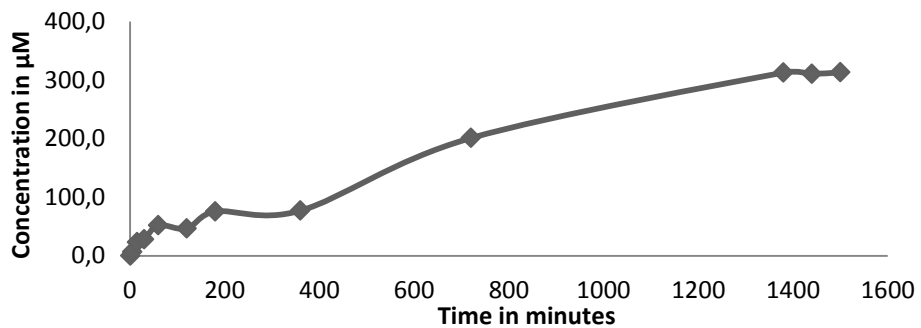
Note: (A) Absorbance versus concentration graph of cryogel beads in in 0.9% Saline solution with 20% DMSO of total solution. (B) Absorbance versus concentration graph of gel beads in 0.9% Saline solution with 20% DMSO of total solution. (C) Concentration versus time graph of gel beads in DMSO.

**A**

### Absorbance Versus Concentration Graph of Dried Gel Beads in 0.9% Saline solution with 40% DMSO of total solution

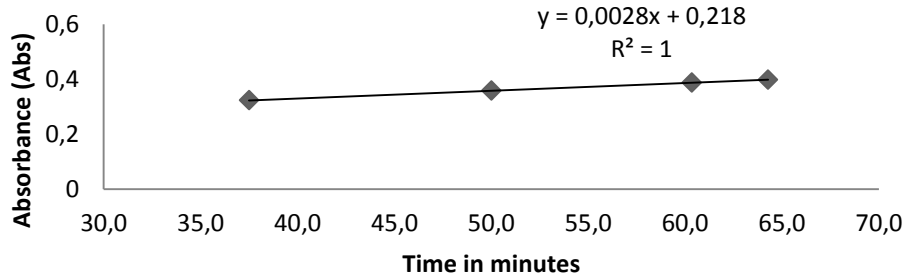
**B**

### Concentration Versus Time Graph of Dried Gel Beads in 0.9% Saline solution with 40% DMSO of total solution

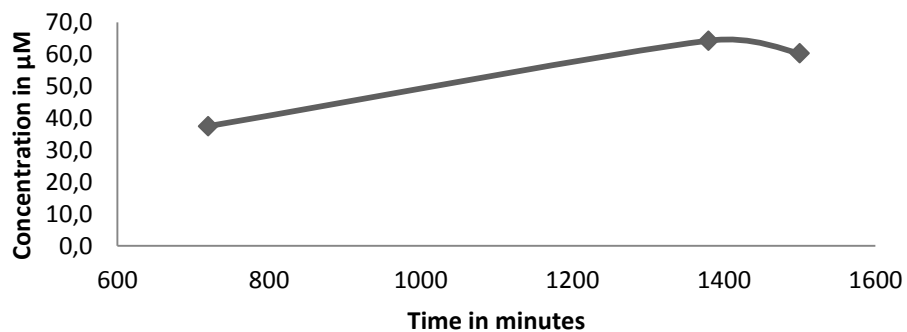


**C**

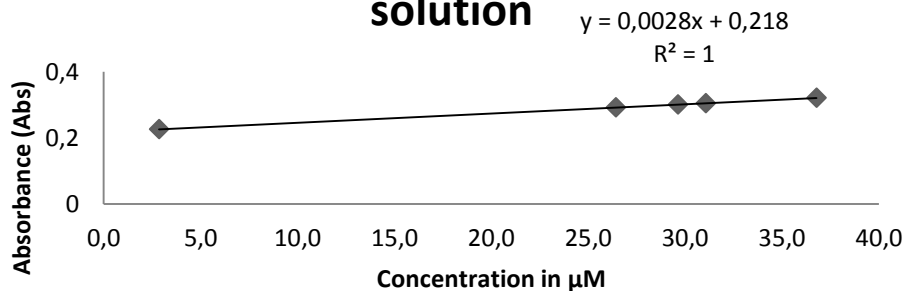
### Absorbance Versus Concentration Graph of Cryogel Beads in 0.9% Saline solution with 40% DMSO of total solution

**D**

### Concentration Versus Time Graph of Cryogel Beads in 0.9% Saline solution with 40% DMSO of total solution

**E**

### Absorbance Versus Concentration Graph of Gel beads in 0.9% Saline solution with 40% DMSO of total solution





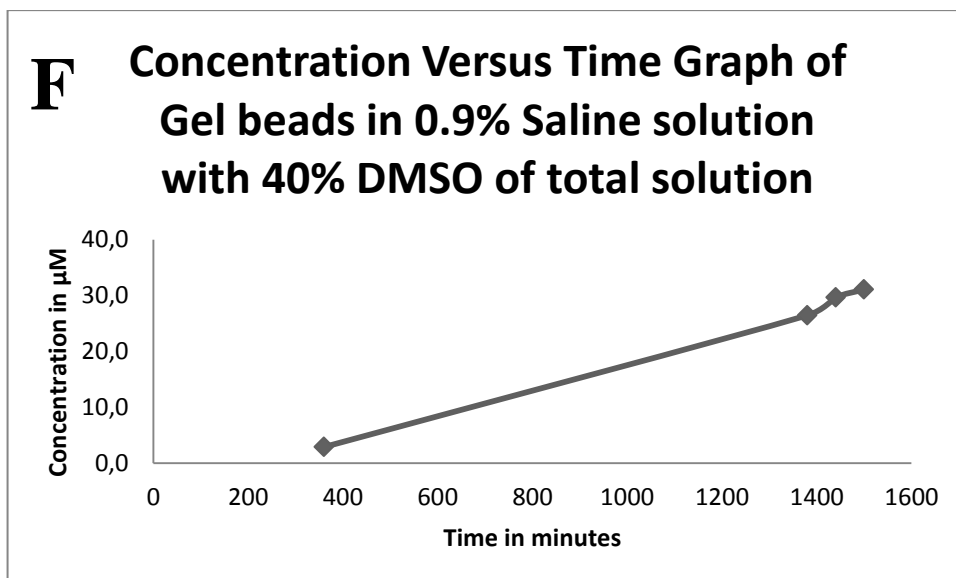


Figure 32: Absorbance versus concentration and concentration versus time graphs of quercetin in 0.9% Saline solution with 40% DMSO of total solution.

Note: (A) Absorbance versus concentration graph of dried beads in 0.9% Saline solution with 40% DMSO of total solution. (B) Concentration versus time graph of dried beads in 0.9% Saline solution with 40% DMSO of total solution. (C) Absorbance versus concentration graph of cryobeads in 0.9% Saline solution with 40% DMSO of total solution. (D) Concentration versus time graph of cryobeads in 0.9% Saline solution with 40% DMSO of total solution. (E) Absorbance versus concentration graph of new beads in 0.9% Saline solution with 40% DMSO of total solution. (F) Concentration versus time graph of new beads in 0.9% Saline solution with 40% DMSO of total solution.

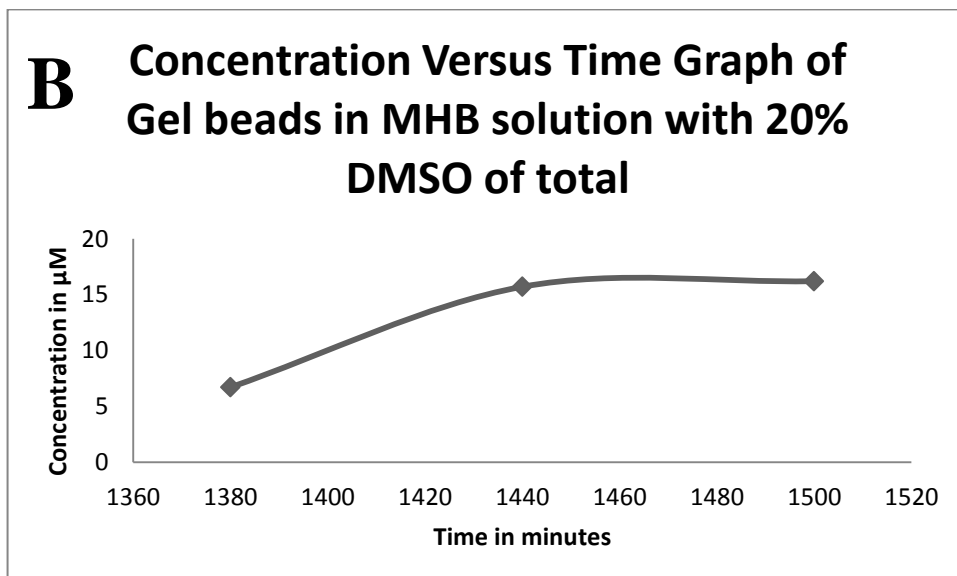
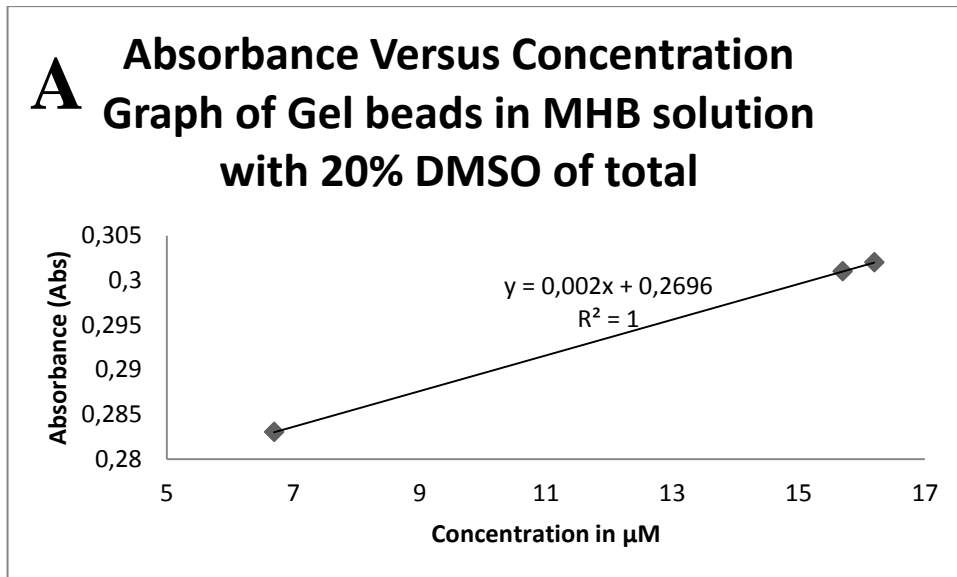
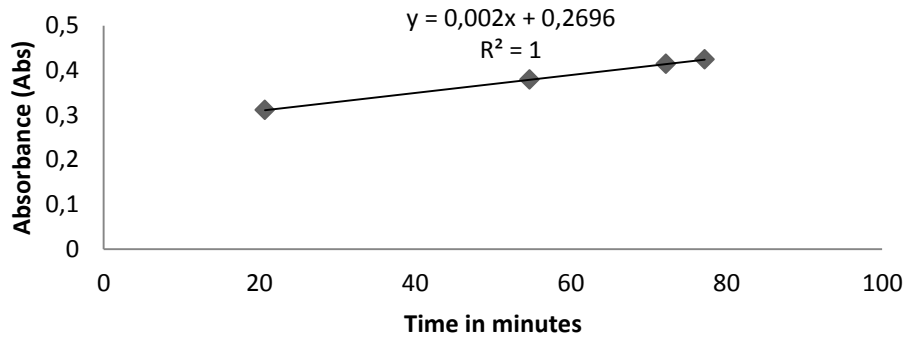


Figure 33: Absorbance versus concentration and concentration versus time graphs of quercetin in MHB solution with 20% DMSO of total solution.

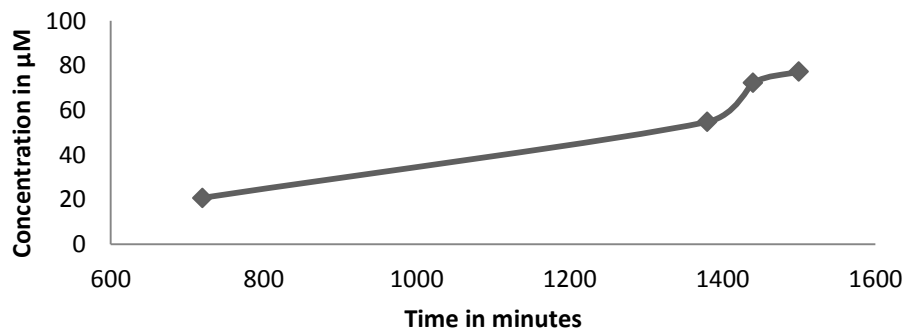
Note: (A) Absorbance versus concentration graph of new beads in MHB solution with 20% DMSO of total solution. (B) Concentration versus time graph of new beads in MHB solution with 20% DMSO of total solution.

**A**

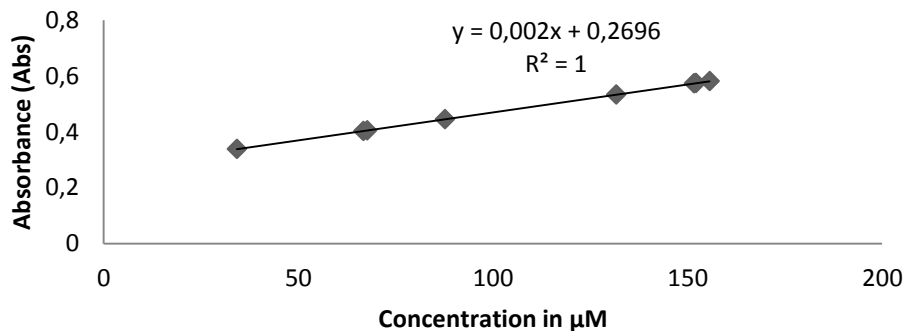
### Absorbance Versus Concentration Graph of Dried Gel Beads in MHB solution with 40% DMSO of total

**B**

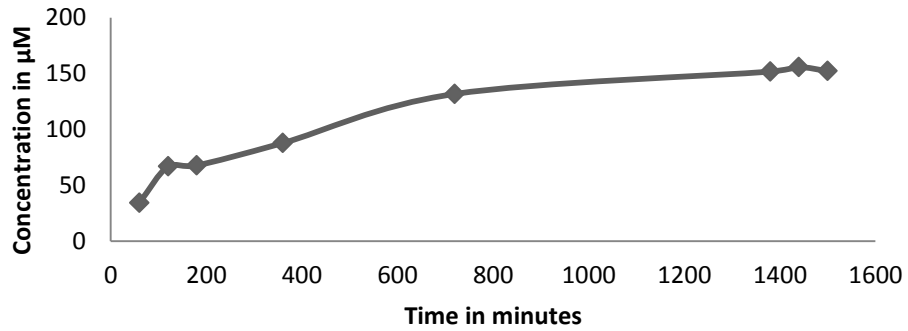
### Concentration Versus Time Graph of Dried Gel Beads in MHB solution with 40% DMSO of total

**C**

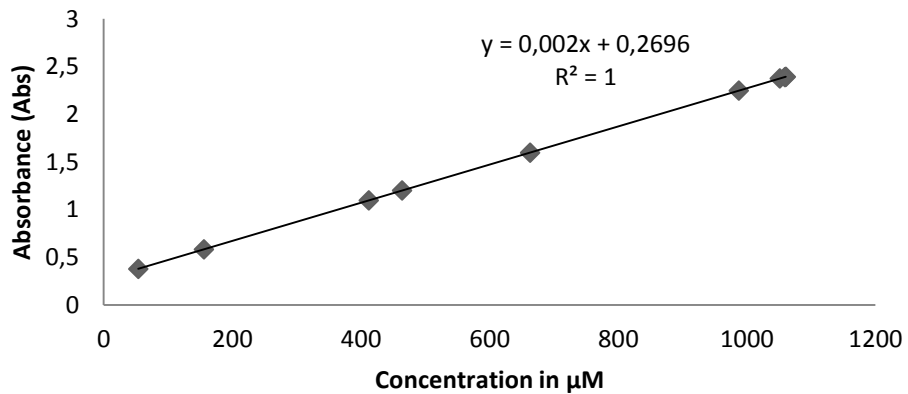
### Absorbance Versus Concentration Graph of Cryogel Beads in MHB solution with 40% DMSO of total



**D** Concentration Versus Time Graph of Cryogel Beads in MHB solution with 40% DMSO of total



**E** Absorbance Versus Concentration Graph of Gel beads in MHB solution with 40% DMSO of total



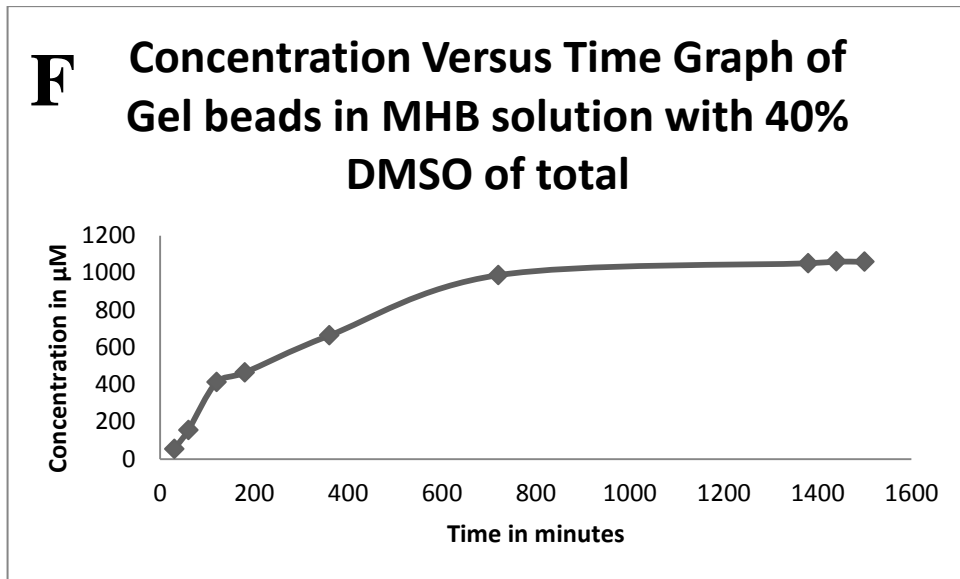
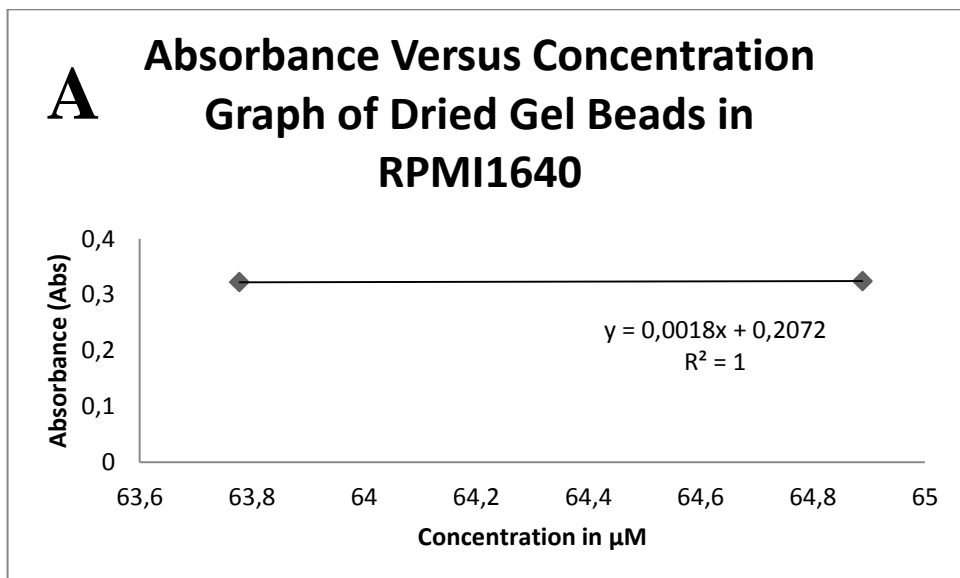
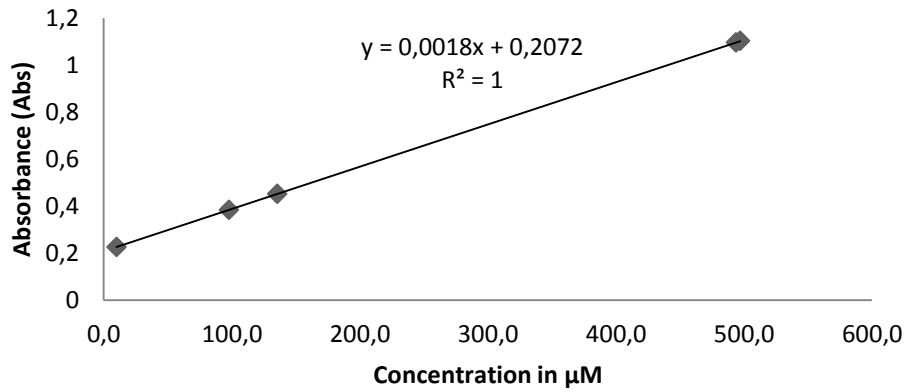


Figure 34: Absorbance versus concentration and concentration versus time graphs of quercetin in MHB solution with 40% DMSO of total solution.

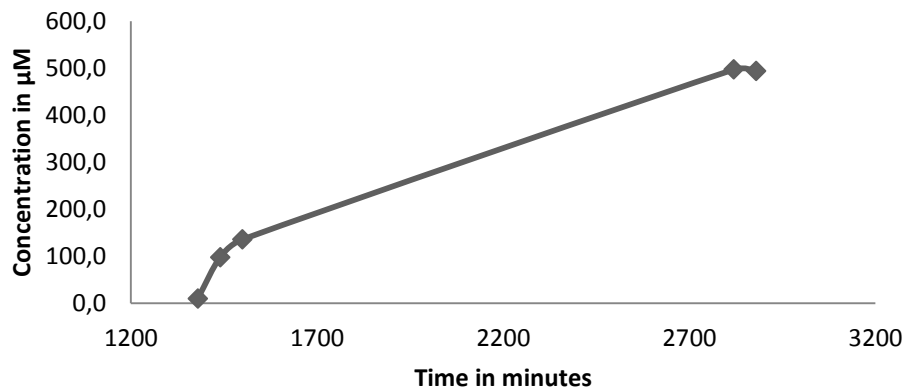
Note: (A) Absorbance versus concentration graph of dried gel beads in MHB solution with 40% DMSO of total solution. (B) Concentration versus time graph of dried gel beads in MHB solution with 40% DMSO of total solution. (C) Absorbance versus concentration graph of cryogel beads in MHB solution with 40% DMSO of total solution. (D) Concentration versus time graph of cryogel beads in MHB solution with 40% DMSO of total solution. (E) Absorbance versus concentration graph of gel beads in MHB solution with 40% DMSO of total solution. (F) Concentration versus time graph of gel beads in MHB solution with 40% DMSO of total solution.



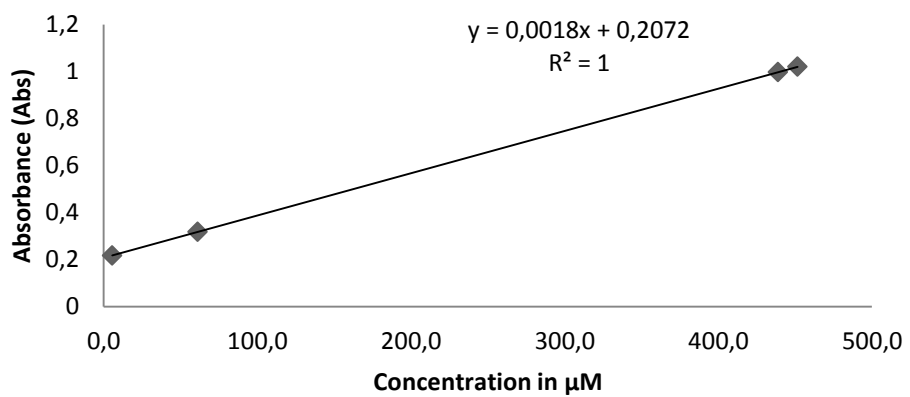
### **B** Absorbance Versus Concentration Graph of Cryogel Beads in RPMI1640



### **C** Concentration Versus Time Graph of Cryogel Beads in RPMI1640



### **D** Absorbance Versus Concentration Graph of Gel beads in RPMI1640



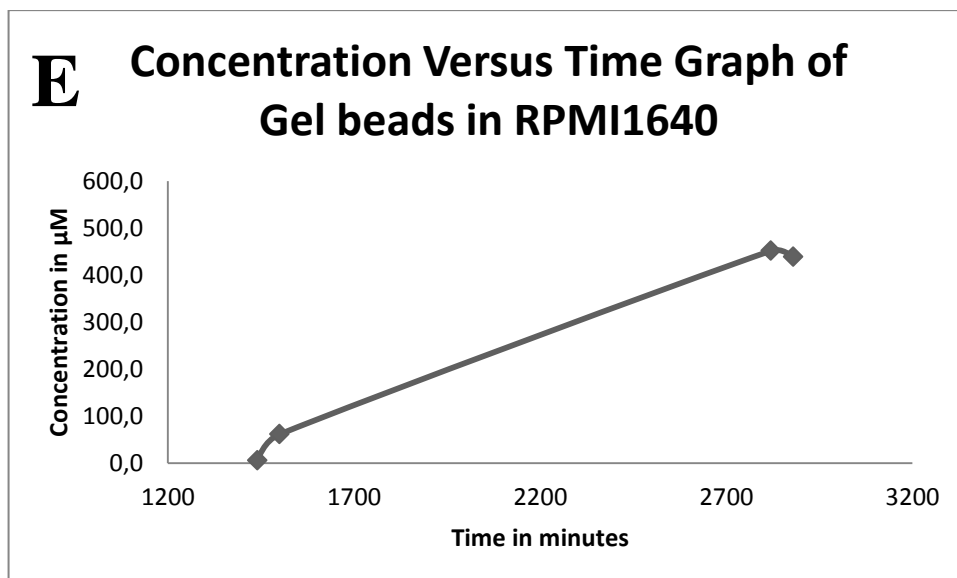


Figure 35: Absorbance versus concentration and concentration versus time graphs of quercetin in RPMI-1640.

Note: (A) Absorbance versus concentration graph of dried gel beads in RPMI-1640. (B) Absorbance versus concentration graph of cryogel beads in RPMI-1640. (C) Concentration versus time graph of cryogel beads in RPMI-1640. (D) Absorbance versus concentration graph of new beads in RPMI-1640. (E) Concentration versus time graph of new beads in RPMI-1640.

### 4.8.3 Release Kinetics Models

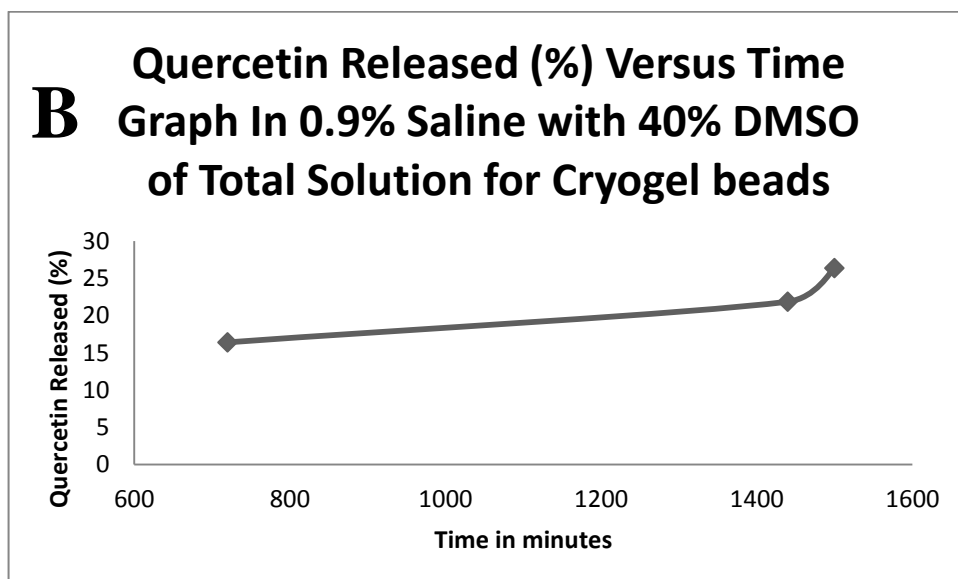
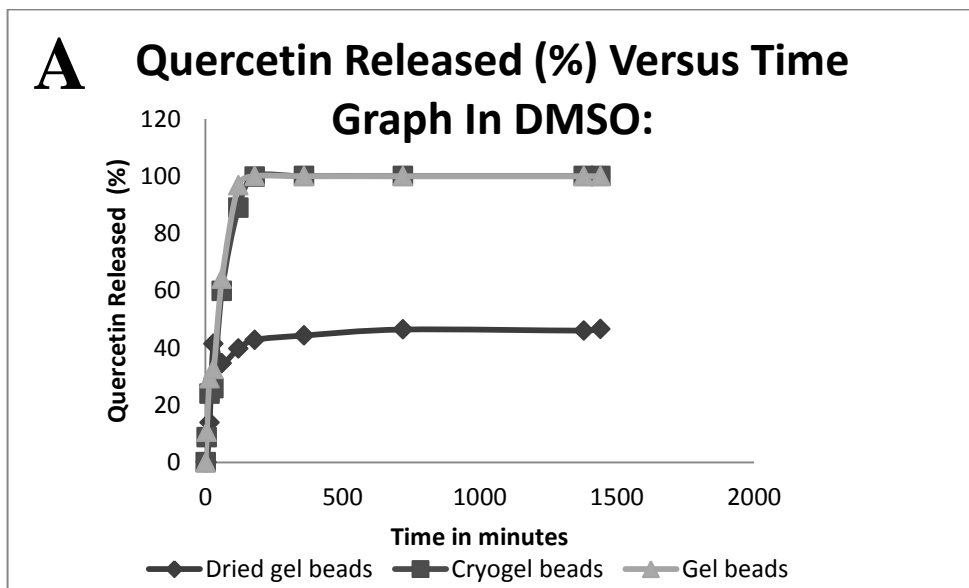
#### 4.8.3.1 Percent Quercetin Released Results

The percent quercetin released was studied for three selected release media, which are DMSO, 0.9% saline solution with 10% DMSO of total solution for time kill assay and RPMI-1640 for cell culture.

For each selected solvent, the concentration of quercetin released was calculated by using calibration curve. Following to this, to find the mass of quercetin released concentration, molecular mass of quercetin (302.24 g/mol) and volume of release medium were multiplied. Finally, Quercetin released percents were calculated. Quercetin Released (%) Versus Time Graphs were constructed (Figure 36).

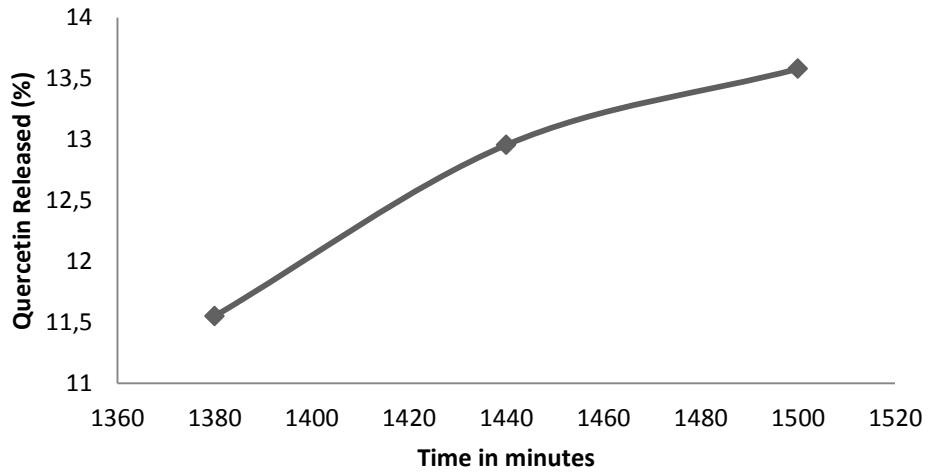
$$\text{Quercetin released (\%)} = (m / m_0) \times 100 \quad (9)$$

Although the quercetin release percents in DMSO were desired, since using pure (100%) DMSO can be toxic for bacteria and cells. 0.9% Saline with 40% DMSO of total solution and RPMI-1640 were chosen for time kill assay and cell culture related assays, respectively. Since, the highest percent release of quercetin were obtained with cryogel and gel beads based on observations and release data, therefore ,cryogel and gel beads are chosen for further bacterial and cell culture tests.

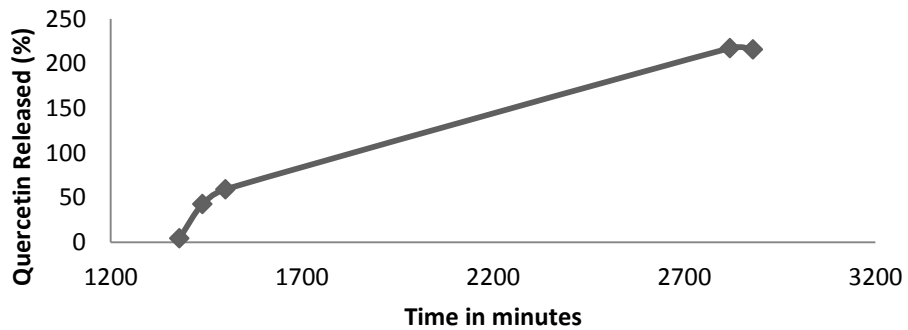




**C** Quercetin Released (%) Versus Time  
Graph In 0.9% Saline with 40% DMSO  
of Total Solution for Gel Beads



**D** Quercetin Released (%) Versus Time  
Graph In RPMI1640 for Cryogel  
Beads:



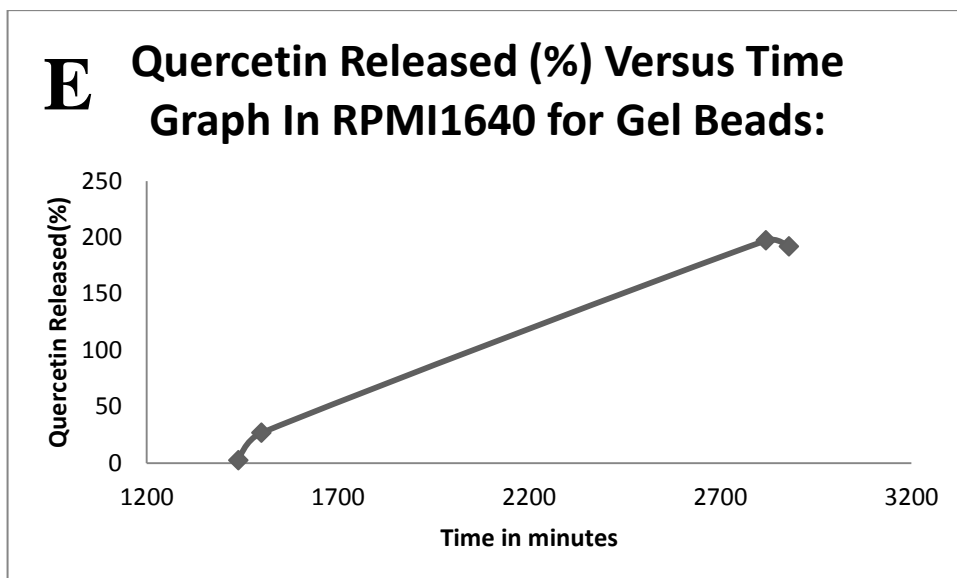


Figure 36: Quercetin released (%) graphs.

Note: (A) Quercetin released (%) versus time graph in DMSO. (B) Quercetin released (%) versus time graph in 0.9% saline with 40% DMSO of total solution for cryogel beads. (C) Quercetin released (%) versus time graph in 0.9% saline with 40% DMSO of total solution for gel beads. (D) Quercetin released (%) versus time graph in RPMI-1640 for cryogel beads. (E) Quercetin released (%) versus time graph in RPMI-1640 for gel beads.

#### 4.8.3.2 Results of Release Kinetics of Quercetin from Alginate Beads

Table 9: Parameters table for four different models.

Release Medium	Types of the Beads	Release Models								
		Zero Order Release Model		First Order Release Model		Higuchi Release Model		Korsmeyer-Peppas Release Model		
		$R^2$	$K_0$	$R^2$	$K_1$	$R^2$	$k_H$	$R^2$	$k_p$	$n$
DMSO	Dried gel beads	0,5646	19,332	0,5629	0,2428	0,7142	37,139	0,5547	1,84458	0,4285
	Cryogel beads	0,9608	43,643	0,9817	1,0953	0,9727	75,008	0,9685	1,41449	0,7191
	Gel beads	0,9569	46,449	0,9504	1,6746	0,9765	80,144	0,9741	1,38053	0,6755
0.9% Saline with 40% DMSO of Total Solution	Cryogel beads	0,8481	1,6963	0,9192	0,0495	0,8638	9,3612	0,7782	0,89068	0,6134
	Gel beads	0,6518	1,3112	0,7121	0,0293	0,7367	7,6224	0,6799	4,47063	1,4214
RPMI-1640	Cryogel beads	0,9321	5,4279	0,7755	0,0386	0,7744	35,077	0,6736	6,438656	3,5072
	Gel beads	0,8887	4,7946	0,7894	0,0203	0,7098	30,379	0,8122	16,2626924	4,9256

Table 10: Types of release mechanism can be determined based on release exponent (n).

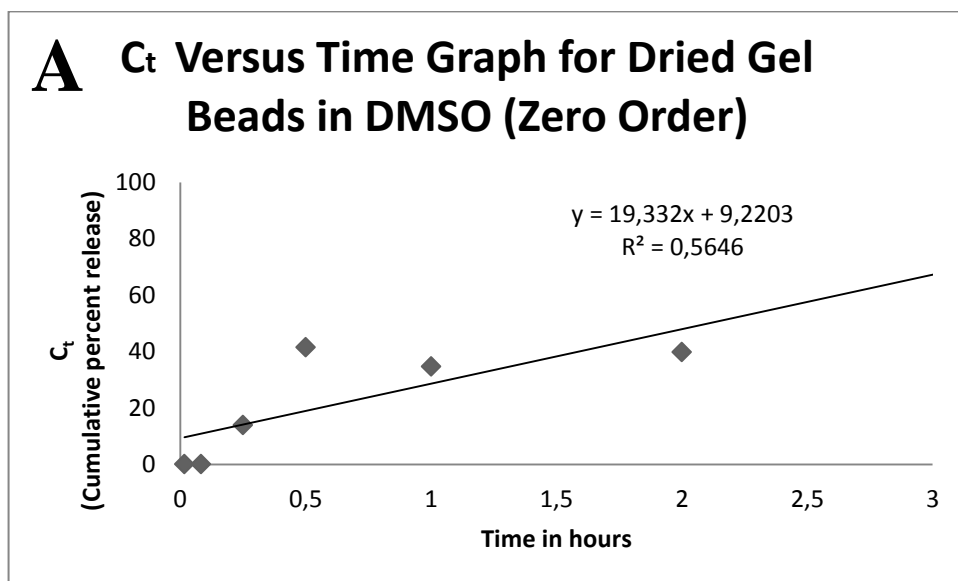
Release exponent (n)	Mechanism of release
<0.45	Both fickian and non-fickian diffusion (Quasi Fickian)
0.5	Fickian Diffusion
0.45<n<0.89	Non-fickian
n=0.89	Case II transport
0.89<n	Super case II transport

The release modellings of quercetin from dried gel beads, cryogel beads and gel beads were studied by using four different models; zero order release model, first order release model, higuchi release model and korsmeyer-peppas release model. The best fit lines for each model were represented in Figure 37, 38, 39 and 40. In addition,  $k_0, k_1, k_H, k_P, n$  and all  $R^2$  parameters are given in table 9a. Aim is to

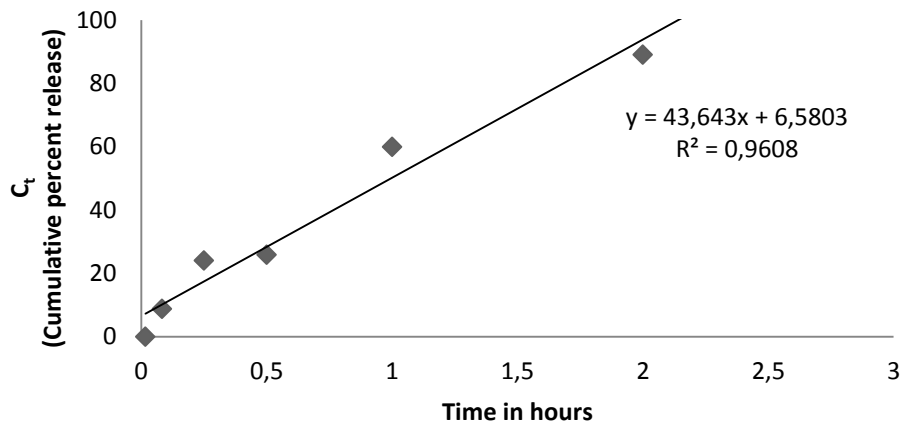
determine the highest  $R^2$  value, the model, which gives the highest  $R^2$  value is the best fit for the bead. According to this table, dried gel beads in DMSO showed the highest  $R^2$  value with zero order release model. This suggest that the release of quercetin was independent from the concentration of quercetin in the beads. Cryogel beads in DMSO showed the highest  $R^2$  value (0.9817) with first order release model. Gel beads in DMSO showed the highest  $R^2$  value (0.9504) with higuchi release model. This suggest that drug concentration was lower in polymer than its solubility and release occurs through the pores in the matrix. In addition, cryogel beads and gel beads in 0.9% saline with 40% DMSO of total solution showed the highest  $R^2$  values with first order release model at 0.9192 and 0.7121, respectively. First order release models were suggesting that the release is dependent on the concentration of quercetin in the bead. It also suggests that the quercetin released in a sustained manner. Cryogel beads and gel beads had the highest  $R^2$  values with zero order release model at 0.9321 and 0.8887 with RPMI-1640. Zero order release model suggesting that quercetin has low solubility and also it suggest that constant release of quercetin per unit time. However, in RPMI-1640, there is no considerable release of quercetin in first 720 minutes. It can be concluded that cryogel beads and gel beads require 720 minutes for the considerable amount of quercetin release. Once the release is started, it will follow the zero order release model up to 48 hours.

n values represent the way of release mechanism of chemical in table 9b. n values for dried gel beads in DMSO is lower than 0.45 indicate that release mechanisms showed both fickian and non-fickian diffusion. This indicates that the chemical in this case quercetin released from non-swell able polymer and during the release studies, it is observed that beads are not swelling in DMSO, however, they do release quercetin through fickian and non-fickian diffusion. n value for cryogel beads and

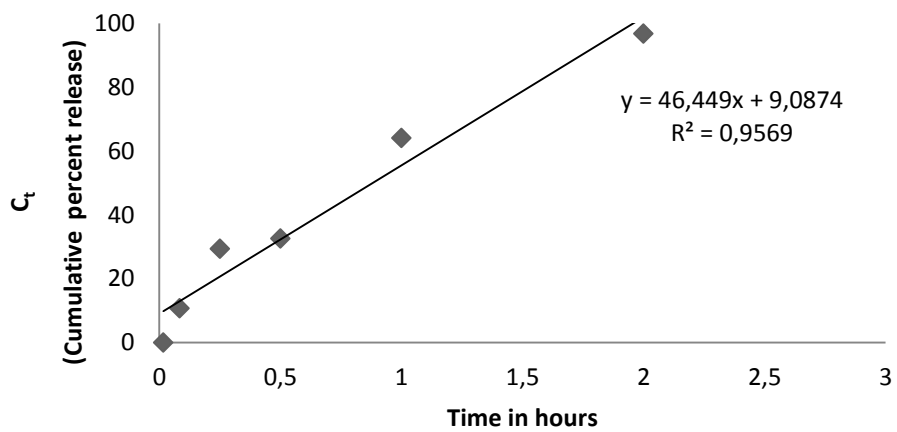
gel beads in DMSO was between 0.45 and 0.89, this indicate non-fickian diffusion. n value for cryogel beads in 0.9% saline with 40% DMSO of total solution is 0,6134, which indicate non-fickian diffusion. Although fickian diffusion has no boundaries, non-fickian dissusion has boundaries between highly swollen and ordered crystalline regions (or dried regions) of the polymer. For gel beads in 0.9% saline with 40% DMSO of total solution, for cryogel beads and gel beads in RPMI-1640, their n values are higher than 1 which indicates super case II transport. This strongly indicate zero order release model. Release from the beads require some times, this time can be required for the swelling of the polymeric material for release of quercetin.



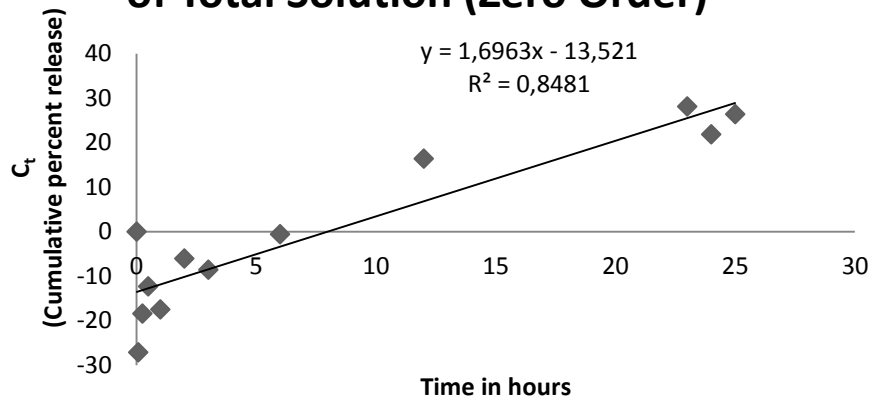
### **B** $C_t$ Versus Time Graph for Cryogel Beads in DMSO (Zero Order)



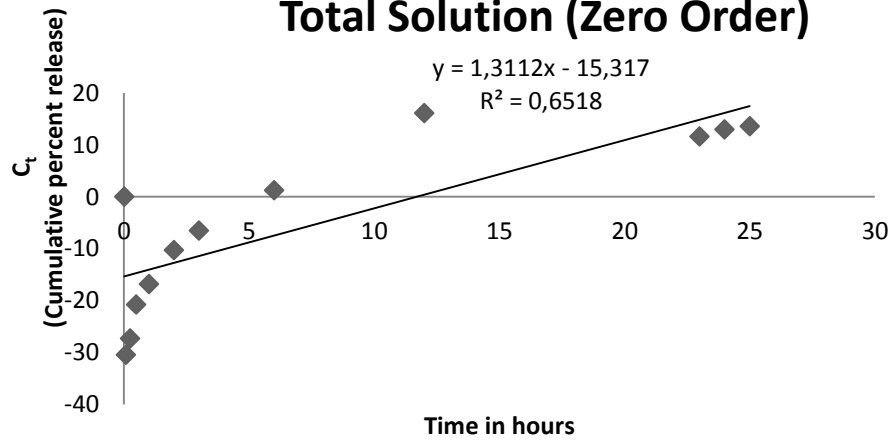
### **C** $C_t$ Versus Time Graph for Gel Beads in DMSO (Zero Order)



**D** **C<sub>t</sub> Versus Time Graph for Cryogel Beads in 0.9% Saline with 40% DMSO of Total Solution (Zero Order)**



**E** **C<sub>t</sub> Versus Time Graph for Gel beads in 0.9% Saline with 40% DMSO of Total Solution (Zero Order)**



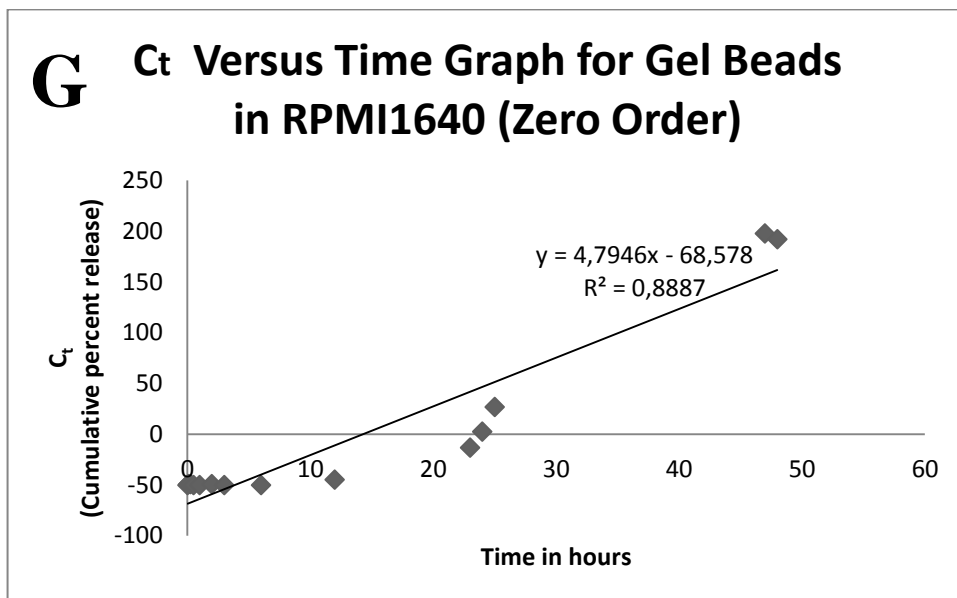
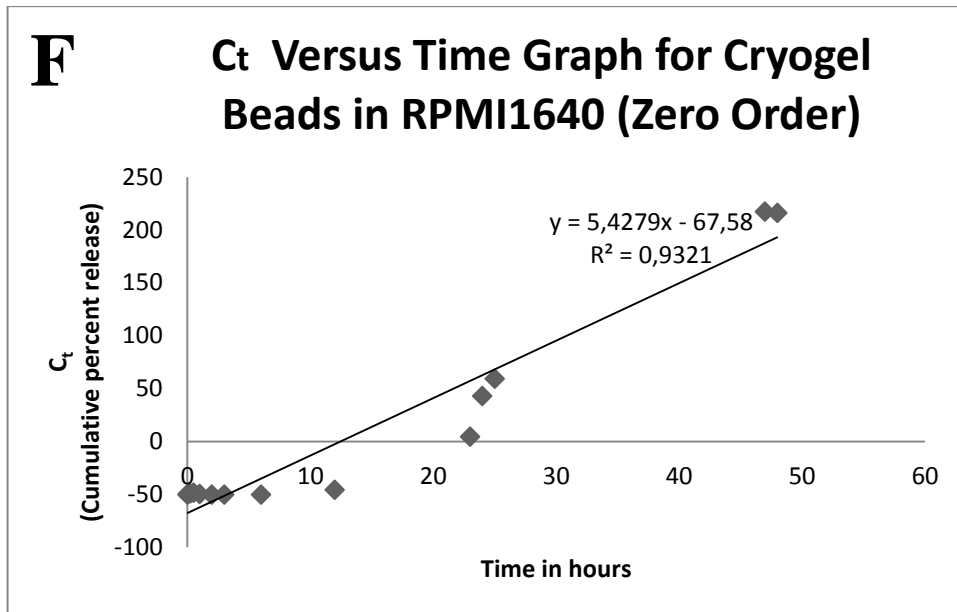
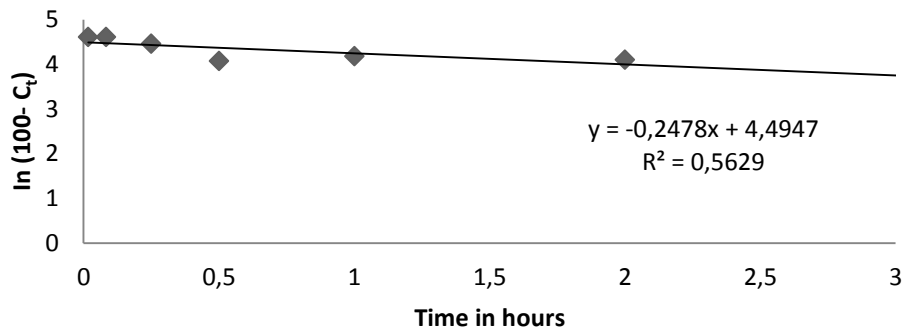


Figure 37: Zero order release models for different types of beads in 3 different types of release media

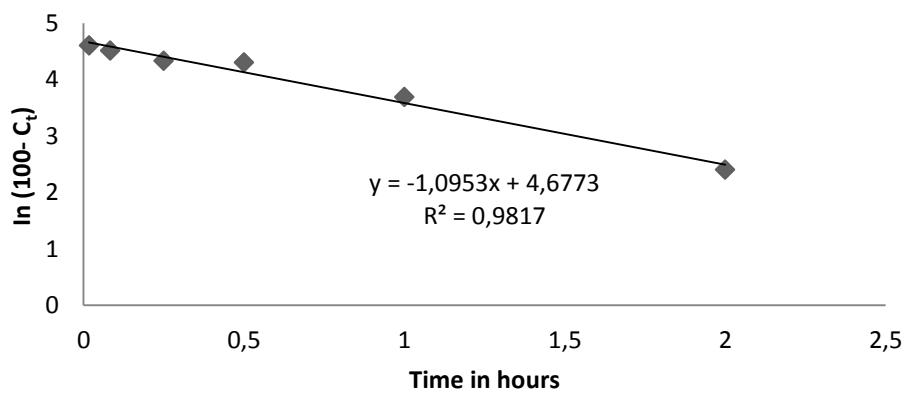
Note: 3 different types of release media; DMSO, 0.9% saline with 40% DMSO of total solution and RPMI-1640.



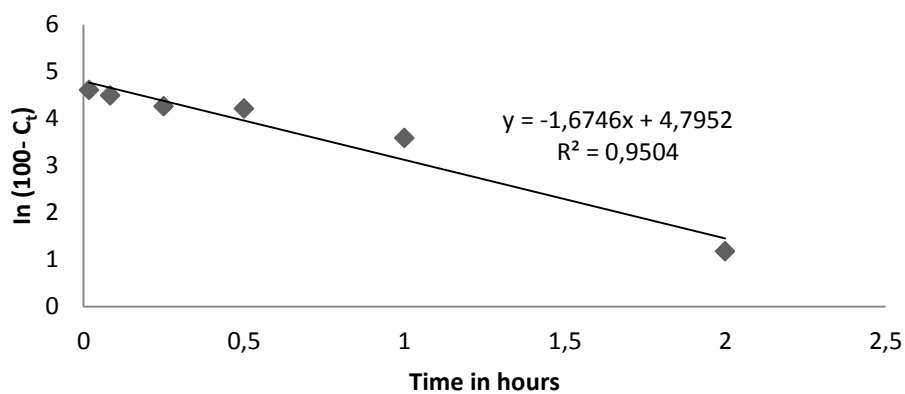
**A** **In (100 - Ct) Versus Time Graph for Dried Gel Beads in DMSO (First Order)**



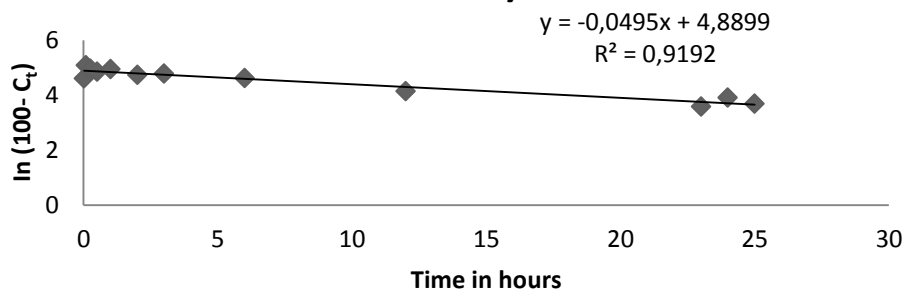
**B** **In (100 - Ct) Versus Time Graph for Cryogel Beads in DMSO (First Order)**



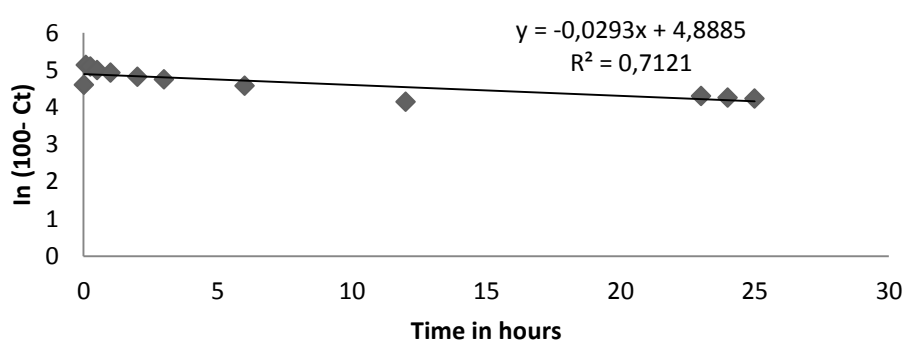
**C** **In (100 - Ct) Versus Time Graph for Gel Beads in DMSO (First Order)**



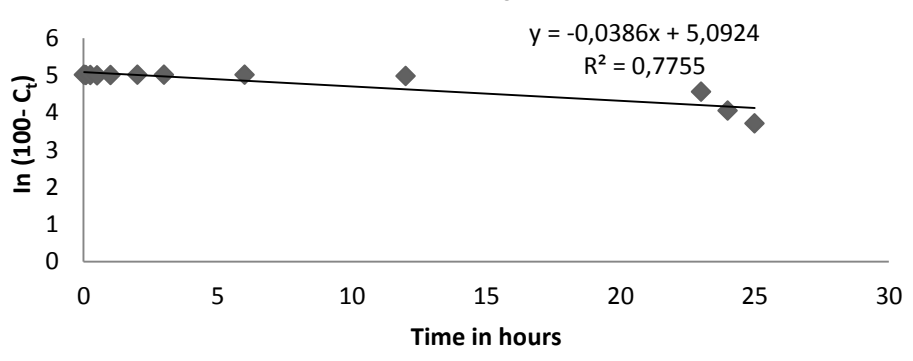
**D** In (100 - Ct) Versus Time Graph for Cryogel Beads in 0.9% Saline with 40% DMSO of Total Solution (First Order)



**E** In (100 - Ct) Versus Time Graph for Gel Beads in 0.9% Saline with 40% DMSO of Total Solution (First Order)



**F** In (100 - Ct) Versus Time Graph for Cryogel Beads in RPMI1640 (First Order)



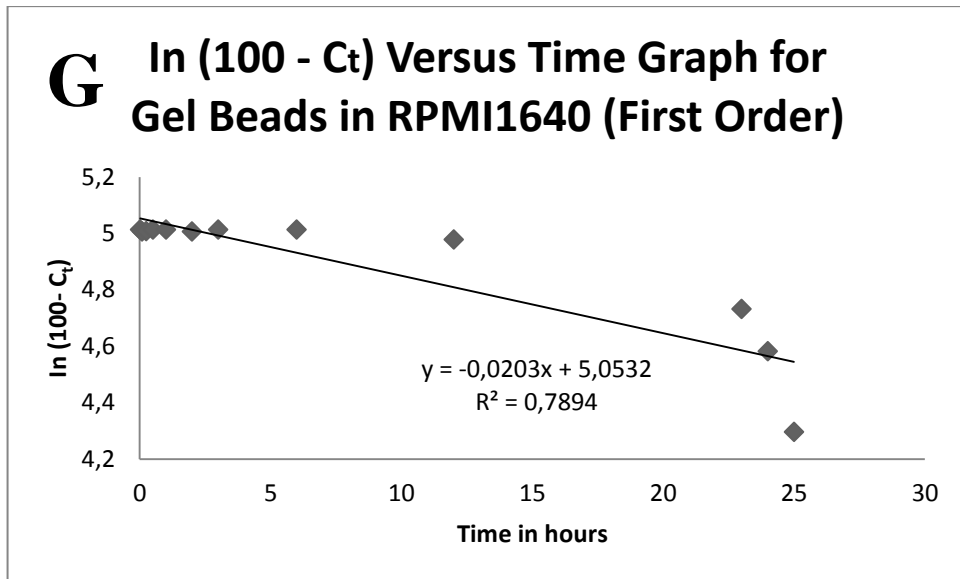
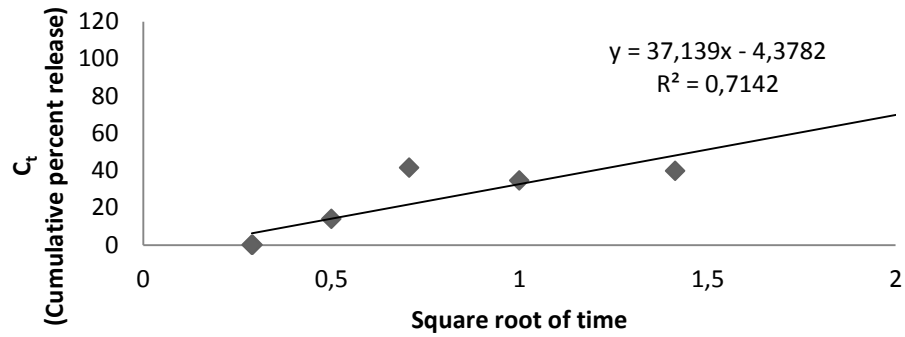


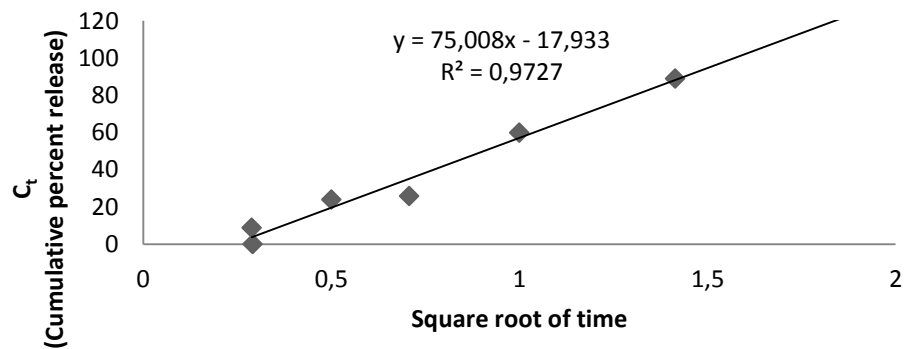
Figure 38: First order release models for different types of beads in 3 different types of release media

Note: 3 different types of release media; DMSO, 0.9% saline with 40% DMSO of total solution and RPMI-1640.

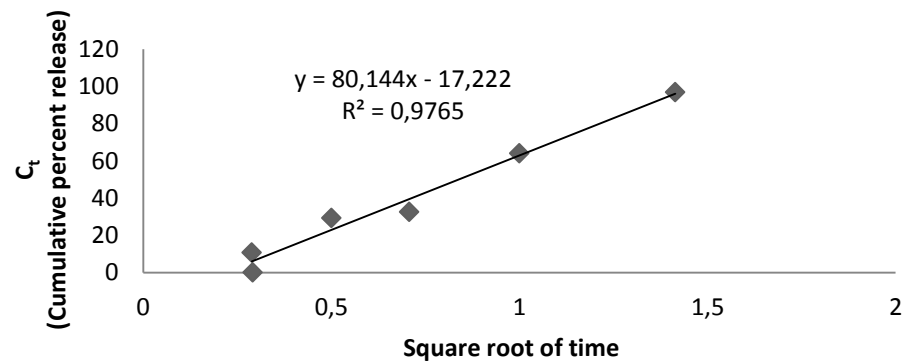
### A $C_t$ Versus Square Root of Time for Dried Gel Beads in DMSO (Higuchi Release Model)



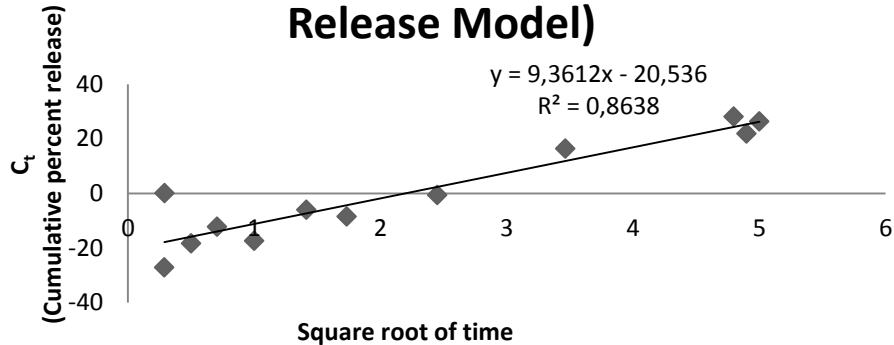
### B $C_t$ Versus Square Root of Time for Cryogel Beads in DMSO (Higuchi Release Model)



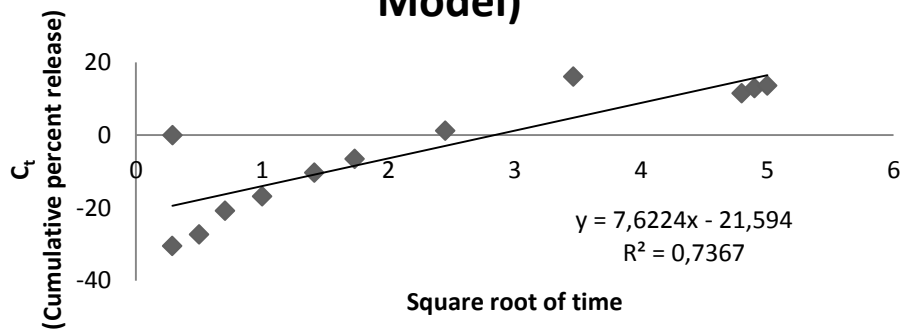
### C $C_t$ Versus Square Root of Time for Gel Beads in DMSO (Higuchi Release Model)



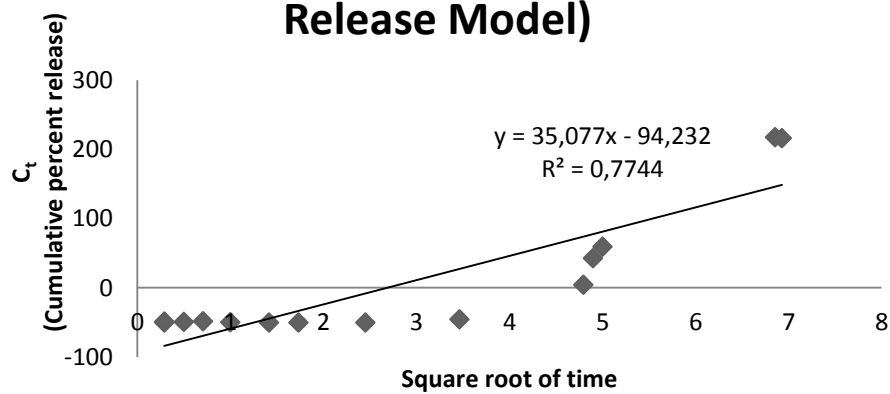
**D**  $C_t$  Versus Square Root of Time for Cryogel Beads in 0.9% Saline with 40% DMSO of Total Solution (Higuchi Release Model)



**E**  $C_t$  Versus Square Root of Time for Gel Beads in 0.9% Saline with 40% DMSO of Total Solution (Higuchi Release Model)



**F**  $C_t$  Versus Square Root of Time for Cryogel Beads in RPMI1640(Higuchi Release Model)



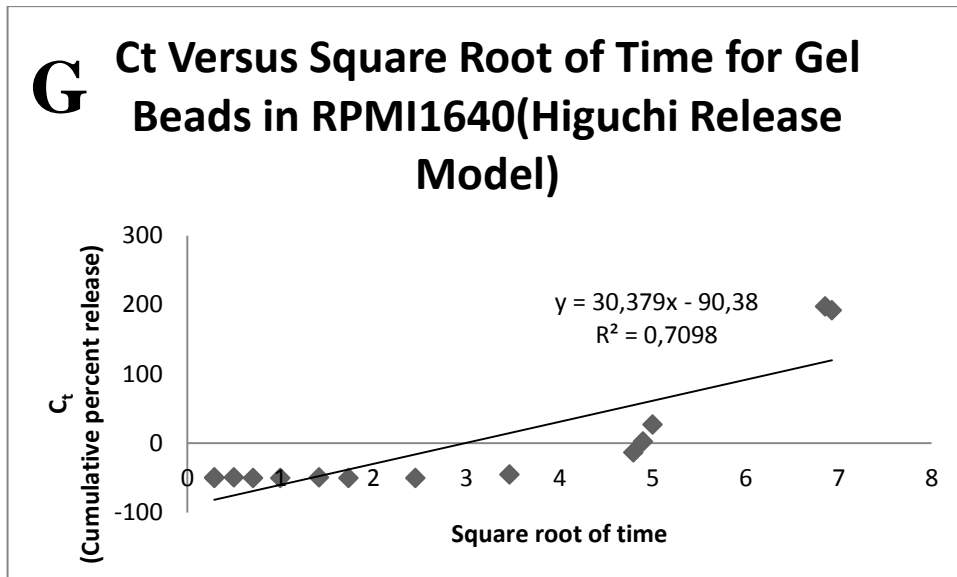
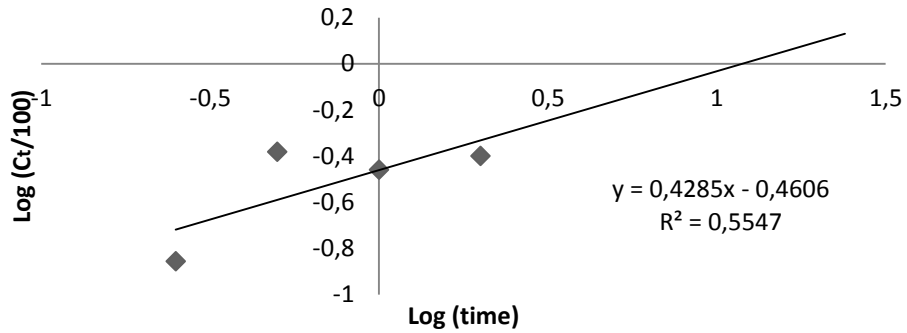


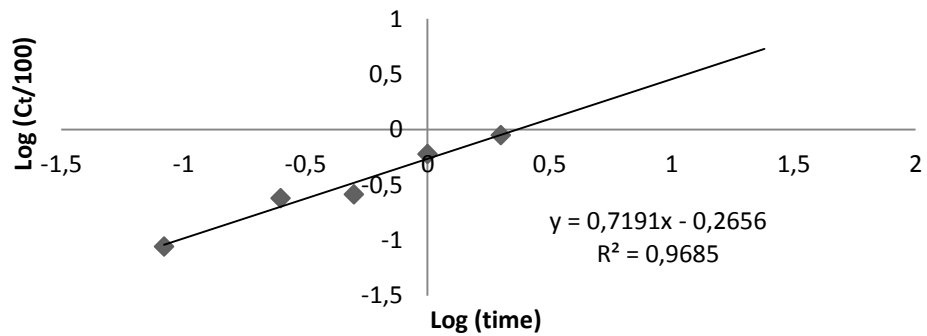
Figure 39: Higuchi Release Models for different types of beads in 3 different types of release media.

Note: 3 different types of release media; DMSO, 0.9% saline with 40% DMSO of total solution and RPMI-1640.

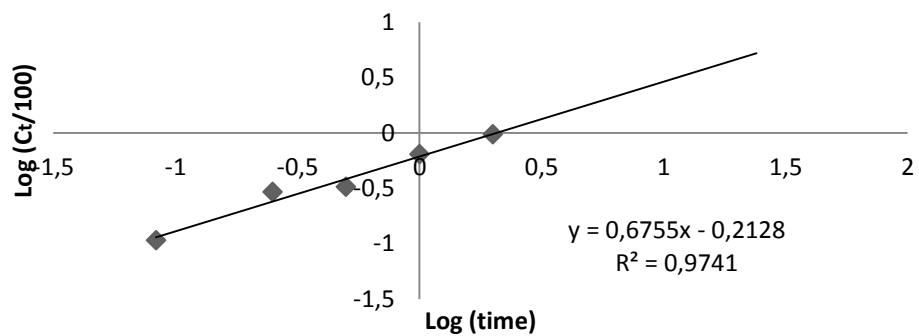
**A** **Log (C<sub>t</sub>/100) Versus Log (time) Graph for Dried Gel Beads in DMSO (Korsmeyer-peppas model)**



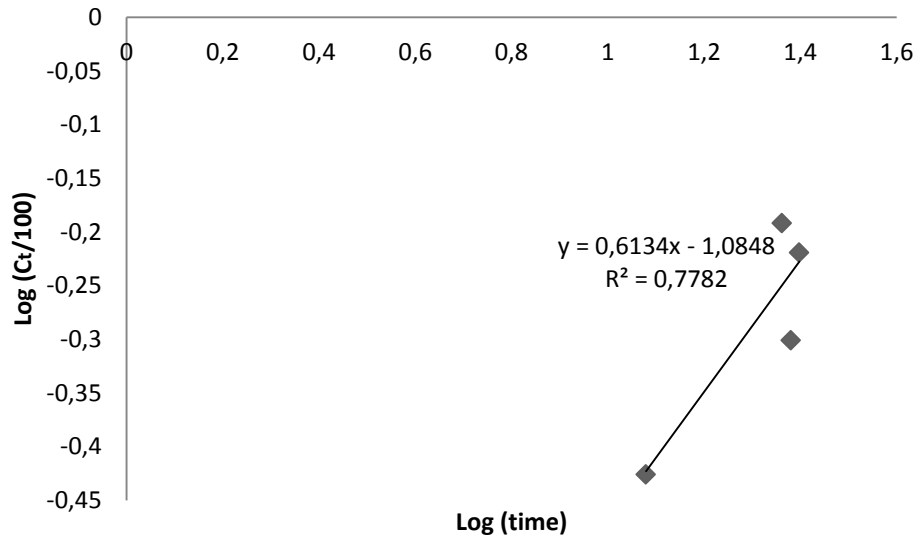
**B** **Log (C<sub>t</sub>/100) Versus Log (time) Graph for Cryogel Beads in DMSO (Korsmeyer-peppas model)**



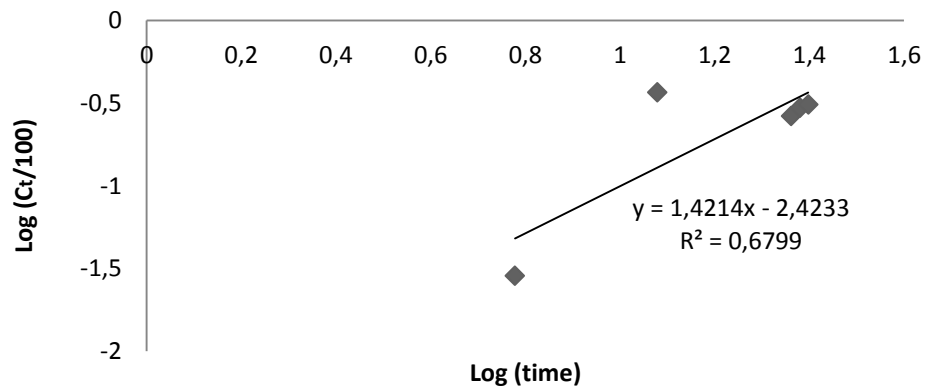
**C** **Log (C<sub>t</sub>/100) Versus Log (time) Graph for Gel Beads in DMSO (Korsmeyer-peppas model)**



**D** Log (C<sub>t</sub>/100) Versus Log (time) Graph for Cryogel Beads in 0.9% Saline with 40% DMSO of Total Solution (Korsmeyer-peppas model)



**E** Log (C<sub>t</sub>/100) Versus Log (time) Graph for Gel Beads in 0.9% Saline with 40% DMSO of Total Solution (Korsmeyer-peppas model)





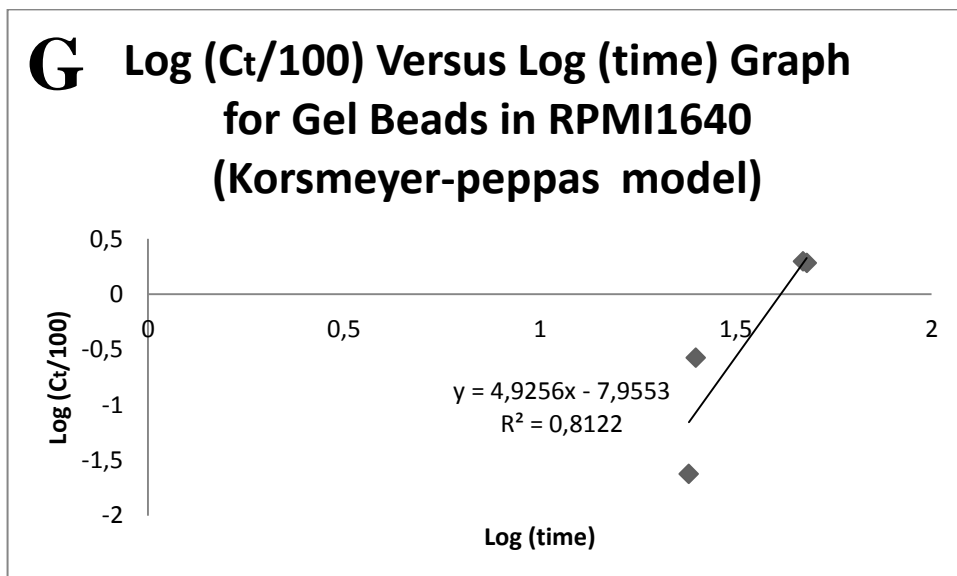
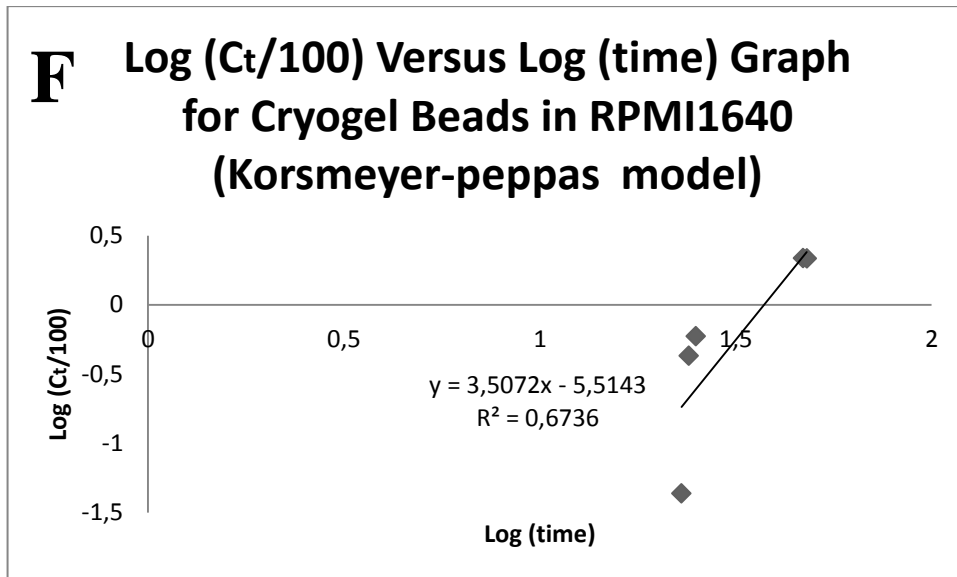


Figure 40: Korsmeyer-peppas models for different types of beads in 3 different types of release media

Note: 3 different types of release media; DMSO, 0.9% saline with 40% DMSO of total solution and RPMI-1640.

## 4.9 MTT Assay (Succinate Dehydrogenase Activity Assay) and IC50

### Determination

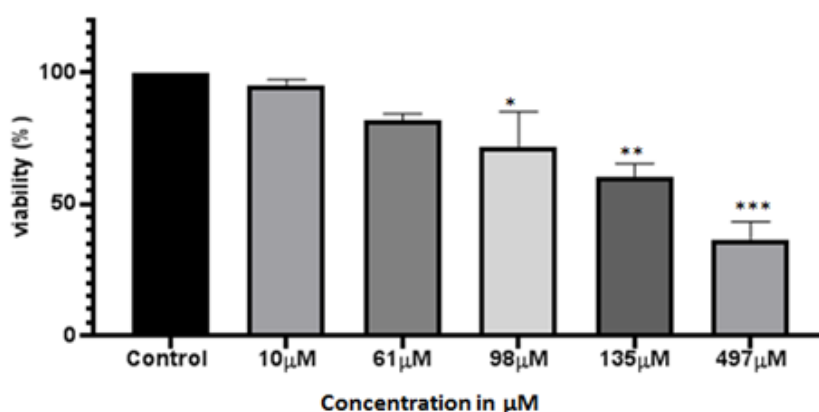
Cell viability and cell proliferation can be determined by conducting MTT Assay. Based on release studies nine different concentration of quercetin from alginate beads were selected to investigate their effects on the papillary thyroid cancer cells (B-CPAP). These concentrations were 5,10,61,98,135,439,452,494 and 497  $\mu\text{M}$  quercetin. Some of these concentrations with unexpected results were omitted from the results to have optimal cell viability graph given in Figure 41 and Table 10. Cell viability was calculated from the absorbance values by using the following equation;

$$\% \text{ Viability} = \frac{OD_{\text{Sample}} - OD_{\text{Blank}}}{OD_{\text{Control (with DMSO)}} - OD_{\text{Blank}}} \times 100 \quad (10)$$

Table 11: Selected concentrations and their effect on B-CPAP cancer cells after 24 hours in terms of % cell viability.

Concentration (in $\mu\text{M}$ )	Average % Cell Viability
Control	100
10	94,83 $\pm$ 1,8
61	82,10 $\pm$ 1,6
98	71,56 $\pm$ 9,5
135	60,00 $\pm$ 3,8
497	36,59 $\pm$ 4,7

**Percent Viability Versus Concentration Graph**



Tukey's multiple comparisons test	Mean Diff.	95,00% CI of diff.	Significant?	Summary
Control vs. 10μM	5,17	-21,28 to 31,62	No	ns
Control vs. 61μM	17,9	-8,551 to 44,35	No	ns
Control vs. 98μM	28,44	1,989 to 54,89	Yes	*
Control vs. 135μM	40	13,55 to 66,45	Yes	**
Control vs. 497μM	63,42	36,96 to 89,87	Yes	***

Figure 41: Percent viability versus concentration graph.

Note: Graph show the effect of different concentration of quercetin based on release studies on the B-CPAP thyroid cancer cells.

Based on the data shown in Figure 41, it was observed that as the concentration of quercetin increased due to release from the beads, the inhibitory effect on the B-CPAP cells was increased. This is concluded due to decrease in percent viability of papillary thyroid cancer cells by increasing the concentration of quercetin in the medium. Figure 42 and Figure 43 show the pictures of B-CPAP cancer cells after quercetin treatment and after MTT treatment, respectively. After MTT treatment, formazan crystals were formed and at low concentration of quercetin, formazan crystals are more common. As the concentration of quercetin increased, there were less observable formazan crystals. This indicates that percent cell viability will decrease with increasing quercetin concentration.

Polyphenols such as quercetin reduce the viability of cancer cells mainly by two modes of action. The first action is by modifying redox status. There are reactive oxygen species (ROS) in organisms such as hydrogen peroxide. These ROS species act as cell replication regulator and also play important roles in signal transduction pathways. The demand for ROS species is high for cancer cells to enable uncontrollable growth. In the presence of polyphenol such as quercetin. It acts as scavenging agent to trap and reduce ROS species. Thus, cancer cells will not find enough cell replication regulator and they will decrease in number. The second mode of action is achieved by interacting with cancer cell functions such as cell cycle and apoptosis. Cancer cells require high amount of cyclin dependent kinase to suppress the p53 tumor suppressor proteins and to produce many cancer cells via uncontrollable cell cycles. Quercetin may inactivate or decrease the amount of cyclin dependent kinase, which leads to stop of cell cycles. Therefore, no more cancer cells will be produced. In addition, quercetin may activate caspase 3 in cancer cells, this will initiate apoptosis in cancer cells. Caspase 3 is an effector protease, it can cleave all many essential materials inside the cancer cells and it will causes programmed death of cancer cells. Therefore, the number of cancer cells will decrease (Kampa et al., 2007).

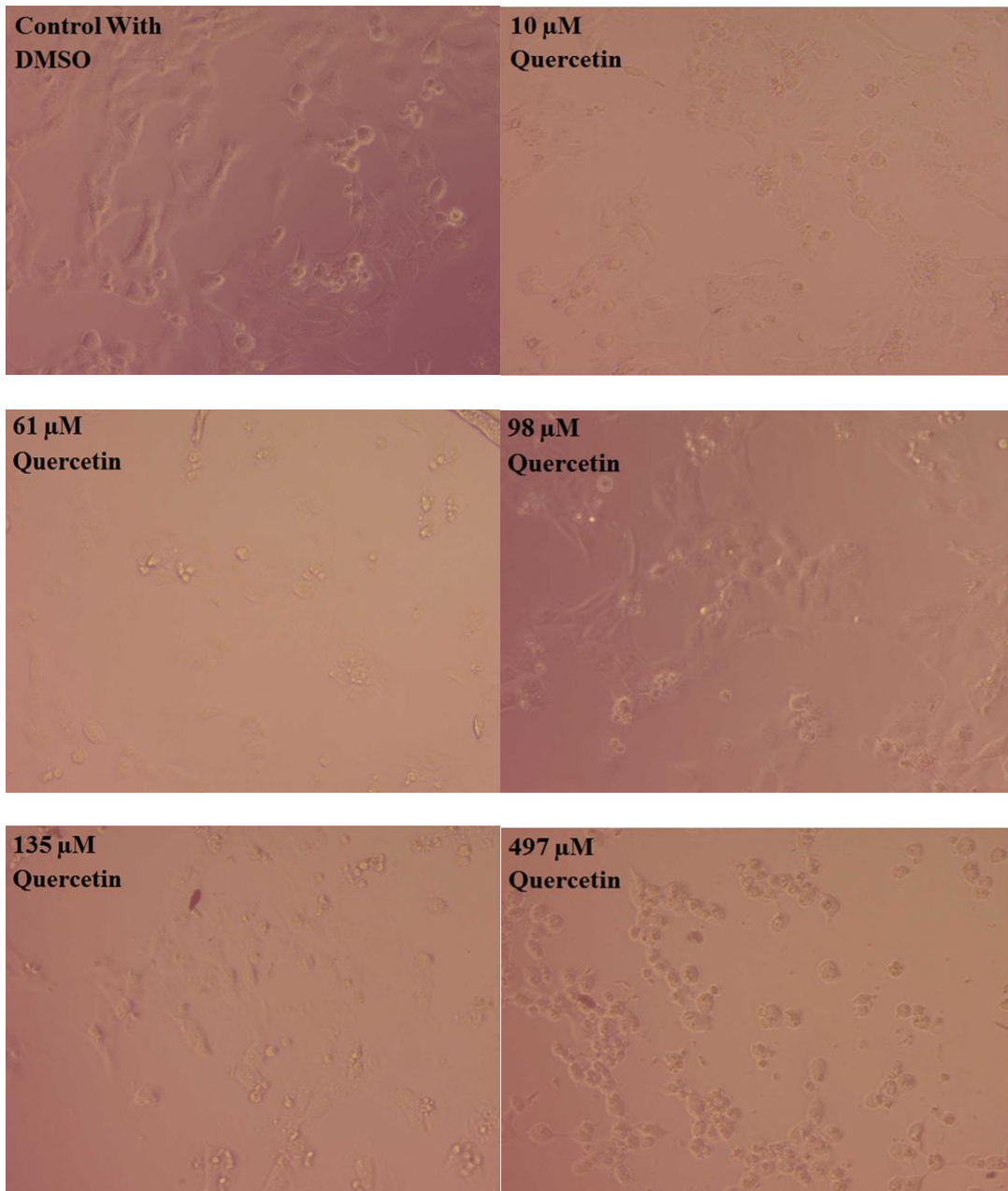


Figure 42: Invert microscope images of B-CPAP cancer cells after treatment with different concentrations of quercetin.

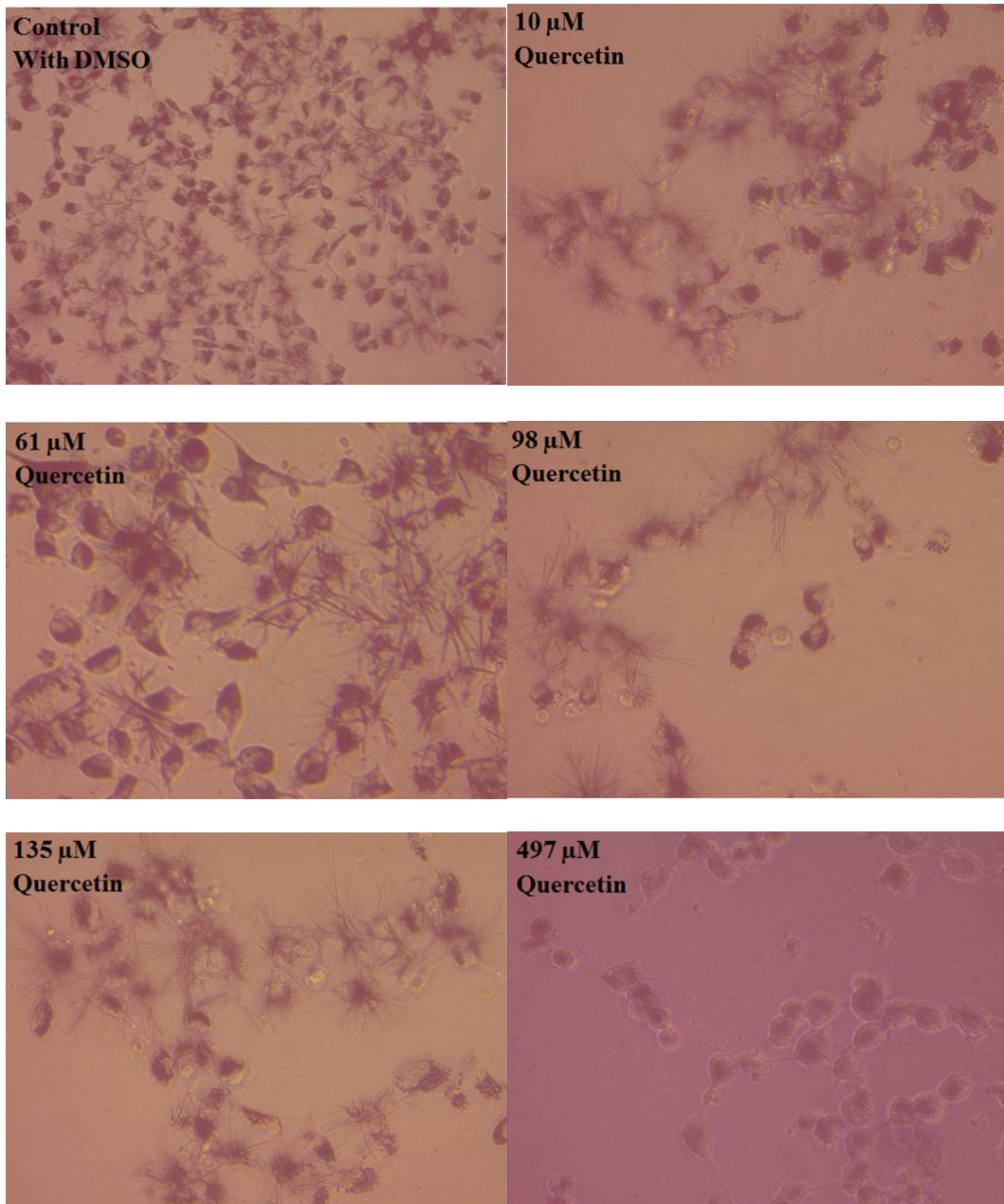


Figure 43: Invert microscope images of B-CPAP cancer cells after MTT treatment.

### 4.9.1 IC50 Determination

IC50 value for the quercetin released from the beads on B-CPAP cancer cells was determined by using the dose-effect and median-effect graphs as given in Figure 44 . IC50 value was found as 268,43  $\mu\text{M}$ . IC50 value providing as concentration of quercetin required to reduce the % viability of B-CPAP cells by half.

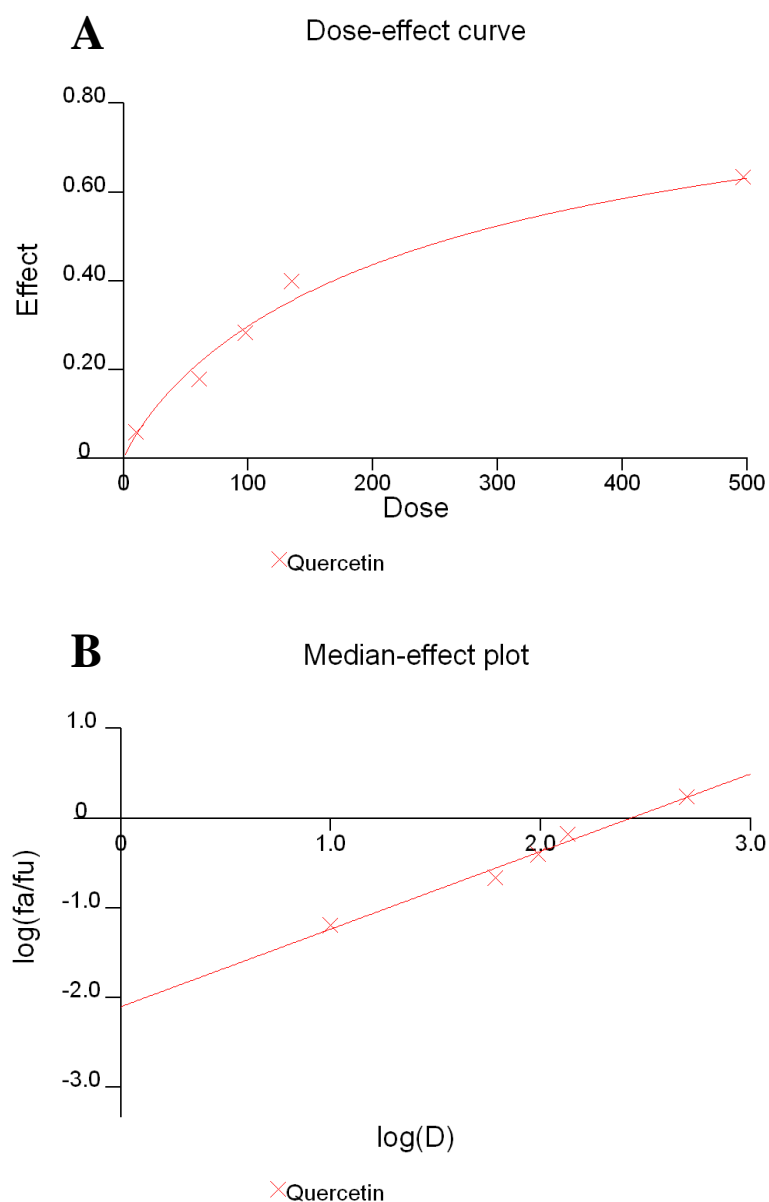


Figure 44: Average % Viability Determination.  
Note: Average % Viability was determined by using (A) Dose-effect curve and (B) Median-effect plot (Plotted in calcsyn software).

#### 4.10 Antioxidant Assay – DPPH (2, 2-diphenyl-1-picrylhydrazyl)

##### Test

Antioxidant test as its name suggest investigation of the oxidation inhibition effect of any compound. By inhibition of oxidation reactions, there will be fewer amounts of free reactive oxygen species and therefore it will less likely to cause cell damage. DPPH test was used to measure radical scavenging activity of molecules. Radical scavenging activity was usually shown in terms of percent inhibition. Percent inhibition can be calculated as follow;

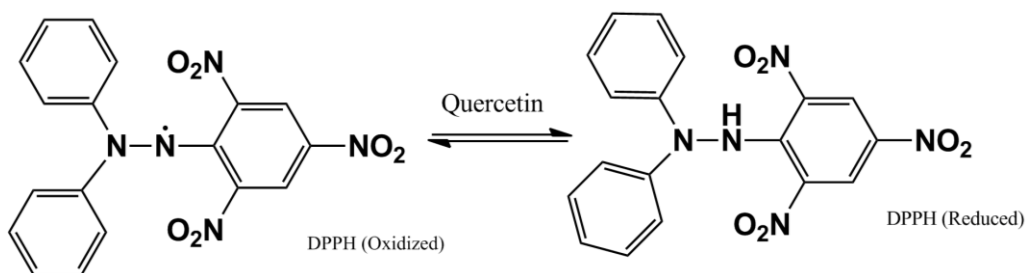
$$\% \text{ inhibition of DPPH radical} = \frac{A_{\text{Control}} - A_{\text{Sample}}}{A_{\text{Control}}} \times 100 \quad (11)$$

$$A_{\text{Control}} = \text{Absorbance of control}$$

$$A_{\text{Sample}} = \text{Absorbance of sample}$$

Quercetin has antioxidant activity, specifically free radical activity. This is clearly shown in Figures 45 and 46, as the concentration of quercetin increased the colour of DPPH changed from purple to yellow. This is due to the free radical activity of quercetin, quercetin donates hydrogen to DPPH and DPPH will be reduced. Reduced DPPH has yellow colour and therefore, the absorbance value at 515 nm decreased. In addition, gallic acid was used as known reference and it was found that quercetin has even better radical scavenging activity than the gallic acid at about 40 % inhibition.





**Mechanism:**

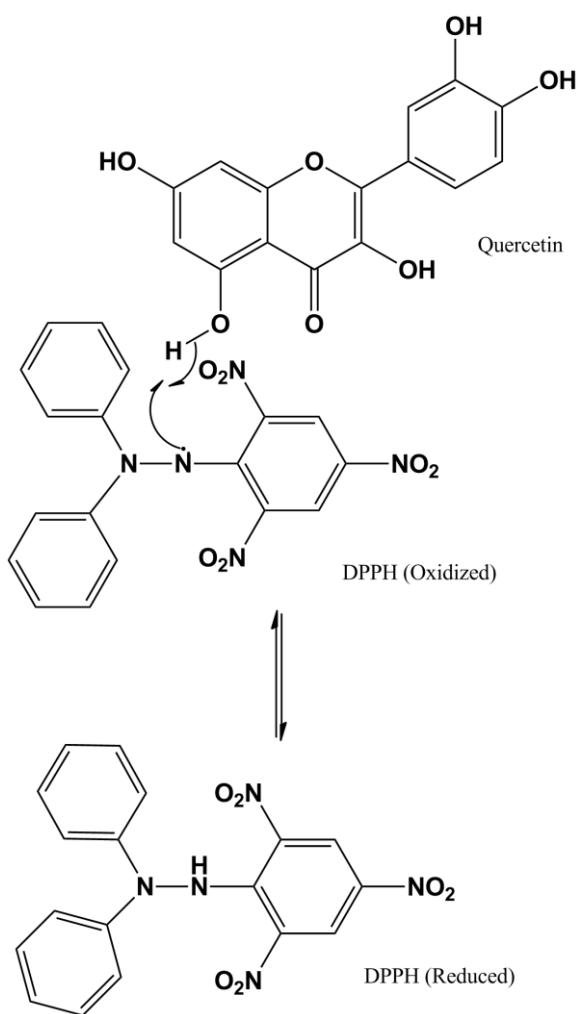


Figure 45: DPPH reduction by quercetin.

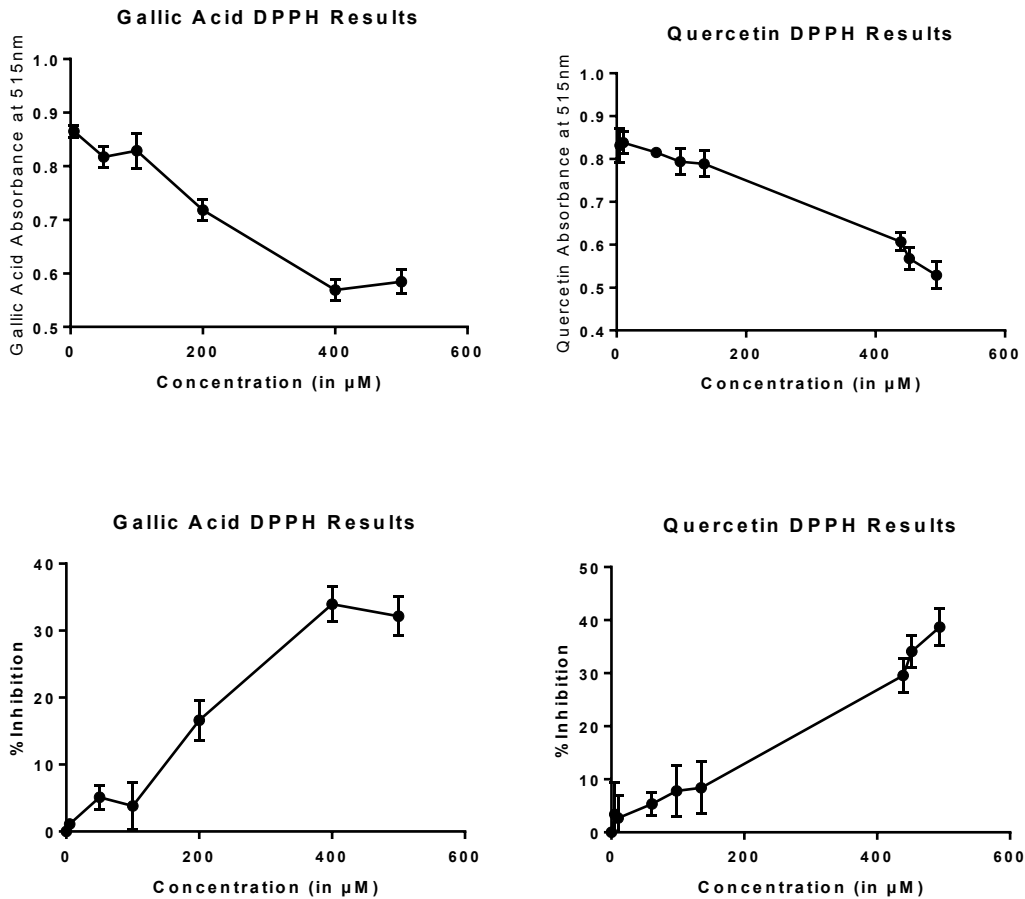


Figure 46: Reduction of DPPH absorbance values at 515 nm.

Note: (A) Reduction of DPPH absorbance values due to free radical scavenging activity of gallic acid. (B) Reduction of DPPH absorbance values due to free radical scavenging activity of quercetin. (C) Percent inhibition of DPPH radical increases up to 32% as the concentration of gallic acid between 5 and 500  $\mu\text{M}$  used. (D) Percent inhibition of DPPH radical increases up to 39% as the increasing concentration of quercetin released from the beads used.

#### 4.11 Time Kill Assay

Based on CFU/mL values from Table 11, CFU/mL versus time graph was constructed in Figure 47. According to Figure 47, in first three values; at time 0, 5, and 10 minutes, the countable colony forming units per mL in normal beads and in cryobeads were lower than the control. This was an expected result, which indicates that quercetin concentrations have antibacterial activity. However, between 15 and 720 minutes, in CFU/mL values, it was observed that in all samples; gel beads, cryogel beads and control the number of colonies are fluctuating and there was no general trend, which indicates that quercetin loaded beads have low amount of quercetin for antibacterial applications. At time 1440 minutes, it was clearly observed that in normal beads and cryobeads, there was clear inhibition of bacterial growth compare to control. This suggest that quercetin loaded beads are suitable for antibacterial applications. However, the concentration of quercetin should be increased, so that it will show its activity earlier.

Table 12: Colony Forming Units per mL (CFU/mL) for *S. aureus* at specific time intervals were calculated from number of colonies obtained on blood agar plates.

<b>Time</b>	<b>B CFU/mL</b>	<b>C CFU/mL</b>	<b>Control CFU/mL</b>
<b>0</b>	46	48	62
<b>5</b>	62	64	108
<b>10</b>	46	42	60
<b>15</b>	62	32	60
<b>30</b>	72	62	120
<b>60</b>	82	96	136
<b>120</b>	68	100	54
<b>180</b>	74	56	100
<b>360</b>	184	90	100
<b>480</b>	98	114	96
<b>600</b>	128	136	94
<b>720</b>	162	106	72
<b>1440</b>	78	90	600

By using the number of colonies, CFU/mL can be calculated by using following equation:

$$\frac{CFU}{mL} = \frac{\text{number of countable colonies} \times \text{dilution factor}}{\text{Volume of culture plate}} \quad (12)$$

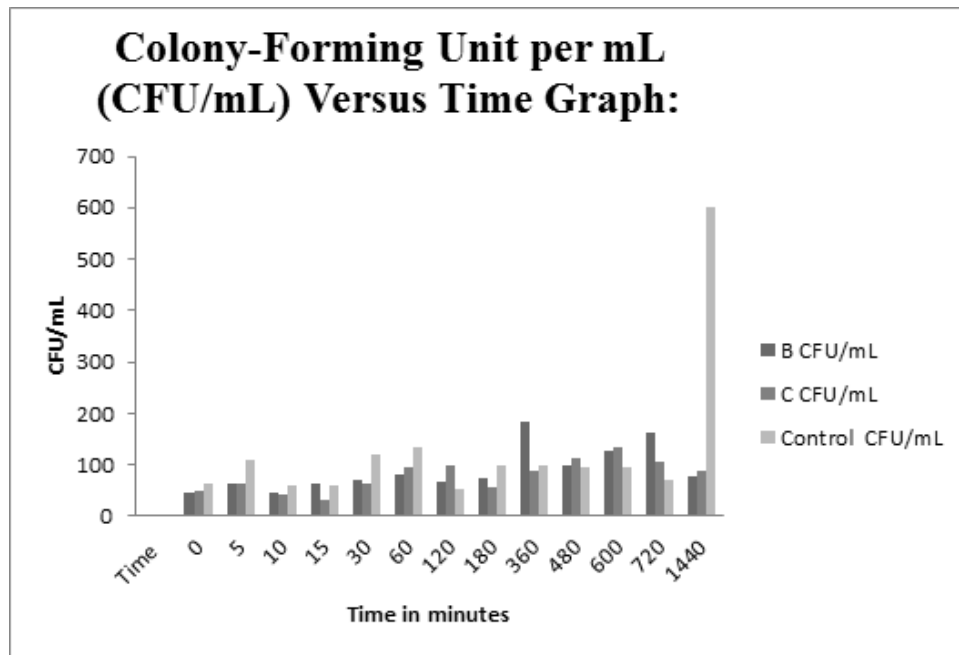


Figure 47: CFU/mL versus time graph.

## Chapter 5

### CONCLUSION

Quercetin was encapsulated by using alginate to form beads. The aim of the encapsulation to enable controlled release of quercetin from the alginate beads and also prevent the fast metabolism or degradation of quercetin in *in vivo* or *in vitro*. It is found that although the swelling profiles were good in phosphate buffer, when it comes to the *in vitro* media such as saline or MHB for antimicrobial activity assays, the swelling in these media were very low. Therefore, it is highly recommended to use the bead either cryogel forms or fresh gel bead forms without drying. In addition, due to the presence of sodium ions in RPMI-1640, it was found that beads showed considerable amount of swelling in RPMI-1640 after 720 minutes. This enable the maximum amount of quercetin released from the beads. It is also found that alginate beads are reacting with ester moiety of casein hydrolysate in MHB and this limits the release of quercetin from the beads. Therefore, for time kill assay, saline solution was suggested to use instead of MHB.

In cell viability assays, it was found that increase in the amount of quercetin from the beads caused decrease in the number of B-CPAP papillary thyroid cancer cells.

In antioxidant activity, DPPH assay, it was found that increasing quercetin concentration released from the beads caused decrease in absorbance at 515 nm for DPPH. Decrease in absorbance of DPPH caused by donation of proton from

quercetin to DPPH. Reduced DPPH would not show peak at 515 nm. Thus, increasing concentration of quercetin caused increase in percent inhibition of free DPPH radicals.

Finally, time kill assay showed that although quercetin is a good antimicrobial agent, the amount of quercetin encapsulated by the beads were not enough. Therefore, the amount of quercetin in the beads should be increased for antimicrobial applications.

Quercetin encapsulated alginate beads were designed as a precaution smart medicine and as a supplement for healthy people and for cancer patients. However, for human use; the results should be replicated with different types of cancer cells and also with the health cell lines. The effect of these beads on healthy cells also plays a critical role. We do not want to reduce healthy cells significantly, while reducing the cancer cells.

In addition, the metabolic pathways were not considered in this thesis. Once quercetin is released from the beads, it will be subjected to metabolism and post modification via the metabolic enzymes. Therefore, the rate of metabolism of quercetin in the body also should be considered and studied before the application with multicellular organisms.

## REFERENCES

- Adebiyi, O.E., Olayemi, F.O., Ning-Hua, T. and Guang-Zhi, Z., 2017. In vitro antioxidant activity, total phenolic and flavonoid contents of ethanol extract of stem and leaf of *Grewia carpinifolia*. *Beni-Suef University Journal of Basic and Applied Sciences*, 6(1), pp.10-14.
- Agüero, L., Zaldivar-Silva, D., Pena, L. and Dias, M.L., 2017. Alginate microparticles as oral colon drug delivery device: A review. *Carbohydrate polymers*, 168, pp.32-43.
- Aijaz, A., Perera, D. and Olabisi, R.M., 2017. Polymeric materials for cell microencapsulation. In *Cell Microencapsulation* (pp. 79-93). Humana Press, New York, NY.
- Alegre-Requena, J.V., Häring, M., Herrera, R.P. and Díaz, D.D., 2016. Regulatory parameters of self-healing alginate hydrogel networks prepared via mussel-inspired dynamic chemistry. *New Journal of Chemistry*, 40(10), pp.8493-8501.
- An, B., Lee, H., Lee, S., Lee, S.H. and Choi, J.W., 2015. Determining the selectivity of divalent metal cations for the carboxyl group of alginate hydrogel beads during competitive sorption. *Journal of hazardous materials*, 298, pp.11-18.
- Anand, D.A.V., Arulmoli, R. and Parasuraman, S., 2016. Overviews of biological importance of quercetin: A bioactive flavonoid. *Pharmacognosy reviews*, 10(20), p.84.

- Asghari, F., Samiei, M., Adibkia, K., Akbarzadeh, A. and Davaran, S., 2017. Biodegradable and biocompatible polymers for tissue engineering application: a review. *Artificial cells, nanomedicine, and biotechnology*, 45(2), pp.185-192.
- Athukoralage, J.S., Graham, S., Grüşchow, S., Rouillon, C. and White, M.F., 2019. A type III CRISPR ancillary ribonuclease degrades its cyclic oligoadenylate activator. *Journal of molecular biology*.
- Ayaz, M., Ullah, F., Sadiq, A., Ullah, F., Ovais, M., Ahmed, J. and Devkota, H.P., 2019. Synergistic interactions of phytochemicals with antimicrobial agents: Potential strategy to counteract drug resistance. *Chemico-biological interactions*.
- Baby, B., Antony, P. and Vijayan, R., 2018. Interactions of quercetin with receptor tyrosine kinases associated with human lung carcinoma. *Natural product research*, 32(24), pp.2928-2931.
- Baghel, S.S., Shrivastava, N., Baghel, R.S., Agrawal, P. and Rajput, S., 2012. A review of quercetin: antioxidant and anticancer properties. *World J Pharm Pharmaceutical Sci*, 1(1), pp.146-60.
- Bajpai, S.K. and Sharma, S., 2004. Investigation of swelling/degradation behaviour of alginate beads crosslinked with Ca<sup>2+</sup> and Ba<sup>2+</sup> ions. *Reactive and Functional Polymers*, 59(2), pp.129-140.



- Bang, S., Choi, J.W., Cho, K., Chung, C., Kang, H. and Hong, S.W., 2016. Simultaneous reduction of copper and toxicity in semiconductor wastewater using protonated alginate beads. *Chemical Engineering Journal*, 288, pp.525-531.
- Bentz, Alexandra B. A Review of Quercetin: Chemistry, Antioxidant Properties, and Bioavailability. *Journal of young investigators*, 2017.
- Birch, J.R. and Arathoon, R., 2018. Suspension culture of mammalian cells. In *Large-Scale Mammalian Cell Culture Technology* (pp. 251-270). Routledge.
- Bruschi, M.L., Borghi-Pangoni, F.B., Junqueira, M.V. and de Souza Ferreira, S.B., 2017. Nanostructured therapeutic systems with bioadhesive and thermoresponsive properties. In *Nanostructures for Novel Therapy* (pp. 313-342). Elsevier.
- Calgarotto, A.K., Maso, V., Junior, G.C.F., Nowill, A.E., Latuf Filho, P., Vassallo, J. and Saad, S.T.O., 2018. Antitumor activities of Quercetin and Green Tea in xenografts of human leukemia HL60 cells. *Scientific reports*, 8(1), p.3459.
- Caliari, S.R. and Burdick, J.A., 2016. A practical guide to hydrogels for cell culture. *Nature methods*, 13(5), p.405.
- Carraher, C.E. and Seymour, R.B., 2003. Seymour/Carraher's polymer chemistry. M. Dekker.

- Catalani, S., Palma, F., Battistelli, S., Nuvoli, B., Galati, R. and Benedetti, S., 2017. Reduced cell viability and apoptosis induction in human thyroid carcinoma and mesothelioma cells exposed to cidofovir. *Toxicology in Vitro*, *41*, pp.49-55.
- Chacon, E., Acosta, D. and Lemasters, J.J., 1997. Primary cultures of cardiac myocytes as in vitro models for pharmacological and toxicological assessments. In *In Vitro Methods in Pharmaceutical Research* (pp. 209-223). Academic Press.
- Chen, L., Guo, P., He, Y., Chen, Z., Chen, L., Luo, Y., Qi, L., Liu, Y., Wu, Q., Cui, Y. and Fang, F., 2018. HCC-derived exosomes elicit HCC progression and recurrence by epithelial-mesenchymal transition through MAPK/ERK signalling pathway. *Cell death & disease*, *9*(5), p.513.
- Chiang, C.L., Ma, C.C.M., Wu, D.L. and Kuan, H.C., 2003. Preparation, characterization, and properties of novolac-type phenolic/SiO<sub>2</sub> hybrid organic–inorganic nanocomposite materials by sol–gel method. *Journal of Polymer Science Part A: Polymer Chemistry*, *41*(7), pp.905-913.
- Cohn, A.L., Day, B.M., Abhyankar, S., McKenna, E., Riehl, T. and Puzanov, I., 2017. BRAFV600 mutations in solid tumors, other than metastatic melanoma and papillary thyroid cancer, or multiple myeloma: a screening study. *Oncotargets and therapy*, *10*, p.965.
- Daemi, H. and Barikani, M., 2012. Synthesis and characterization of calcium alginate nanoparticles, sodium homopolymannuronate salt and its calcium nanoparticles. *Scientia Iranica*, *19*(6), pp.2023-2028.

- Danks, A.E., Hall, S.R. and Schnepf, Z., 2016. The evolution of 'sol-gel' chemistry as a technique for materials synthesis. *Materials Horizons*, 3(2), pp.91-112.
- Dash, S., Murthy, P.N., Nath, L. and Chowdhury, P., 2010. Kinetic modeling on drug release from controlled drug delivery systems. *Acta Pol Pharm*, 67(3), pp.217-23.
- de Souza Armini, R., Bernabé, C.S., Rosa, C.A., Siller, C.A., Schimitel, F.G., Tufik, S., Klein, D.F. and Schenberg, L.C., 2015. In a rat model of panic, corticotropin responses to dorsal periaqueductal gray stimulation depend on physical exertion. *Psychoneuroendocrinology*, 53, pp.136-147.
- Destruel, P.L., Zeng, N., Maury, M., Mignet, N. and Boudy, V., 2016. In vitro and in vivo evaluation of in situ gelling systems for sustained topical ophthalmic delivery: state of the art and beyond. *Drug discovery today*, 22(4), pp.638-651.
- Devi, N., Sarmah, M., Khatun, B. and Maji, T.K., 2017. Encapsulation of active ingredients in polysaccharide-protein complex coacervates. *Advances in colloid and interface science*, 239, pp.136-145.
- Draget, K.I. and Taylor, C., 2011. Chemical, physical and biological properties of alginates and their biomedical implications. *Food Hydrocolloids*, 25(2), pp.251-256.
- Falini, B., Martelli, M.P. and Tiacci, E., 2016. BRAF V600E mutation in hairy cell leukemia: from bench to bedside. *Blood*, 128(15), pp.1918-1927.

- Farhadi, F., Khameneh, B., Iranshahi, M. and Iranshahy, M., 2019. Antibacterial activity of flavonoids and their structure–activity relationship: An update review. *Phytotherapy research*, 33(1), pp.13-40.
- Fellinger, T.P., 2017. Sol–gel carbons from ionothermal syntheses. *Journal of Sol-Gel Science and Technology*, 81(1), pp.52-58.
- Feng, C., Yang, M., Lan, M., Liu, C., Zhang, Y., Huang, B., Liu, H. and Zhou, Y., 2017. ROS: crucial intermediators in the pathogenesis of intervertebral disc degeneration. *Oxidative medicine and cellular longevity*, 2017.
- Geoghegan, F., Wong, R.W.K. and Rabie, A.B.M., 2010. Inhibitory effect of quercetin on periodontal pathogens in vitro. *Phytotherapy Research*, 24(6), pp.817-820.
- Graulus, G.J., Mignon, A., Van Vlierberghe, S., Declercq, H., Fehér, K., Cornelissen, M., Martins, J.C. and Dubruel, P., 2015. Cross-linkable alginate-graft-gelatin copolymers for tissue engineering applications. *European Polymer Journal*, 72, pp.494-506.
- Güran, M., Şanlıtürk, G., Kerküklü, N.R., Altundağ, E.M. and Yalçın, A.S., 2019. Combined effects of quercetin and curcumin on anti-inflammatory and antimicrobial parameters in vitro. *European Journal of Pharmacology*, p.172486.
- Hecht, H. and Srebnik, S., 2016. Structural characterization of sodium alginate and calcium alginate. *Biomacromolecules*, 17(6), pp.2160-2167.

Henderson, T.M., Ladewig, K., Haylock, D.N., McLean, K.M. and O'Connor, A.J., 2013. Cryogels for biomedical applications. *Journal of Materials Chemistry B*, 1(21), pp.2682-2695.

Ighodaro, O.M. and Akinloye, O.A., 2018. First line defence antioxidants-superoxide dismutase (SOD), catalase (CAT) and glutathione peroxidase (GPX): Their fundamental role in the entire antioxidant defence grid. *Alexandria Journal of Medicine*, 54(4), pp.287-293.

Islam, S., Bhuiyan, M.R. and Islam, M.N., 2017. Chitin and chitosan: structure, properties and applications in biomedical engineering. *Journal of Polymers and the Environment*, 25(3), pp.854-866.

Iwashina, T., 2013. Flavonoid properties of five families newly incorporated into the order Caryophyllales. *Bull Natl Mus Nat Sci*, 39, pp.25-51.

Jaiswal, N. and Rizvi, S.I., 2014. Onion extract (*Allium cepa* L.), quercetin and catechin up-regulate paraoxonase 1 activity with concomitant protection against low-density lipoprotein oxidation in male Wistar rats subjected to oxidative stress. *Journal of the Science of Food and Agriculture*, 94(13), pp.2752-2757.

Jenke, D.R., 2014. Extractables and leachables considerations for prefilled syringes. *Expert opinion on drug delivery*, 11(10), pp.1591-1600.

Jia, J., Richards, D.J., Pollard, S., Tan, Y., Rodriguez, J., Visconti, R.P., Trusk, T.C., Yost, M.J., Yao, H., Markwald, R.R. and Mei, Y., 2014. Engineering alginate as bioink for bioprinting. *Acta biomaterialia*, 10(10), pp.4323-4331.

Kabay, T., 2019. Effects of Different Potassium Doses On Development of High Temperature-Sensitive Bean Plants. *Feb-Fresenius Environmental Bulletin*, 28(1), pp.320-325.

Kampa, M., Nifli, A.P., Notas, G. and Castanas, E., 2007. Polyphenols and cancer cell growth. In *Reviews of physiology, biochemistry and pharmacology* (pp. 79-113). Springer, Berlin, Heidelberg.

Kaygusuz, H., Evingür, G.A., Pekcan, Ö., von Klitzing, R. and Erim, F.B., 2016. Surfactant and metal ion effects on the mechanical properties of alginate hydrogels. *International journal of biological macromolecules*, 92, pp.220-224.

Kuete, V., Karaosmanoğlu, O., and Sivas, H., 2017. Anticancer Activities of African Medicinal Spices and Vegetables. *Medicinal Spices and Vegetables from Africa*, pp.271–297.

Kulkarni Vishakha, S., Butte Kishor, D. and Rathod Sudha, S., 2012. Natural polymers—A comprehensive review. *International Journal of Research in Pharmaceutical and Biomedical Sciences*, 3(4), pp.1597-1613.

- Kumar, S., Chauhan, N., Gopal, M., Kumar, R. and Dilbaghi, N., 2015. Development and evaluation of alginate–chitosan nanocapsules for controlled release of acetamiprid. *International journal of biological macromolecules*, 81, pp.631-637.
- Lakhanpal, P. and Rai, D.K., 2007. Quercetin: a versatile flavonoid. *Internet Journal of Medical Update*, 2(2), pp.22-37.
- Lawal, M.V., 2019. Modified Starches as Direct Compression Excipients–Effect of Physical and Chemical Modifications on Tablet Properties: A Review. *Starch-Stärke*, 71(1-2), p.1800040.
- Li, D., Lv, C., Liu, L., Xia, Y., She, X., Guo, S. and Yang, D., 2015. Egg-box structure in cobalt alginate: a new approach to multifunctional hierarchical mesoporous N-doped carbon nanofibers for efficient catalysis and energy storage. *ACS central science*, 1(5), pp.261-269.
- Li, Y., Yao, J., Han, C., Yang, J., Chaudhry, M., Wang, S., Liu, H. and Yin, Y., 2016. Quercetin, inflammation and immunity. *Nutrients*, 8(3), p.167.
- Lou, G., Liu, Y., Wu, S., Xue, J., Yang, F., Fu, H., Zheng, M. and Chen, Z., 2015. The p53/miR-34a/SIRT1 positive feedback loop in quercetin-induced apoptosis. *Cellular Physiology and Biochemistry*, 35(6), pp.2192-2202.
- Luo, Y. and Wang, Q., 2014. Recent development of chitosan-based polyelectrolyte complexes with natural polysaccharides for drug delivery. *International journal of biological macromolecules*, 64, pp.353-367.

- Lushchak, V.I., 2014. Free radicals, reactive oxygen species, oxidative stress and its classification. *Chemico-biological interactions*, 224, pp.164-175.
- Lu, Z. and Hunter, T., 2018. Metabolic kinases moonlighting as protein kinases. *Trends in biochemical sciences*, 43(4), pp.301-310.
- Mane, S., Ponrathnam, S. and Chavan, N., 2015. Effect of chemical cross-linking on properties of polymer microbeads: A review. *Can. Chem. Trans*, 3(4), pp.473-485.
- Mattila, J.T. and Thomas, A.C., 2014. Nitric oxide synthase: non-canonical expression patterns. *Frontiers in immunology*, 5, p.478.
- Murawski, A., Diaz, R., Inglesby, S., Delabar, K. and Quirino, R.L., 2019. Synthesis of Bio-based Polymer Composites: Fabrication, Fillers, Properties, and Challenges. In *Polymer Nanocomposites in Biomedical Engineering* (pp. 29-55). Springer, Cham.
- Murugan, A.K., Qasem, E., Al-Hindi, H., Shi, Y. and Alzahrani, A.S., 2016. Classical V600E and other non-hotspot BRAF mutations in adult differentiated thyroid cancer. *Journal of translational medicine*, 14(1), p.204.
- Mutlu Altundağ, E., Kasacı, T., Yılmaz, A.M., Karademir, B., Koçtürk, S., Taga, Y. and Yalçın, A.S., 2016. Quercetin-induced cell death in human papillary thyroid cancer (B-CPAP) cells. *Journal of thyroid research*, 2016.



- Orive, G., Hernández, R.M., Gascón, A.R., Calafiore, R., Chang, T.M.S., De Vos, P., Hortelano, G., Hunkeler, D., Lacík, I. and Pedraz, J.L., 2004. History, challenges and perspectives of cell microencapsulation. *TRENDS in Biotechnology*, 22(2), pp.87-92.
- Panche,A.N., Diwan, A.D. and Chandra, S.R.,2016.Flavonoids: an overview. *J Nutr Sci*. 5:47
- Panzella, L. and Napolitano, A., 2017. Natural phenol polymers: Recent advances in food and health applications. *Antioxidants*, 6(2), p.30.
- Patel, N., Lalwani, D., Gollmer, S., Injeti, E., Sari, Y. and Nesamony, J., 2016. Development and evaluation of a calcium alginate based oral ceftriaxone sodium formulation. *Progress in biomaterials*, 5(2), pp.117-133.
- Perim, M.C., Borges, J.D.C., da Silva, E.M.L., Araújo, T.A.D.S., da Silva, A.C.O., da Silva, V.C., Carreiro, S.C., Cunha, A.F. and Pranchevicius, M.C.D.S., 2018. In vitro antibacterial and time-kill assay of ethanolic extract of Davilla nitida bark on multidrug resistant bacteria isolated from diabetic foot lesions. *Natural product research*, pp.1-6.
- Plieva, F.M., Savina, I.N., Deraz, S., Andersson, J., Galaev, I.Y. and Mattiasson, B., 2004. Characterization of supermacroporous monolithic polyacrylamide based matrices designed for chromatography of bioparticles. *Journal of Chromatography B*, 807(1), pp.129-137.

- Pongjanyakul, T. and Rongthong, T., 2010. Enhanced entrapment efficiency and modulated drug release of alginate beads loaded with drug–clay intercalated complexes as microreservoirs. *Carbohydrate Polymers*, 81(2), pp.409-419.
- Rahal, A., Kumar, A., Singh, V., Yadav, B., Tiwari, R., Chakraborty, S. and Dhama, K., 2014. Oxidative stress, prooxidants, and antioxidants: the interplay. *BioMed research international*, 2014.
- Rasines-Perea, Z. and Teissedre, P.L., 2017. Grape polyphenols' effects in human cardiovascular diseases and diabetes. *Molecules*, 22(1), p.68.
- Rudin, A. and Choi, P., 2013. *Introductory Concepts and Definitions. The Elements of Polymer Science & Engineering*, pp.1–62.
- Sachan, N.K., Pushkar, S., Jha, A. and Bhattacharya, A., 2009. Sodium alginate: the wonder polymer for controlled drug delivery. *J. Pharm. Res*, 2(8), pp.1191-1199.
- Saiselet, M., Floor, S., Tarabichi, M., Dom, G., Hébrant, A., van Staveren, W. and Maenhaut, C., 2012. Thyroid cancer cell lines: an overview. *Frontiers in endocrinology*, 3, p.133.
- Scarano, A., Butelli, E., De Santis, S., Cavalcanti, E., Hill, L., De Angelis, M., Giovinazzo, G., Chieppa, M., Martin, C. and Santino, A., 2018. Combined dietary anthocyanins, flavonols, and stilbenoids alleviate inflammatory bowel disease symptoms in mice. *Frontiers in nutrition*, 4, p.75.

- Schuster, E., Sott, K., Ström, A., Altskär, A., Smisdom, N., Gebäck, T., Lorén, N. and Hermansson, A.M., 2016. Interplay between flow and diffusion in capillary alginate hydrogels. *Soft Matter*, 12(17), pp.3897-3907.
- Seeli, D.S., Dhivya, S., Selvamurugan, N. and Prabakaran, M., 2016. Guar gum succinate-sodium alginate beads as a pH-sensitive carrier for colon-specific drug delivery. *International journal of biological macromolecules*, 91, pp.45-50.
- Shaari, N. and Kamarudin, S.K., 2015. Chitosan and alginate types of bio-membrane in fuel cell application: an overview. *Journal of Power Sources*, 289, pp.71-80.
- Soukoulis, C., Cambier, S., Hoffmann, L. and Bohn, T., 2016. Chemical stability and bioaccessibility of  $\beta$ -carotene encapsulated in sodium alginate o/w emulsions: Impact of  $\text{Ca}^{2+}$  mediated gelation. *Food hydrocolloids*, 57, pp.301-310.
- Souza, C.D.S., Felicio, L.B.A., Ferreira, J., Kurachi, C., Bentley, M.V.B., Tedesco, A.C. and Bagnato, V.S., 2009. Long-term follow-up of topical 5-aminolaevulinic acid photodynamic therapy diode laser single session for non-melanoma skin cancer. *Photodiagnosis and Photodynamic Therapy*, 6(3-4), pp.207-213.
- Teixeira, J., Chavarria, D., Borges, F., Wojtczak, L., Wieckowski, M.R., Karkucińska-Wieckowska, A. and Oliveira, P.J., 2019. Dietary polyphenols and mitochondrial function: role in health and disease. *Current medicinal chemistry*.
- Thombre, A.G., Wu, X.Y. and am Ende, M.T., 2019. Controlled Release Technology and Design of Oral Controlled Release Dosage Forms. *Chemical Engineering in*

*the Pharmaceutical Industry: Drug Product Design, Development, and Modeling*, pp.381-407.

Toklu, H.Z. and Tumer, N., 2015. Oxidative stress, brain edema, blood-brain barrier permeability, and autonomic dysfunction from traumatic brain injury. *Brain Neurotrauma: Molecular, Neuropsychological, and Rehabilitation Aspects*; Kobeissy, FH, Ed.

Tsao, R., 2010. Chemistry and biochemistry of dietary polyphenols. *Nutrients*, 2(12), pp.1231-1246.

Voo, W.P., Ooi, C.W., Islam, A., Tey, B.T. and Chan, E.S., 2016. Calcium alginate hydrogel beads with high stiffness and extended dissolution behaviour. *European Polymer Journal*, 75, pp.343-353.

Walker, E.H., Pacold, M.E., Perisic, O., Stephens, L., Hawkins, P.T., Wymann, M.P. and Williams, R.L., 2000. Structural determinants of phosphoinositide 3-kinase inhibition by wortmannin, LY294002, quercetin, myricetin, and staurosporine. *Molecular cell*, 6(4), pp.909-919.

Wang, M., Yuan, Z., Cheng, S., Leitch, M. and Xu, C.C., 2010. Synthesis of novolac-type phenolic resins using glucose as the substitute for formaldehyde. *Journal of applied polymer science*, 118(2), pp.1191-1197.

- Wang, Y., Li, X., Wu, C., Zhao, Y., Gao, B.Y. and Yue, Q., 2014. The role of sodium alginate in improving floc size and strength and the subsequent effects on ultrafiltration membrane fouling. *Environmental technology*, 35(1), pp.10-17.
- Wei, G. and Ma, P.X., 2009. Partially nanofibrous architecture of 3D tissue engineering scaffolds. *Biomaterials*, 30(32), pp.6426-6434.
- Williamson, G., 2017. The role of polyphenols in modern nutrition. *Nutrition bulletin*, 42(3), pp.226-235.
- Xu, F., Sridharan, B., Durmus, N.G., Wang, S., Yavuz, A.S., Gurkan, U.A. and Demirci, U., 2011. Living bacterial sacrificial porogens to engineer decellularized porous scaffolds. *PloS one*, 6(4), p.e19344.
- Yadav, R., Devi, A., Tripathi, G. and Srivastava, D., 2007. Optimization of the process variables for the synthesis of cardanol-based novolac-type phenolic resin using response surface methodology. *European polymer journal*, 43(8), pp.3531-3537.
- Yang, J., Zhu, Y., Xu, T., Pan, C., Cai, N., Huang, H. and Zhang, L., 2016. The preservation of living cells with biocompatible microparticles. *Nanotechnology*, 27(26), p.265101.
- Younes, I. and Rinaudo, M., 2015. Chitin and chitosan preparation from marine sources. Structure, properties and applications. *Marine drugs*, 13(3), pp.1133-1174.

- Zhang, Y., Chen, S., Wei, C., Rankin, G.O., Ye, X. and Chen, Y.C., 2018. Flavonoids from Chinese bayberry leaves induced apoptosis and G1 cell cycle arrest via Erk pathway in ovarian cancer cells. *European journal of medicinal chemistry*, 147, pp.218-226.
- Zhang, C., Wang, R., Zhang, G. and Gong, D., 2018. Mechanistic insights into the inhibition of quercetin on xanthine oxidase. *International journal of biological macromolecules*, 112, pp.405-412.
- Zhou, J., Fang, L., Liao, J., Li, L., Yao, W., Xiong, Z. and Zhou, X., 2017. Investigation of the anti-cancer effect of quercetin on HepG2 cells in vivo. *PloS one*, 12(3), p.e0172838.